Spring 2021

Measuring Strain-Mediated Magnetoelectric Effects In Magnetically Self-Assembled Multiferroic Janus Nanofiber Chains: A Quest for New Techniques to Study Multiferroic Nanomaterials

Bryan Lucas Chávez

Measuring Strain-mediated Magnetoelectric Effects in Magnetically Self-Assembled Multiferroic Janus Nanofiber Chains: A Quest For New Techniques to Study Multiferroic Nanomaterials

by

Bryan Lucas Chávez

Bachelors of Science
Allegheny College 2013

Submitted in Partial Fulfillment of the Requirements

for the Degree of Doctor of Philosophy in

Physics

College of Arts and Sciences

University of South Carolina

2021

Accepted by:

Thomas M. Crawford, Major Professor

Yanwen Wu, Committee Member

Yuriy V. Pershin, Committee Member

Andrew B. Greytak, Committee Member

Tracey L. Weldon, Interim Vice Provost and Dean of the Graduate School

Acknowledgments

First, I would like to thank Dr. Thomas "Mas" Crawford for taking the chance on me and allowing me to join his research group. It has been an exciting journey, and I am indebted to you for your guidance. You have always been there with new ideas when I was struggling and have helped me be more creative in my scientific endeavors.

I would like to thank my advisement committee, Dr. Yanwen Wu, Dr. Andrew Greytak, and Dr. Yuriy Pershin for the encouragement and helpful advice throughout this process.

Thank you to the UofSC Physics and Astronomy Department staff for always helping me with funding, classes, and general graduate student life. Thank you specifically to Sam Beals for being one of the friendliest and helpful persons I have enjoyed working with.

Many thanks to all of our collaborators at the University of Florida, specifically Dr. Matthew Bauer and Dr. Maeve Budi for making the samples I used throughout this project. Many thanks to Dr. Jennifer Andrew for giving helpful advice on these materials and the project as a whole.

Thanks to my friends inside and outside of the university, in the swing dance community, game nights crew, disc golf crew, and fellow fraternity brothers: David Baker, Zach Woods, Chris Alduino, William "Shep" Schroer, and Saba Arash. A special thanks to the Magician's Monday crew for keeping me sane even through COVID: Kimi Chavez, Chris McLauchlin, Brigid Byrne, Mark Barnes II, and Michelle Denlar.

Thank you to the many lab mates throughout the trek we call graduate school. Thank you to Sara FitzGerald for helping me with the PPMS and just having some of the best physics and coding advice. Thank you, Rahman Motasebzadeh, for being my study buddy during the qualifying exam time. Thank you to Cory Dolbashian for being my partner in the journey to get "something" from these fibers and praying to god the Mira survived all our experiments. An honorable mention for being semi-work colleagues goes to Heath Smith and Adam Fisher. Thank you to the undergrads who have assisted with this project: Kevin Sosnowski and Annastasia Haynie.

Thank you to Dr. Doros Petasis (Allegheny College) and Dr. Sara Majetich (Carnegie Mellon University) for guiding me early in my undergraduate carrier. Thank you for giving me perspective and guidance. I would not be here if it were not for you. Thank you to my many close friends from Allegheny College: Dr. John Milligan, Kyle Kruse, Sara Bottini, and Clay Moran.

A huge thanks to my family for supporting me throughout this process, even when you may not understand what I was doing or why it took so long. Special thanks to my little sister and roommate for most of graduate school: Kimi Chavez. Though you were only supposed to be here a year, it would not have been the same without you. Thank you to my parents, Rick and Kathy Chavez, for raising me and helping fuel my curiosity for life and the world. I could not have made it this far without you, both personally and professionally.

Lastly, thank you to two great scientists and teachers I had who are no longer with us. Thank you for sparking my interest and love for physics when I was just a neophyte: Dr. Ralph Wuerker and Paul Kanter.

Abstract

Bi-phasic composite multiferroics couple piezoelectric and magnetostrictive properties via an interfacial strain, allowing for control of their magnetic properties with electric fields and vice versa. Nanofibers have a larger area-to-volume ratio than thin films and are not affected by substrate clamping, leading to a predicted magnetoelectric coupling an order of magnitude higher than those found in thin-film multiferroics. Nanofibers have potential applications in photonics, nanoelectronics, biosensing, and optoelectronics. This work focuses on measuring magnetoelectric effects in electrospun nanofibers made of barium titanate ($BaTiO_3$) and cobalt ferrite ($CoFe_2O_4$). To transform the disordered as-spun mat of fibers into a functional architecture for devices, they are ground to various lengths with an average diameter of $\sim$800 nm, and then magnetically self-assembled in a polymer solution. Temperature-dependent magnetometry shows that cobalt ferrite and barium titanate are coupled, confirmed with an observed magnetization shift at $\sim$393 K. I studied the self-assembly of these fibers in an external magnetic field and observed that the fibers chain end-to-end with different dynamics compared to magnetic nanoparticles. Due to geometric and electrochemical effects, in-fluid chaining proved unsuccessful as an *in-situ* probe of the magnetoelectric coupling of these promising multiferroic nanomaterials. I successfully used a novel scattered magneto-optical Kerr effect geometry to probe voltage-induced changes in magnetization. The observed magnetoelectric effects show 50-110 Oe/V changes in coercivity, typically non-hysteretic behaviors, and "collapsing" hysteresis loops. In conclusion, I successfully tested new techniques to measure the magnetoelectric effects in self-assembled multiferroic nanofiber aggregates.

Table of Contents

List of Tables

List of Figures

Chapter 1

Introduction

This document will explain the research endeavors that I took to measure the magnetoelectric effect in multiferroic nanofibers. This work came about from a collaboration between Dr. Thomas "Mas" Crawford (University of South Carolina) and Dr. Jennifer Andrew (University of Florida), with the original goal of finding novel ways to measure the magnetoelectric coupling in multiferroic nanofibers. While most of the multiferroic community is concerned with thin-film heterostructures, we endeavored to look at nanofibers due to their possible applications in the biomedical industry to optoelectronics. It became apparent early in the project why most of the community stays away from nanofiber and nanoparticle systems due to the difficulties in characterizing them. The cylindrical nature and the degrees of freedom inherent in the system compound the challenges in characterizing them. As a fellow researcher said to us, "these are very messy materials to deal with." Although not deterred, we soldiered on to expand on the current knowledge of multiferroics.

This work has three key phases: sample fabrication (magnetic field-driven chaining), magnetoelectric chaining experiment, and magnetoelectric magneto-optical Kerr effect experiments. Each took significant time to master and control all possible problems. Early on in this project, it became evident that the fibers did not self-assemble predictably, making it difficult to make consistent samples for the initial experiments, i.e. Faraday Effect experiment. This led to a study of the magnetic field-driven chaining dynamics where I found that the nanofibers do not chain in the same way as nanoparticles. This difference in the chaining dynamics led to a

hypothesis that I could probe the magnetoelectric effect using self-assembly. Using this, I devised an experiment to probe the chaining dynamics in which electric and magnetic fields were applied perpendicular to each other and recorded the *in-situ* chaining dynamics. Although the initial tests seemed promising with further revisions and eliminating possible systematic errors, the experiment did not prove sensitive enough to extract a coupling constant. With the knowledge gleaned from the chaining experiments in sample fabrication and measurement, a new experiment was devised using the magneto-optical Kerr effect (MOKE). Using a novel scattering MOKE geometry that my colleague, Dr. Cory Dolbashian, designed, I was able to probe the converse magnetoelectric effect (dM/dE) in immobilized chained fiber samples. I was able to measure the magnetoelectric effects in multiple geometries, which showed very different results. These are the first results ever seen using MOKE on self-assembled multiferroic nanofibers. Although the voltage-induced changes are typically non-hysteretic, they detectably change the magnetization, coercivity, and remanence.

In this document, I will start by reviewing relevant information on magnetic and multiferroic materials. Then I will explain the sample fabrication for each experiment and the experimental setups. Continuing, I will discuss the temperature-dependent magnetization data, the magnetic and magnetoelectric chaining data, and the MOKE data. Lastly, I will summarize the results and conclusions of these experiments.

Chapter 2

Magnetism and Magnetic Materials/Nanoparticles

2.1 Overview of Magnetic Materials

Magnetic materials are integral to our everyday lives, with uses varying from magnetic hard drives to magnetic resonance imaging (MRI). In this chapter, I will give a general overview of magnetic materials to refresh the readers' memory of relevant magnetic topics. For a complete discussion on magnetic materials, see [1, 2]. The core types of magnetic materials are: ferromagnetic, ferrimagnetic, paramagnetic, diamagnetic, and anti-ferromagnetic [3]. What distinguishes these different magnetic material types is how they respond to an external magnetic field and their internal spin structure. Diamagnetic materials(i.e., Cu, He, H_2O) repel external magnetic fields and decrease the magnetic field strength; an ideal diamagnetic material is a superconductor. Paramagnetic materials (i.e., Na, Al) are weakly magnetic, their magnetization is linearly proportional to the external magnetic field, and they show no hysteresis. Anti-ferromagnetic materials(i.e., MnO, FeO) are distinguished from paramagnetic materials by a difference in magnetic susceptibility below the Neél temperature [1]. Ferro/Ferrimagnetic materials(i.e., Fe, Fe_3O_4) are the most commonly used magnetic materials with a few defining features: magnetic saturation, magnetic remanence, and coercivity [1]. Ferro/ferrimagnetic materials are used in everything from bar magnets, hard drives, and hyperthermia cancer treatment to inductors.

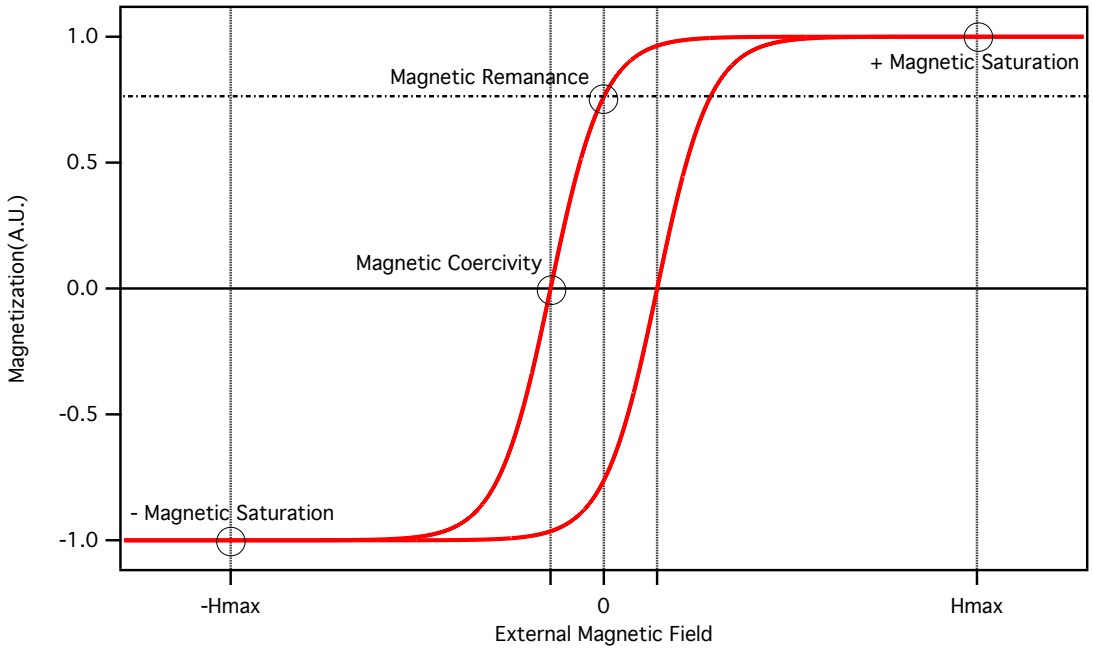

Figure 2.1 Ideal Hysteresis Loop: An ideal Hysteresis loop for a Ferro/Ferrimagnetic material [1].

Magnetic saturation (M_s) happens when an applied external magnetic field forces all domains in a material to point in the same direction, i.e. the material is as magnetic as it can be. Remanence (M_r) is a measurement of how magnetic a material is when no external magnetic fields are applied and is indicative of a material that shows magnetic hysteresis. Remanence can change depending on how the external magnetic field is applied, i.e. the field history, which is called hysteresis [1]. It should be noted that diamagnetic, paramagnetic, and anti-ferromagnetic materials do not experience magnetic hysteresis. Magnetic coercivity is the magnetic field needed to reduce the magnetic moment of a material to zero. Although coercivity is also seen in ferroelectric materials, I will always use coercivity to talk about magnetic materials. All of these properties are defined in Figure 2.1. Another important property is the magnetic permeability (μ), which is the slope of the magnetic flux (B) versus the applied magnetic field (H), typically measured at an initial and maximum state [1]. For ferro/ferrimagnetic materials, this means their magnetic permeability is field-

dependent due to their hysteresis. The hysteresis loop's shape tells us important information about the domain structure and how applied stress affects it.

The internal structure of a magnetic material works by having many different magnetic domains. A domain can be thought of as many tiny magnetic dipoles or spins that interact with each other. The process of how domains align depends on two main things: crystalline anisotropy and shape anisotropy. Crystalline anisotropy is simply dependent on the inherent crystal structure of a material [1]. Shape anisotropy tells that we must also consider the macroscopic shape (i.e., rod, sphere, square) of the material we are dealing with. Shape anisotropy is defined by the relationship of magnetization to the de-magnetization field in a material. By understanding how these anisotropies interact, we can understand the "easy" and "hard" magnetic axes of a material. The easy axis is simply the direction that a magnetic material can be magnetized with the least amount of field needed to flip the magnetization from positive to negative saturation, whereas the hard axis requires the most amount of field. Conceptually, if we look at Figure 2.1, this type of loop would be indicative of the hard axis, whereas if the loop were a perfect square loop with sharp transitions from positive to negative, it would be the easy axis. Typically, the easy and hard axes are perpendicular to each other. For a rod or elongated nanofibers, the easy axis ends up being along the long axis of a fiber [1].

Since domains can be approximated as a magnetic dipole we can understand some of their dynamics by looking at the magnetic dipole energy. The energy that a magnetic dipole has is,

$$E_{dipole} = -\vec{m} \bullet \vec{H} = -mHcos(\theta), \tag{2.1}$$

where E_{dipole} is the energy for a single dipole, $\vec{m}$ is the magnetic moment, $\vec{H}$ is the applied field, and θ is the angle between $\vec{m}$ and $\vec{H}$. We see from this that the preferential direction for the domains is in the same direction as the magnetic field [1].

This domain evolution can be affected by an applied stress which will be covered in the next section.

2.2 Magnetostriction and Stress Effects on Hysteresis

Magnetostriction is a phenomenon where a substance's dimensions change in the presence of an external magnetic field. This induced shape change is defined as,

$$\lambda = \frac{\Delta l}{l}, \tag{2.2}$$

where λ is the magnetostriction ratio, l is the initial length of the measured material, and Δl is the change in length. Magnetostriction is an inherently small effect(10^{-6}) even for materials with "large" magnetostriction, like cobalt ferrite. Magnetostriction depends on the field orientation, crystal structure, and a saturation value where the material will no longer increase in size. Even though it is a small effect, the opposite effect, where an applied stress is placed on a material, can cause significant changes in magnetization, a process called the inverse magnetostrictive effect or magnetomechanical effect [1]. Figure 2.2 shows what happens to a material with a positive magnetostriction ratio like iron. The magnetostriction constant for polycrystalline cobalt ferrite like our sample is $\lambda_p = -110 \times 10^{-6}$ [1].

If stress is applied to a magnetic material, then the domain structure will change, and therefore the measured magnetization will change. The magnetization changes depend on the crystal structure, applied stress, shape anisotropy, and the magnetostriction curve's shape. If, for instance, λ goes from positive to negative at some set magnetic field, the Villari reversal point, then the stress-induced magnetization will flip from increasing to decreasing. Bozorth *et al.* found that the magnetostriction curves are completely positive or negative for polycrystalline cobalt ferrites depending on whether the magnetic field is applied perpendicular or parallel to the easy axis [4].

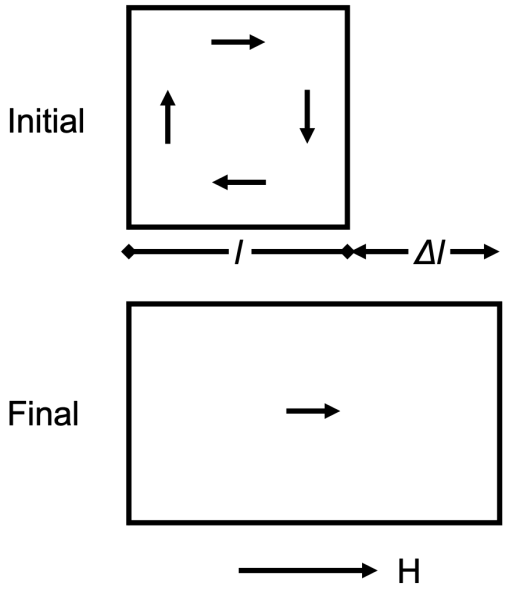

Figure 2.2 Magnetostriction Diagram: This show a possible initial and final state for a material that exhibits positive magnetostriction [1].

The energy associated with magnetostriction for a polycrystalline material is defined as,

$$E_{me} = -\frac{3}{2}\lambda_p \sigma cos^2(\theta), \tag{2.3}$$

where E_{me} is the magnetoelastic energy, λ_p is the polycrystalline magnetostriction constant, σ is the stress, and θ is the angle between M_s and σ [1]. From this, we can see that when a stress is applied, the magnetization will want to rotate toward the stress to minimize the energy. If the magnetization and stress are already aligned, then this effect will produce a minimal change in the magnetization curve.

Figure 2.3 is what I would expect to happen to the magnetization if the applied stress is along the easy axis of a magnetic material with negative magnetostriction. The opposite would occur if the stress were applied perpendicular to the easy axis of the material. The concept behind the inverse magnetostrictive effect can be demonstrated by Figure 2.2 if the magnetic field(H) is replaced with a tensile stress. Therefore, if one elongated a material with a positive λ, then the magnetization would also increase, or the opposite for compression [1].

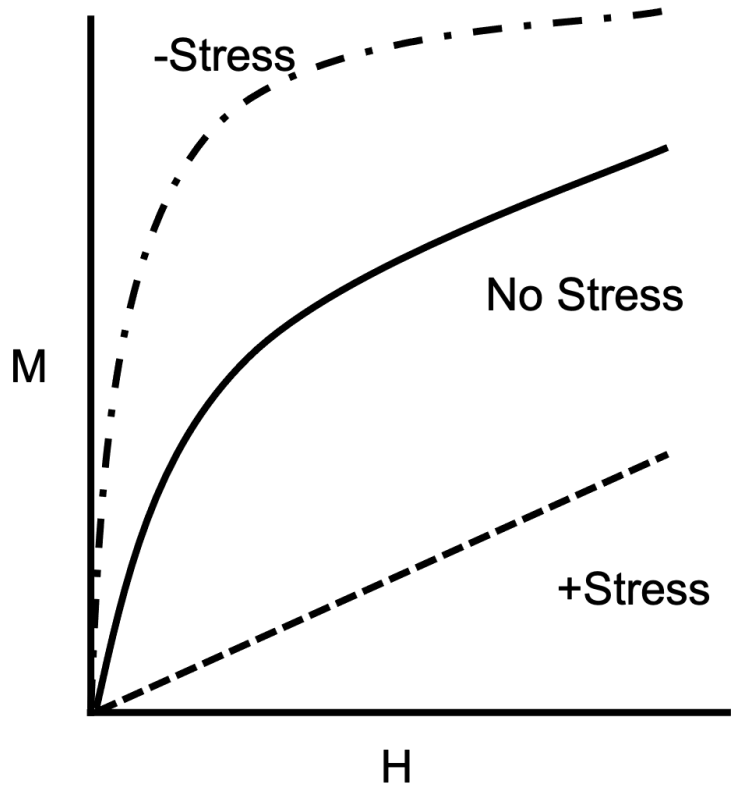

Figure 2.3 Inverse Magnetostrictive Effect: This shows representative changes in the magnetization due to applied stress if a material has a negative magnetostrictive ratio, like cobalt ferrite [1].

2.3 Dipole-Dipole Magnetic Chaining in Janus Nanofibers

Self-assembly of nanofibers into structured composites is a potential means to leverage their enhanced properties. Self-assembly methods include electric- and magnetic-field-assisted alignment and Langmuir-Blodgett film-formation [5, 6]. In particular, in magnetic-field-driven assembly, when a magnetic field is applied to a suspension of magnetic particles, their moments align with the external magnetic field and experience an attractive dipolar interaction. This kind of chaining has been studied extensively in nanoparticle systems [7, 8, 9, 10, 11, 12, 13, 14, 15]. One recent experiment studied the dynamic assembly of isolated clusters of ferromagnetic rods in aqueous solution at small fields ~ 1 mT [16]. One of the seminal experiments in this

field was conducted by Fermigier and Gast on paramagnetic latex nanoparticles [9]. Figure 2.4 shows typical chaining of Janus nanofibers.

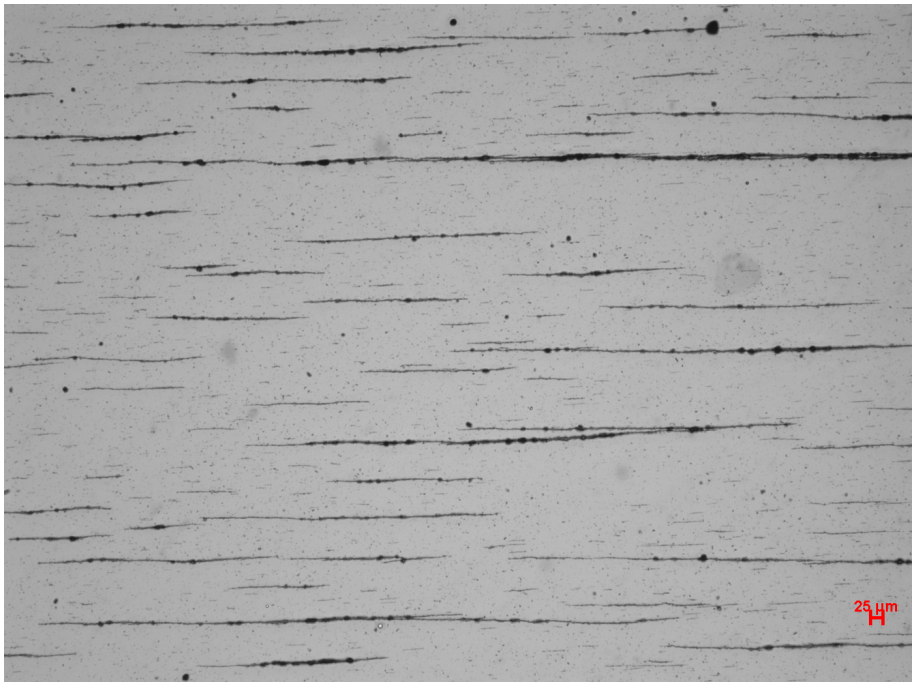

(a)

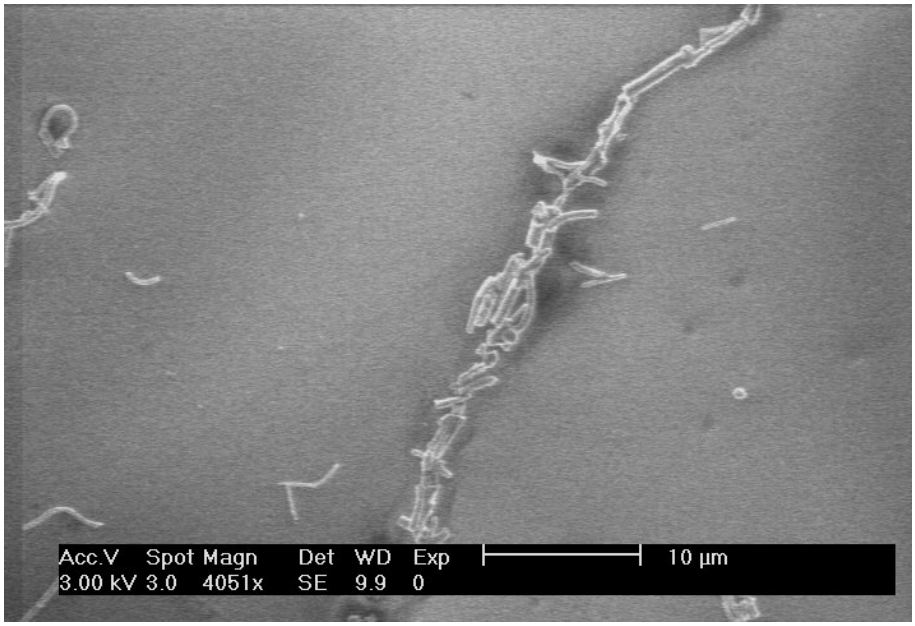

(b)

Figure 2.4 Nanofiber Chaining: Typical chaining of Janus nanofibers, a) under optical miscroscopy (1kOe) and b) SEM image of nanofiber chain.

2.3.1 Torque, Magnetic Energy and Diffusion

In the presence of an external field, a dipole will experience a torque and align parallel to the field. Magnetic nanoparticles and nanofibers can be approximated as idealized dipoles, which allows for simple calculations of how they respond to a magnetic force. Ferro/ferri-magnetic nanoparticles aggregate into chains both with and without an external magnetic field [16, 17], although in the absence of an external field, the nanoparticle chains tend to be randomly oriented with large angular dispersion. The torque produced by the external magnetic field on a magnetic dipole moment is,

$$\tau = \vec{m} \times \vec{H} = |mH|sin(\theta), \tag{2.4}$$

where $\vec{m}$ is the magnetic moment, and $\vec{H}$ is the external magnetic field [1]. Figure 2.5 shows a schematic of an idealized Janus fiber experiencing a torque due to an external magnetic field.

This attractive force will increase with the external magnetic field, and the dipoles will tend to align parallel to the field and each other, minimizing their energy, which is given by

$$U(R, \theta) = \frac{\mu_0 m^2}{4\pi R^3}(1 - 3cos^2(\theta)), \tag{2.5}$$

where μ_0 is the permeability of free space, R and θ are the distance and angle between the dipole centers, assuming one of the moments is parallel to the field, and m is the magnetic moment [3]. The moment is given by M(H)*V, where M(H) is the volume magnetization at a particular field and V is the particle volume. A schematic of this interaction is shown in Figure 2.6, which shows two magnetic nanoparticles in a uniform magnetic field.

The magnetic field of a fiber is spatially nonuniform, and a second fiber subjected to this spatial field gradient feels an attractive force that drives the fibers together and causes them to chain end to end [8, 9]. As the number of fibers increases, the number of chains and the length of those chains also increase. Chain length is ultimately

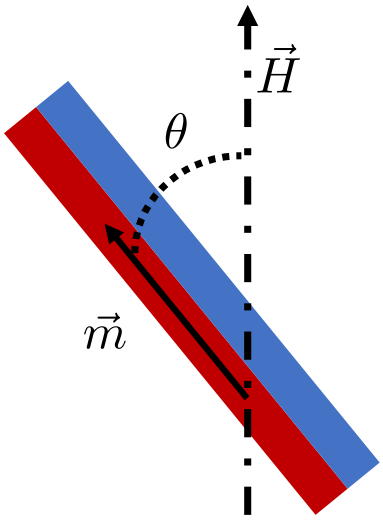

Figure 2.5 Torque on Janus Nanofiber: Torque on a Janus fiber due to an external magnetic field. Blue is $BaTiO_3$ and red with an arrow is the $CoFe_2O_4$, H is the external magnetic field and θ is the angle between the magnetic moment of the fiber and the external magnetic field.

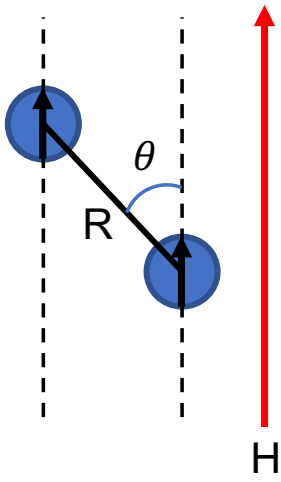

Figure 2.6 Dipole Interaction of Two Nanoparticles: Idealized magnetic nanoparticles interacting with each other and an external magnetic field.

limited by the number of available nearby fibers, i.e. the initial concentration, and the drag force (dependent on the chain's length) that a nearby chain experiences.

Diffusion limits chain length by limiting a chain's ability to travel and attract other fibers. For low Reynolds numbers, the diffusion of a sphere is described by the Stokes-Einstein equation, which can be adapted for rod-shaped particles. When this

is done, the parallel and perpendicular diffusion parameters are,

$$D_{\parallel} = \frac{kTln(l/d)}{2\pi\eta l} \tag{2.6a}$$

$$D_{\perp} = \frac{kTln(l/d)}{4\pi\eta l}, \tag{2.6b}$$

where k is Boltzmann constant, T is the temperature, l is the length of the fiber, d is the diameter of the fiber, and η is the viscosity [17, 18]. A chain's ability to diffuse decreases as the fibers aggregate, assuming a constant diameter, and as the viscosity of the solution increases, i.e. curing, thus slowing aggregation.

The previously described physics was combined with the Smoluchowski coagulation equation, and this led to diffusion-limited cluster aggregation for magnetic and ferroelectric nanoparticles [19]. In both experiment and simulation, nanoparticle chaining is well modeled using a dynamic scaling power law called diffusion-limited cluster aggregation(DLCA) [8, 9, 14, 17, 19, 10, 20]. DLCA describes how the average mass or length grows over time in a colloidal system. In DLCA, the power law exponents generally do not depend on either concentration or magnetic field, although this model has been reported to fail for larger particles with diameters ~ 1 μm [7].

For nanoparticle chaining, DLCA is applied by first determining the average chain length ($\langle L(t)\rangle$) and the weighted chain length ($\langle S(t)\rangle$) which are given as follows,

$$\langle L(t)\rangle = \frac{\sum\limits_{s} n_s(t)s}{\sum\limits_{s} n_s(t)} \tag{2.7a}$$

$$\langle S(t)\rangle = \frac{\sum\limits_{s} n_s(t)s^2}{\sum\limits_{s} n_s(t)s}. \tag{2.7b}$$

Here n_s is the number of chains with length s [20, 19, 17]. At long times, $\langle L(t)\rangle$ and $\langle S(t)\rangle$ follow dynamic scaling theory such that $\langle L(t)\rangle \sim t^{z'}$ and $\langle S(t)\rangle \sim t^{z}$. z′ and z are the dynamic scaling exponents for $\langle L(t)\rangle$ and $\langle S(t)\rangle$ respectively. They are normally assumed to be equal and independent of concentration and magnetic field strength. Fermigier and Gast observed a scale parameter, z′, of 0.5 with respect to

time and 4/3 for the magnetic field, as expected for diffusion-limited chaining [9]. For isotropic diffusion aggregation, the scaling factor has been reported to be ∼1.4 [14]. Miyazima *et al.* modeled both mass-independent and diffusion-limited chaining and found scaling parameters of z = 1 and z = 0.5, respectively [19].

Vicsek and Family developed a power scaling law for aggregation,

$$n_s \sim t^{-w} s^{-\tau} f(s/t^z), \tag{2.8}$$

where w is a scaling exponent that describes the reduction of n_s, τ is a static exponent that describes the relation between cluster size and cluster density, and the function $f(s/t^z)$ approaches 1 when $s << t^z$ and 0 for $s >> t^z$. At long times, Equation 2.8 simplifies to $n_s \sim t^{-w}$. Using this, a crossover parameter, $\Delta = w/z$, can be calculated, which helps in identifying the type of aggregation that is occurring. The crossover parameter is defined as,

$$\Delta = \begin{cases} 2 - \tau & CC \\ 2 & FC \end{cases} \tag{2.9}$$

where CC chaining, chain-chain, is dominated by chains aggregating with chains, and FC chaining, fiber-chain, is dominated by chains aggregating with "individual" fibers or small chains [7]. For diffusion-limited chaining, if $\Delta > 1$ then z = z′ and if $\Delta < 1$ then z′ =w [13, 11]. Erb *et al.* used the crossover exponent to analyze the chaining of 10 μm nonmagnetic particles in ferrofluids and found that the scaling exponents changed as a function of concentration and magnetic field. Following their approach, I used the three different scaling exponents and the crossover parameter extracted from optical images to characterize my system. The results of the magnetic chaining are described in Chapter 6.

Different types of chaining can happen, depending on the strength and concentration of the solution. The typical types of chaining that can occur are shown in Figure 2.7. At low concentration or low field strength, the particles will form small chains

with some isolated particles(Figure 2.7b-i.), i.e. FC regime. If the field is increased, then the particles will want to form more linear chains that are longer like in Figure 2.7b-ii, i.e. between the CC and FC regime. If the concentration is increased, then it will be preferential for the width of the chain to grow, but the additional chains will need to be shorter than the chain they are aggregating with [12], like Figure 2.7b-iii. Lastly, if both concentration and magnetic field are increased, then the solution will start cross-linking, where the chains will break and attach to each other, forming a more solid film. The CC regime of chaining happens in these last two conditions.

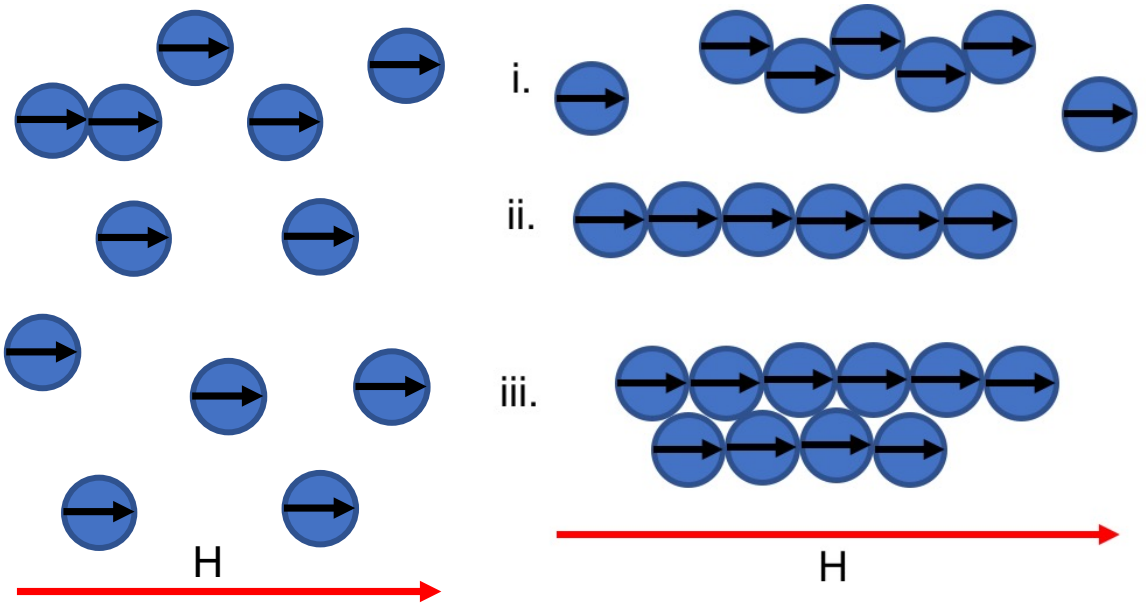

(a) (b)

Figure 2.7 Diagram of Chain Regime: a) is the initial state right after the magnetic field is turned on, b) are possible chaining configurations that can happen depending on the concentration and the strength of the magnetic fields.

Chapter 3

Multiferroic Materials

In this chapter, I will give an overview of multiferroic materials and the magnetoelectric effect. Multiferroic materials exhibit two or more "ferroic" properties, i.e. ferroelectrics, ferro/ferrimagnetics. Typical multiferroics show a combination of properties such as: magnetostriction, magnetocaloric, piezoelectric, and magnetoelectictricy [21]. Multiferroics are broken into two distinct types: single-phase and bi-phasic or composite. Single-phase multiferroics(i.e., $BiFeO_3$, $TbMnO_3$) have proven to be elusive because ferromagnetic and ferroelectric properties are inherently weak in a single material and typically need to be cooled below room temperature to exhibit multiferroicity [21, 22, 23, 24].

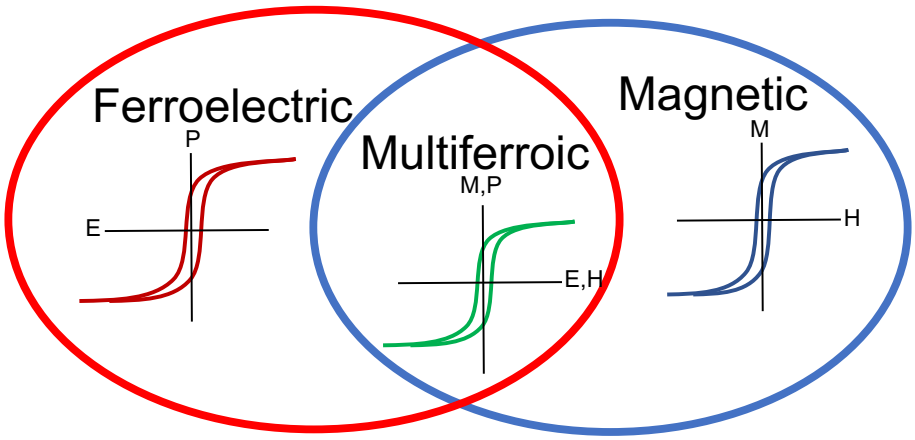

Figure 3.1 Relationship between Ferroelectrics, Magnetic and Multiferroic materials.

On the other hand, bi-phasic composite multiferroics couple piezoelectric and magnetostriction via interfacial strain and are not limited by the same factors [21]. Composite multiferroics take two different materials and "glue" them together, there-

fore artificially producing coupling. By combining two different materials with different intrinsic properties, one can make a composite that is coupled. Depending on the shape, geometry, and size of the material, their coupling can either improve or hinder the magnetoelectric effect [24]. Figure 3.1 shows the combination of properties that are exhibited by magnetic, ferroelectric, and multiferroic materials. Nanofibers have a larger area-to-volume ratio than thin films and are not affected by substrate clamping, leading to a predicted magnetoelectric coupling an order of magnitude higher than found in thin-film multiferroics [25, 26, 27]. Substrate clamping is where the material is restricted from expanding or contracting because the substrate is not elastic [21].

Multiferroic materials couple magnetic properties to electric properties, allowing for the control of magnetic properties with electric fields and vice versa. This versatility has led to an interest in using them in the fields of data storage, optical electronics, spintronics, and biomedical devices [21, 24, 28]. Multiferroic materials exhibit the magnetoelectric(ME) effect which conceptually is described in two ways,

$$\begin{aligned} \alpha_E &= \frac{\text{electric polarization}}{\text{strain}} \times \frac{\text{strain}}{\text{magnetic field}} &&= \frac{\Delta P}{\Delta H}, \\ \alpha_H &= \frac{\text{magnetization}}{\text{strain}} \times \frac{\text{strain}}{\text{electric field}} &&= \frac{\Delta M}{\Delta E}, \end{aligned} \tag{3.1}$$

where α_E is the magnetoelectric coupling induced by an external magnetic field, α_H is the opposite, P is the electric polarization, H is the magnetic field, M is the magnetization, and E is the electric field [21].

Bi-phasic multiferroics are typically made by deposition of thin films onto a substrate allowing for well-controlled nanoscale heterostructures [21]. Combining a magnetostrictive material like $CoFe_2O_4$ with a piezoelectric like $BaTiO_3$ produces an interface where strain in one component changes the intrinsic properties of the other [21, 24]. As explained in Chapter 2.2, magnetostriction is a property of ferro/ferrimagnetic materials where they will expand or contract in the presence of an

external magnetic field [1]. Piezoelectricity is a similar effect that happens when ferroelectrics are biased by an external voltage or electric field [29]. The connectivity in a composite multiferroic is important in predicting the strength of the magnetoelectric coupling [23]. Figure 3.2 shows typical connectivity, where 0 stands for 0-D objects(spherical nanoparticles), 1 is 1-D objects(rods, fibers), 2 is for 2-D objects(sheets, thin films), and 3 is for 3-D objects(bulk material).

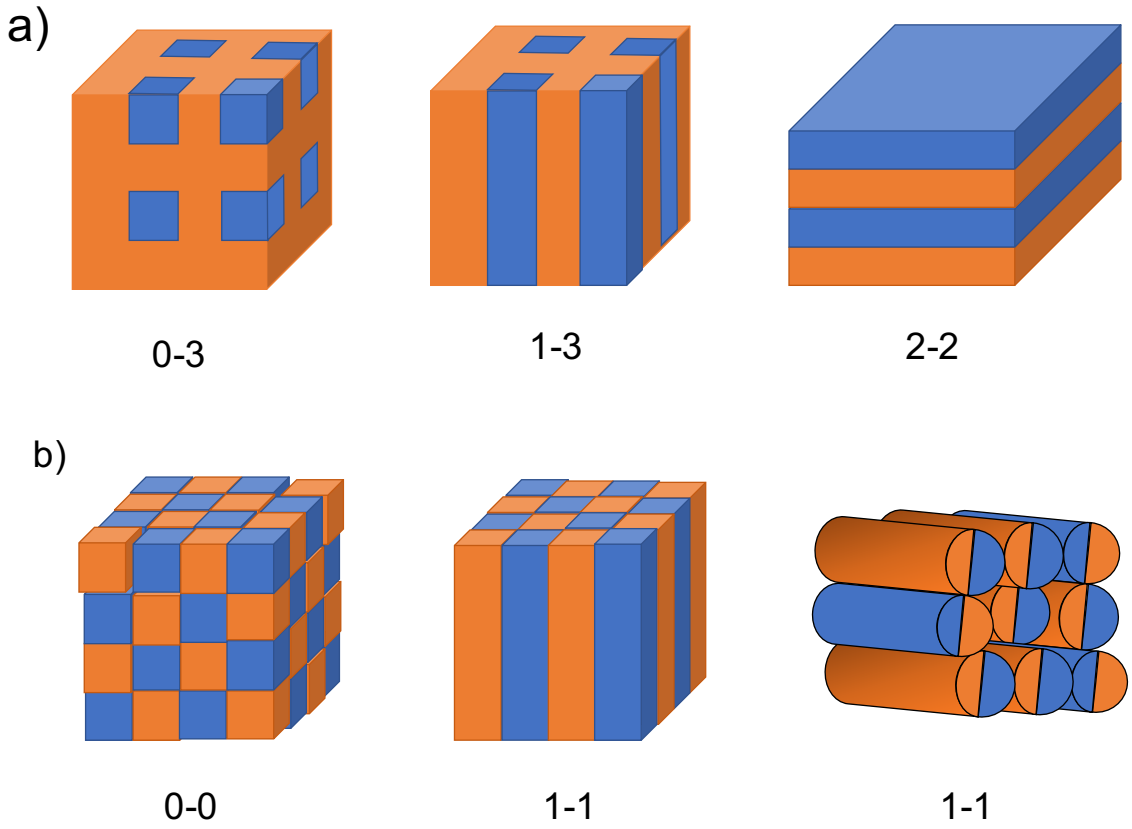

Figure 3.2 Composite Materials Connectivity: a) Typical connectivity made through thin film methods, b) are possible nanoscale connectivity where the bottom right 1-1 is the connectivity of our nanofibers [23].

Thin-film heterostructures, although easier to control, are limited to 0-3, 1-3, 2-2 connectivity which have lower predicted ME coupling [25]. Ideal nanocomposites will have 1-1 or 0-0, which correspond to Janus nanofibers or nanoparticles. For comparison, the current maximum magnetoelectric coupling for thin-film architectures with 2-2 connectivity is 5.6 V cm^{-1} Oe^{-1}, while nanofibers with 1-1 connectivity

have been reported to be 7.8 V cm^{-1} Oe^{-1} [28, 26]. Our collaborators measured a coupling (dE/dH) constant of 514±27 mV cm^{-1} Oe^{-1} on nanowire arrays [30]. Due to these properties, there has been a push to synthesize and characterize nanoscale multiferroic materials.

3.1 Magnetoelectric Effect

As presented in Equation 3.1, the magnetoelectric effect is defined by a change in either the magnetization or electric polarization of a material by either an electric field or magnetic field, respectively. The direct magnetoelectric effect (DME) constant, shown in Equation 3.2, has units of Volts per centimeter Oersted (V/cm-Oe), and the converse magnetoelectric effect (CME) constant, shown in Equation 3.3, is measured in units of Siemens per meter (s/m). The ME effect is further broken down into an AC and DC magnetic field regimes that see different responses. The AC ME effect will see a linear increase in the response, i.e. the measured voltage, with increasing AC magnetic field frequency [21]. Whereas when measured with a DC magnetic field, the ME effect response will be non-linear, typically butterfly loops, for the DC magnetic fields [24, 31]. At low DC magnetic fields, the ME effect can be assumed to be linear, but as the field increases this breaks down due to the non-linearity of magnetostriction [31, 32]. The DME and CME are as follows,

$$P_i = \alpha_{ij}^E H_j \tag{3.2}$$

$$\mu_0 M_i = \alpha_{ji} E_j \tag{3.3}$$

$$\alpha_{ij} = \epsilon_0 \epsilon_{ik} \alpha_{kj}^E, \tag{3.4}$$

where P is the electric polarization, M is the magnetization, H and E are the magnetic and electric fields, μ_0 is the magnetic permeability, ϵ_0 is the electric permittivity, ϵ_{ik} is the relative permittivity, α_{ij} is the linear magnetoelectric coefficient due to the electric field and α_{ij}^E is the linear magnetoelectric coefficient due to the magnetic

field [24, 32]. It should be noted that there is disagreement in the literature about whether the CME and DME are equivalent [21, 32].

To calculate the strain-mediated ME effect for bi-phasic composites, the strain tensor is needed [24]. The strain-mediated magnetoelectric effect is defined using the stress tensor as follows,

$$\varepsilon = \mathbf{S}\sigma + \mathbf{d}E + \mathbf{q}H \tag{3.5a}$$

$$D = \mathbf{d}\sigma + \boldsymbol{\kappa}E + \boldsymbol{\alpha}H \tag{3.5b}$$

$$B = \mathbf{q}\sigma + \boldsymbol{\alpha}E + \boldsymbol{\mu}H, \tag{3.5c}$$

where $\mathbf{S}$ is the elastic compliance, $\boldsymbol{\kappa}$ is the dielectric permittivity, $\boldsymbol{\mu}$ is the magnetic permeability, $\boldsymbol{\alpha}$ is the intrinsic magnetoelectric coefficient, $\mathbf{d}$ is the peizoelectric coefficient, $\mathbf{q}$ is the piezomagnetic coefficient, σ is the stress, and ε is the strain, D is the electric displacement, and B is the magnetic induction [21]. Zhang *et al.* simplified this for a fiber with 1-1 connectivity, aligned and poled in the same direction(x_1). In this case, Equation 3.5 changes as follows,

$$\varepsilon_1 = S_{11}\sigma_1 + d_{k1}E_k + q_{k1}H_k \tag{3.6a}$$

$$D_i = d_{i1}\sigma_1 + \kappa_{ik}E_k \tag{3.6b}$$

$$B_i = q_{i1}\sigma_1 + \mu_{ik}H_k. \tag{3.6c}$$

The intrinsic magnetoelectic coefficient, α, is dropped because cobalt ferrite(CFO) and barium titanate(BTO) do not have intrinsic magnetoelectric coupling. The direct magnetoelectric coupling is now defined as,

$$\alpha_{ik} = -\frac{d_{i1}q_{k1}}{S_{11}}. \tag{3.7}$$

Thus, for composite multiferroics, the magnetoelectric coupling is transferred by piezoelectric and magnetostrictive properties. Zhang *et al.* calculated the magnetoelectric coupling of lead zirconate titanate(PZT) and CFO nanofibers compared to

their thin-film counterparts [25]. Their calculation predicts a magnetoelectric coupling an order of magnitude higher than their thin-film counterparts [26, 33, 34, 35].

Janus particles consist of two materials with equal volumes that are fused together such that they have a uniform planar interface. For nanofibers and nanoparticles, this means each material looks like a hemi-cylinder and hemisphere, respectively. An idealized diagram of a Janus nanofiber is shown in Figure 2.5. It draws its name from the Roman god Janus, the god of transitions, and duality, who had two heads placed back to back. Multiferroic Janus nanofibers have been created by a few groups [34, 33], including through electrospinning, a technique which will be described in Section 4.1.

Multiferroic Janus nanofibers are typically made from sol-gel solutions of ferroelectric BTO or PZT combined with CFO. These materials are chosen because of their high values of magnetostriction and piezoelectricity, and because the tetragonal perovskite(BTO) and cubic spinel(CFO) structure encourages self-segregation and produces better interfaces [34]. Jones *et al.* studied how the orientation of the BTO and CFO crystal structure affects the ME coupling in these materials. They rewrote Equation 3.7 as,

$$ME(\theta) = \lambda_{hkl} \bullet e^*_{333}(\theta), \tag{3.8}$$

where $ME(\theta)$ is the magnetoelectric coefficient, λ_{hkl} is the saturation magnetostrictive strain, and $e^*_{333}(\theta)$ is the piezoelectric coefficient in an arbitrary orientation(θ) [36]. This brought to light that the magnetoelectric effect might not always occur along the same direction, as it is electrically or magnetically poled. Therefore, it is important to measure the coupling in multiple directions, i.e. with electric and magnetic fields parallel and perpendicular to each other.

In thin-film multiferroics, the magnetoelectric effect can be measured using a lock-in technique, pulsed magnetic field, vibrating sample magnetometer(VSM), SQUID magnetometry, and dielectric property measurements [31]. The most widely used measurement technique is the lock-in technique, where a magnetoelectric voltage(MEV)

is measured across the sample as the frequency of an AC magnetic field is increased [37]. This measurement has inherent difficulties due to leakage currents, induced voltages, and erroneous resonance signals [21]. VSM and SQUID measurements are limited by the space to attach electrodes to the sample [34]. Capacitance and PvsE hysteresis are typically used to confirm that a material is a multiferroic, but few studies use it to observe the ME coupling [31].

A few techniques have been developed to measure the magnetoelectric coupling in nanoscale multiferroics: lock-in technique, scanning probe microscopy(SPM), and magneto-optical Kerr effect(MOKE) [31, 26, 35, 27]. The issue with all these measurements is that they obtain local measurements, like with the SPM techniques, or observe a global average, i.e. lock-in technique. MOKE has the pitfall of generally needing a smooth surface to get a good signal, which is not typically the case for nanoparticle systems. New techniques for measuring nanoscale multiferroics that are reliable and transferable to multiple systems are needed.

Chapter 4

Experimental Techniques

4.1 Sample Preparation

Our Janus nanofibers consist of two hemi-cylinders produced by simultaneously electrospinning sol-gel solutions of $BaTiO_3$ (62% mass) and $CoFe_2O_4$(38%) [34]. Electrospinning is a versatile manufacturing process that can produce large amounts of nanofibers quickly. The process extrudes a polymer solution through an electrically charged syringe tip and accelerates it toward a grounded collection plate. The typical potential difference between the syringe and collection plate is $\sim$10 kV [34]. The nanofiber diameter can be tuned by adjusting the solution viscosity, syringe voltage, and distance to the collection plate. This same process can also be used to make nanoparticles, using a process called electrospraying. Electrospinning produces an as-spun mat of fibers that is not very useful in measuring the magnetoelectric effect or assembling the fibers into a functional device. To produce bi-phasic Janus fibers, the electrospinning setup is adapted to include two syringes that combine the two materials into a single fiber [23]. Because $CoFe_2O_4$ is a cubic spinel and $BaTiO_3$ is a perovskite, their crystal structure encourages them to self-segregate, producing an interface for strain mediation [34]. Our collaborators made our nanofibers at the University of Florida in the lab of Dr. Jennifer Andrew. A schematic of the electrospinning process is shown in Figure 4.1.

To suspend the fibers in solution, they are first ground with a mortar and pestle. The ground-up nanofibers have various lengths but an average diameter of

~800nm [34]. The nanofibers are coated with citric acid, and the pH of the solution is raised to ~10 to improve colloidal stability using 0.1M NaOH. Polyvinyl alcohol (PVA) is dissolved into the solution to increase viscosity with the ratio of 0.25 g PVA to 10 mL DIW. The citric acid, NaOH, and PVA improve the colloidal stability, but sedimentation happens after ~45 minutes due to the nanofibers' size and the CFO's magnetization. I found that this fiber/PVA/water solution produced the most consistent fiber sample out of the solutions attempted. The general procedure to produce the nanofiber solutions is shown in Appendix C.

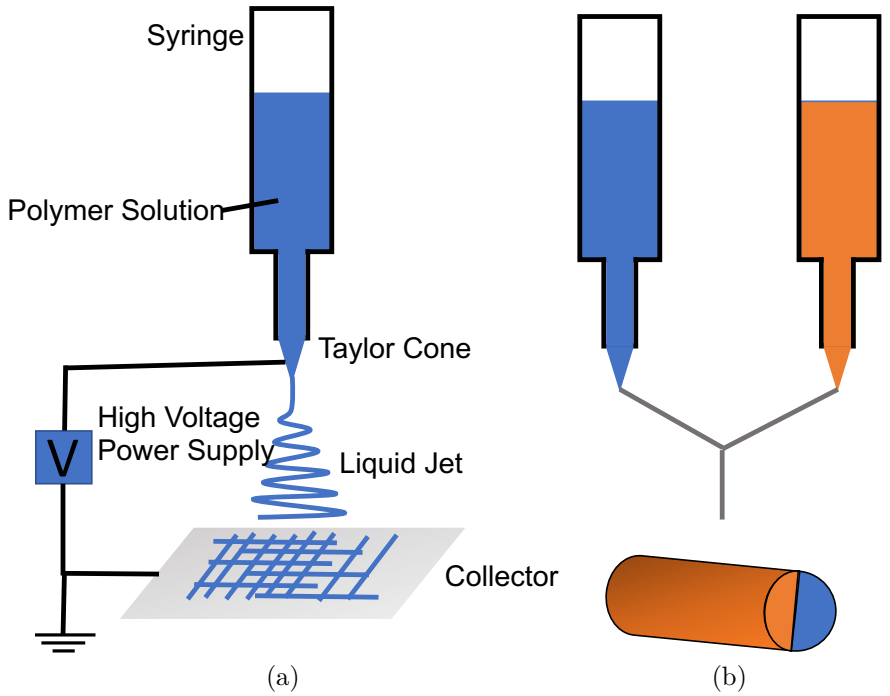

Figure 4.1 Electrospinning Diagram: a) Basic setup for electrospinning and b) Biphasic electrospinning setup.

To make a self-assembled fiber sample, a tip sonicator (2 minutes at 50% Amplitude) is used to re-suspend the fibers and then the solution(typically $\sim 25 - 50\mu$L) is spin-coated or drop-cast on clean glass slides. The sample is placed in an electromagnet or on top of three bar magnets to air cure in a magnetic field. Three different types of glass substrates were used: clean glass wafers(VWR VistaVision^{TM} Cover

Glasses), Indium Tin Oxide(ITO) coated glass, and glass coated with interdigitated gold(Au/Ti) electrodes.

For the magnetic chaining study, three different concentrations of fibers (0.25, 0.18, 0.083 mg/mL) and a range of magnetic fields were used to measure how they affect nanofiber chaining. As the PVA/water/fiber solution air cures in the magnetic field, an *in situ* microscope takes a 10 minute video of the chaining dynamics. After the sample is fully cured, the sample is then imaged with another microscope to obtain a final nanofiber chain length measurement.

For the magnetoelectric chaining setup, a Hele-Shaw [38] fluid cell was built with conductive ITO coated glass, which can apply an electric field perpendicular to the plane of the magnetic chaining. The PVA/water/fiber solution is sealed in a 120 μm hydrophobic well with a diameter of 9 mm. Once the sample is sealed, it is placed in a static magnetic field produced by either two bar magnets(200 Oe) or an electromagnet incorporated into a microscope. The initial Hele-Shaw sample setup is shown in Figure 4.2a. Although initially the measurement seemed to indicate magnetoelectric coupling, subsequent measurements showed electroplating of the ITO and electrochemical interaction above 25 kV/m. To remedy this, a dielectric coating was added to the surface of the ITO to mitigate these effects, initially Kapton tape($\sim$25μm) and then $\sim$1μm of polymethyl methacrylate (PMMA). The 950 PMMA A9 (MicroChem) was spin coated onto the ITO glass slides at 5000 rpm and then baked in an oven at 170°C for 30 minutes. This produced a uniform thin film of PMMA with a thickness of 1.078$\pm$0.11 μm. The thickness was checked by doing a scratch test with a profilometer. This was essential, because without it the top ITO glass slide would become completely metalized, similar in appearance to a mirror. This final sample setup is shown in Figure 4.2b. Once the sample is made, it is placed in the microscope/electromagnetic setup, and alligator clips are attached so that both an electric

and magnetic field can be applied simultaneously using computer-controlled power supplies. The control code is in Appendix E.

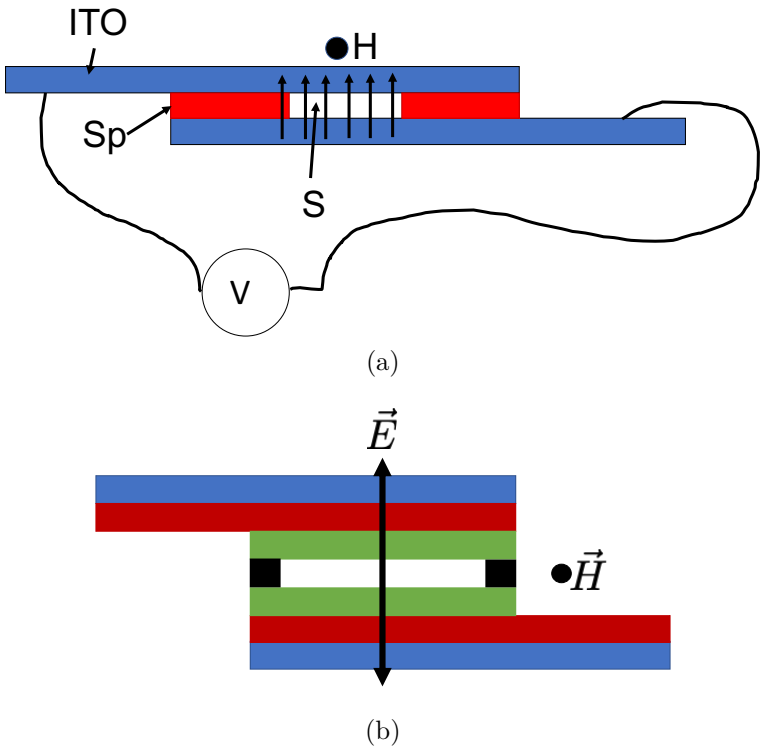

Figure 4.2 Hele-Shaw Setups: a) the sample(S) is sitting between two ITO glass slides which have a spacer(Sp) of 120 μm. The magnetic field is coming out of the page and electric field is perpendicular to the magnetic field. b) Hele-Shaw Setup Mark II: Two ITO coated microscope slides(blue and red), Passivation layer PMMA(green), and 125 μm spacer (black).

Two different sample geometries were produced for the magnetoelectric magneto-optical Kerr effect (MEMOKE) samples: parallel plate capacitors and coplanar electrodes. First, a parallel plate capacitor setup is made in a very similar way to the magnetoelectric chaining setup already described. The main difference between the two setups was that instead of a 120 μm space, the cured sample(fiber/PVA) was the spacer, and the sample was fully air-cured before the top ITO glass slide was attached. This method allows for higher electric fields to be applied with lower voltages. The top ITO glass slide was held in place with PMMA(950 PMMA A9) and a small bead of super glue around the edges. Wires were then attached to the ITO

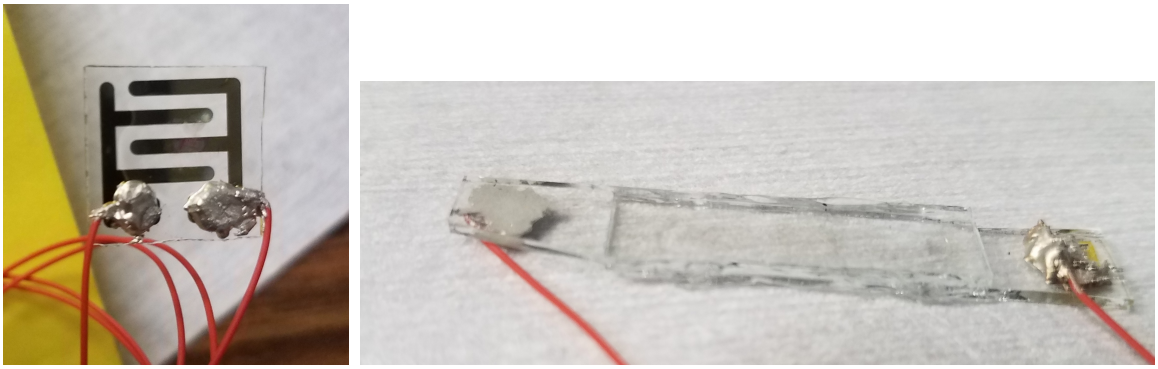

(a) (b)

Figure 4.3 Picture of Test Samples for MOKE: a) test sample of coplanar electrode(interdigitated capacitor) setup and b) a parallel plate sample.

slides using silver epoxy, and the whole sample was placed in the ScMOKE setup. A picture of a parallel plate sample can be seen in Figure 4.3b.

The second MOKE sample setup used coplanar electrodes, either straight electrodes or interdigitated, made by depositing thin films of Cu or Au onto glass slides. The thickness of the electrodes was between 150 and 200 nm. The thin films were deposited either by magnetron sputtering (interdigitated electrodes) or e-beam evaporation (straight electrodes). After the fibers are cured on the electrode, wires are connected to provide the voltage. Care was taken to avoid shorting between the electrodes. After fabrication, the sample is placed in the MOKE setup. A test coplanar setup can be seen in Figure 4.3a.

4.2 Chaining Video Analysis

4.2.1 Magnetic Chaining Video Setup

To measure chaining *in situ* a microscope was incorporated into an electromagnet as shown in Figure 4.4. The real-time measurements were taken with a Canon Rebel T2i EOS 550D over 10 minutes, with 24 frames per second. The videos were spliced into frames 5 seconds apart and processed with the NIH software ImageJ [39]. The

video consists of 1920x1080 pixels^2 with RGB color scale, and covers an area of 2991.36x1620.32μm^2. For this magnification, one pixel was approximately equal to the fiber diameter, making it difficult to account for the smallest fibers but not hindering measurement of the length distribution. After the samples were air-cured, they were imaged separately to obtain the final length and angular distribution.

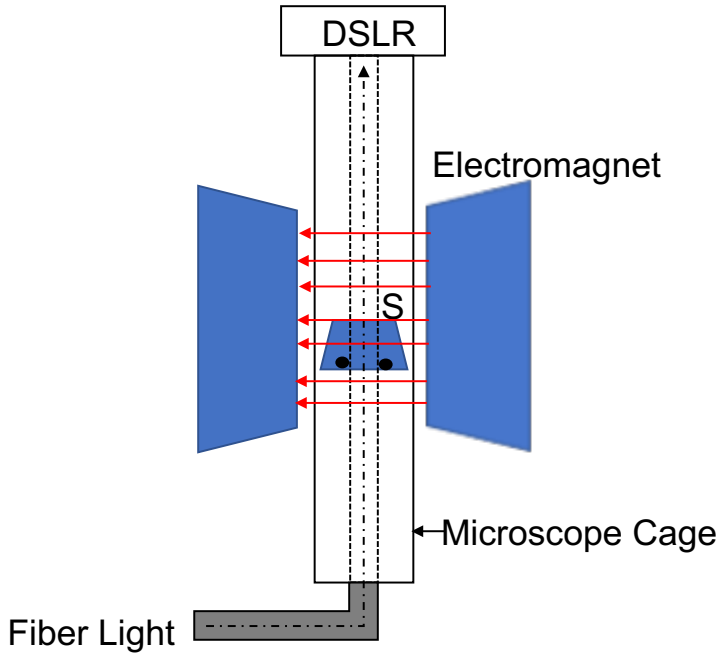

Figure 4.4 *In Situ* Microscope: S is the PVA/water/fiber sample sitting in a sample holder between the electromagnet poles. The microscope cage contains all of the microscope's optical elements, and the DSLR camera is secured above the microscope cage.

Post-curing grayscale images were taken in bright-field with a Nikon Eclipse LV150 microscope using a 5x Plan Fluor objective and a CCD camera(QImaging Exi Aqua, Monochrome) with an area of 1392x1040 pixels^2, i.e. a field of view of 1795.68x1341.6μm^2. To ensure consistency, the images are taken at the center of the sample where it takes the longest time to cure. Again, the images are processed using ImageJ [39]. I used thresholding to separate the fibers from the background. The image is then smoothed to limit noise due to small particles and optical artifacts. The

thresholded pictures are compared with the original image. A representative sample of the chaining images and its thresholded counterpart is shown in Figure 4.5a-b.

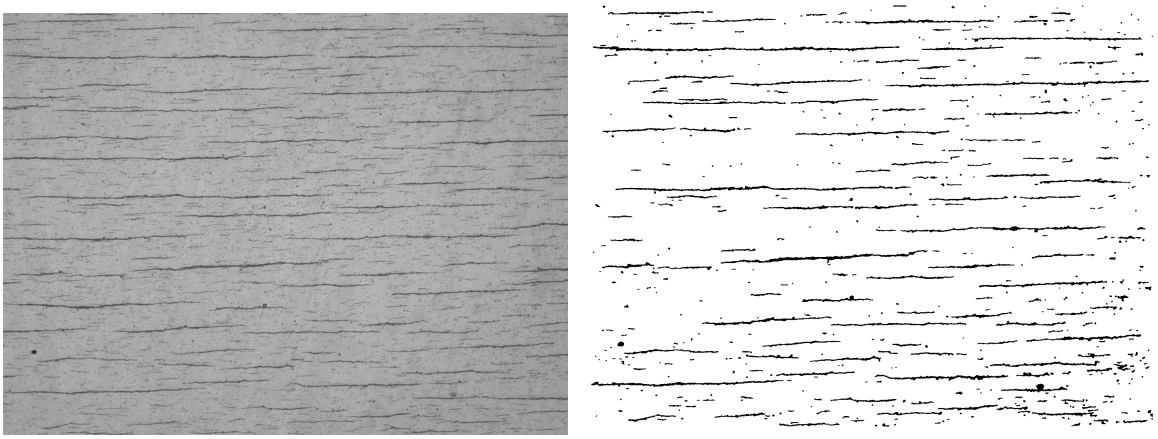

(a) Original Image (b) Thresholded Image

Figure 4.5 Original and Thresholded Nanofiber Images: a) Shows the chaining original image at 1000 Oe and b) shows the threshold image with filtered out background and fibers that touch the edges.

4.2.2 Magnetoelectric Chaining Video Setup

For the magnetoelectric chaining setup, electromagnetic coils were incorporated into an existing Nikon Eclipse LV100 microscope. The real-time measurements were taken with a 10x Plan Fluor objective(Dark-Field) and a CCD camera(QImaging Exi Aqua, Monochrome) with an area of 1392x1040 pixels^2, i.e. a field of view of 890.8x665.5μm^2. The Hele-Shaw cell samples were held in-place by a vacuum in the center of the microscope's objective field of view. The applied magnetic field and voltage were monitored and controlled by a computer which allowed for seamless control of the experiment. The videos were 45 minutes long, with a frame rate of 1 frame per second. As before, everything was processed with ImageJ [39]. This setup brought a couple of advantages over the old system, namely that the videos could be significantly longer, and the image quality was better. The drawbacks were that the system needed

continuous monitoring during a run due to focus drift, and it could not reach as large a magnetic field.

4.2.3 Image Analysis

After the images or videos were taken, they were loaded into ImageJ, properly sliced, scaled to the correct dimensions, and timestamps were applied to the images. The following procedure was used for image analysis and was derived from an existing procedure created by Domínguez-García *et al.* [40].

Image Analysis Procedure:

1. Increase Image Contrast
2. Apply Kuwahara Filtering
3. Apply Smoothing
4. Find Edges
5. Invert Image
6. Apply Otsu Thresholding
7. Convert to Binary
8. Fill holes
9. Erode
10. Visual Check with original
11. Analyze Particles

Kuwahara filtering was used because it preserves the position and sharpness of the edges of a chain. Otsu thresholding is a method to find objects in an image, and it is particularly good for nanoparticles and nanofibers [11]. To confirm this, I processed

the same image with different thresholding algorithms and found the Otsu produced the best results for our samples. The summary graph is shown in Figure 4.6. As our eyes are often still the best image analysis tools after a video has been processed, I watched and compared the videos with the original to make sure it was not picking up any optical anomalies. Optical anomalies can be anything from scratches, air bubbles, or dust particles that fall into the image during a run. At the lowest fields, large clumps (not chains) of fibers can form that produce a lot of scattered light which distorts the image contrast. This particular part of the image analysis was very time consuming, especially if ImageJ picked up some optical anomaly that was not actually in the video or if the chains were large enough that it could not detect the smallest chains. If this did happen, the video was processed again but with slightly different cutoff thresholds.

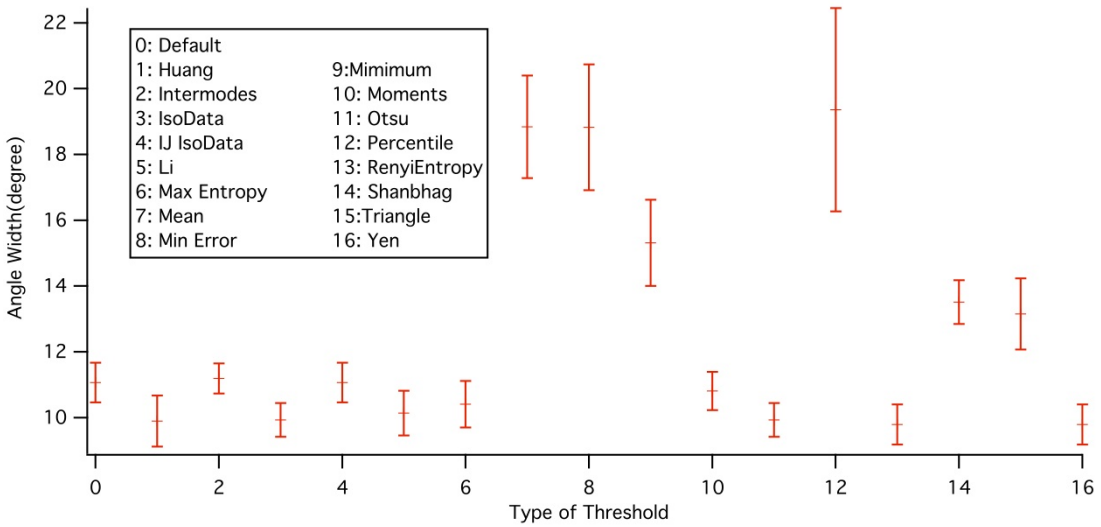

Figure 4.6 Types of Thresholding: Dispersion of results with different thresholding methods. Otsu produced the most consistent results.

ImageJ's particle analysis and directionality subroutines were used to obtain chain length, orientation, and angular dispersion. The angular dispersion is the standard deviation of the Gaussian distribution of fiber orientations. The particle analysis works by fitting an ellipse around the thresholded particles, and the program obtains

the length, width, orientation, and other relevant user-defined parameters. This allows us to measure how well-aligned the chained fibers are with respect to the field. The real-time chaining videos are processed in the same way, except that n_1 is also extracted. n_1 is the number of smallest or "individual" fibers in an image. n_1 is more difficult to extract since our fibers are of various lengths, but we focus on the smallest fibers with an aspect ratio less than 2. These particles are the smallest building blocks of chains, and thus n_1 should decrease with time as the average chain length increases. The experiment was repeated at least three times at each field to ensure that the data were consistent and to average out optical abnormalities. After the image and video data are extracted, the data are fit at long times to obtain the scaling parameters. The data are explained in Chapter 6 but representative graphs are shown in Figure 4.7. The ImageJ macros can be found in Appendix D.

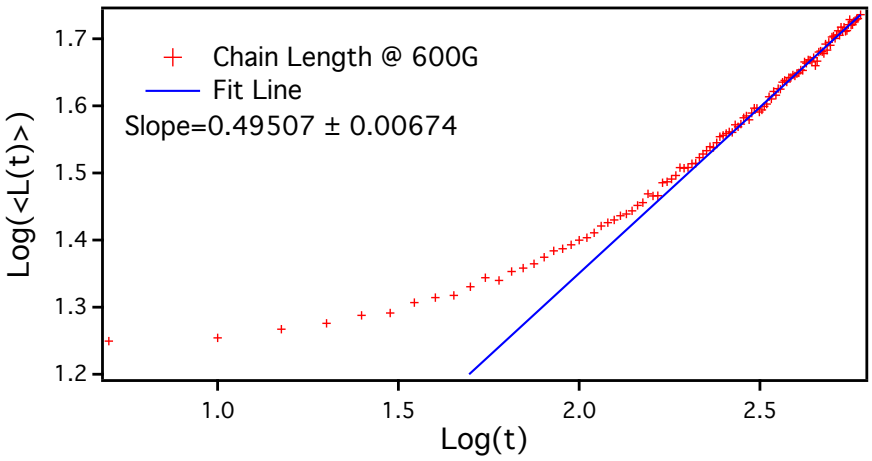

(a)

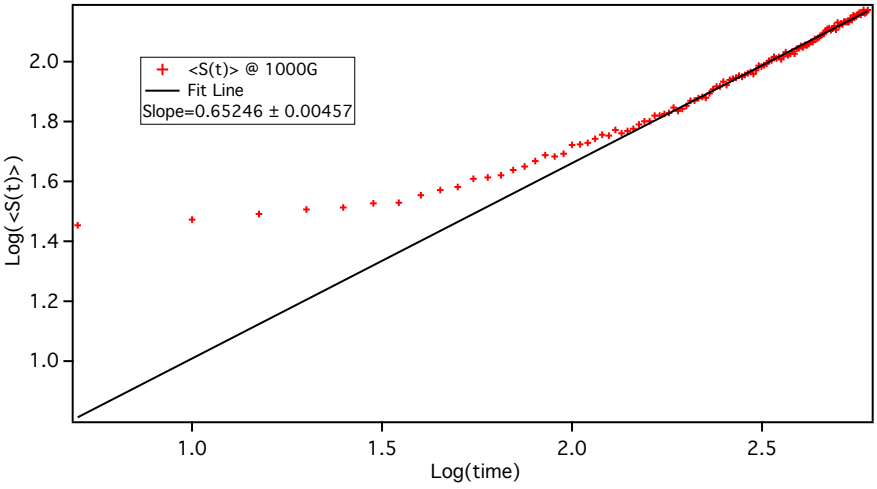

(b)

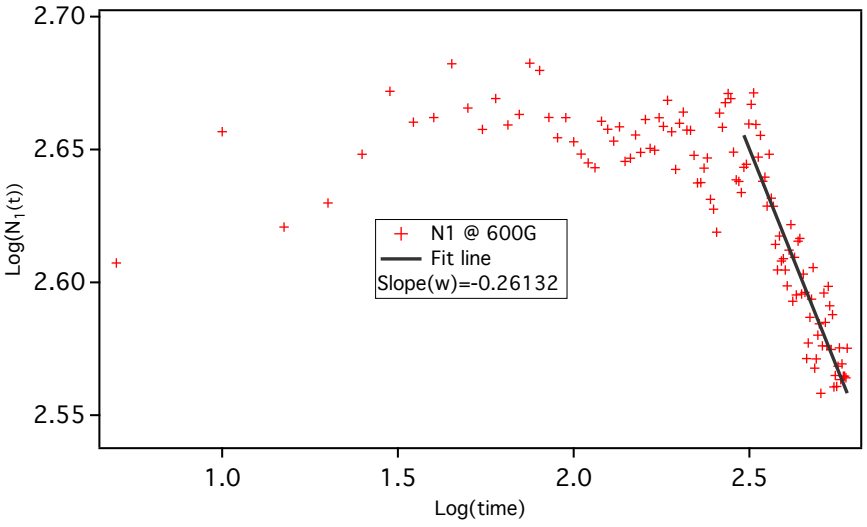

(c)

Figure 4.7 Typical Chaining Data Graph: This is what the extracted data from the videos typically looked like for the three scaling parameters. a) z′, b) z, and c) w.

4.3 Magneto-optical Kerr Effect (MOKE)

The Magneto-optical Kerr effect is an optical effect where the linear state of polarization changes when reflected from a magnetic material. The effect was discovered by John Kerr when he reflected polarized light off the surface of a polished bar magnet [41]. This effect is geometrically dependent with three distinct orientations: Longitudinal(LMOKE), Transversal(TMOKE), and Polar(PMOKE). The different geometries for MOKE are shown in Figure 4.8.

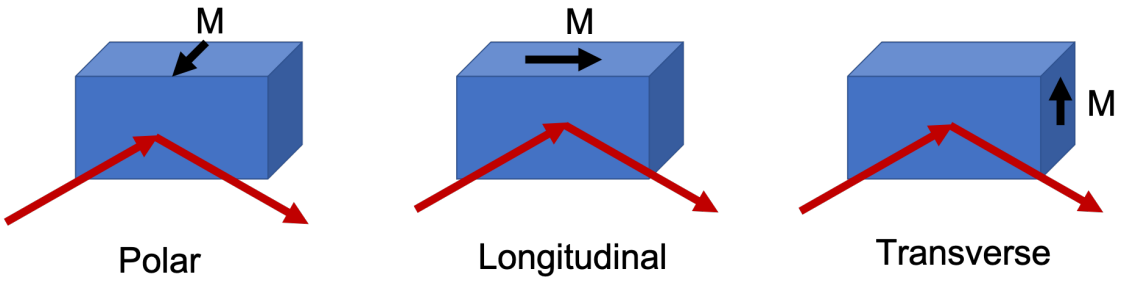

Figure 4.8 Types of MOKE Geometries: This shows the difference in the direction of the magnetic moment for different MOKE types [42].

MOKE can be further broken down in accordance with the polarization direction of the incident light. The polarization of light is defined as: $\hat{s}$ polarization which is perpendicular to the plane of incidence, and $\hat{p}$ polarization which is parallel to the plane of incidence [41, 43]. In our experiment, $\hat{s}$ is normal to the surface of the optical table, and $\hat{p}$ is parallel to the surface of the table. Combining these polarizations and the magnetic geometries, six different outcomes can be deduced using the Lorentz force. MOKE in its most basic form can be thought of as an extension of the Lorentz force,

$$\vec{F} = -q(\vec{v} \times \vec{B}) \tag{4.1}$$

where $\vec{F}$ is the induced force, q is the charge of the particle, $\vec{v}$ is the velocity of the particle, and $\vec{B}$ is the magnetic field [3]. The polarized light induces the surface electrons to vibrate as a function of the electric field and when in the presence of the

magnetic field, will bend so $q\vec{v}$ can be replaced with the electric field. The magnetic field can be replaced with the induced magnetization(M_{ind}) which is dependent on the applied magnetic field. Thus leading to following,

$$\hat{F} \sim \vec{E} \times \vec{M_{ind}}. \tag{4.2}$$

Using the right-hand rule, one can infer the direction of the Kerr rotation. The rotation diagrams for the longitudinal and transverse geometries are shown in Figure 4.9.

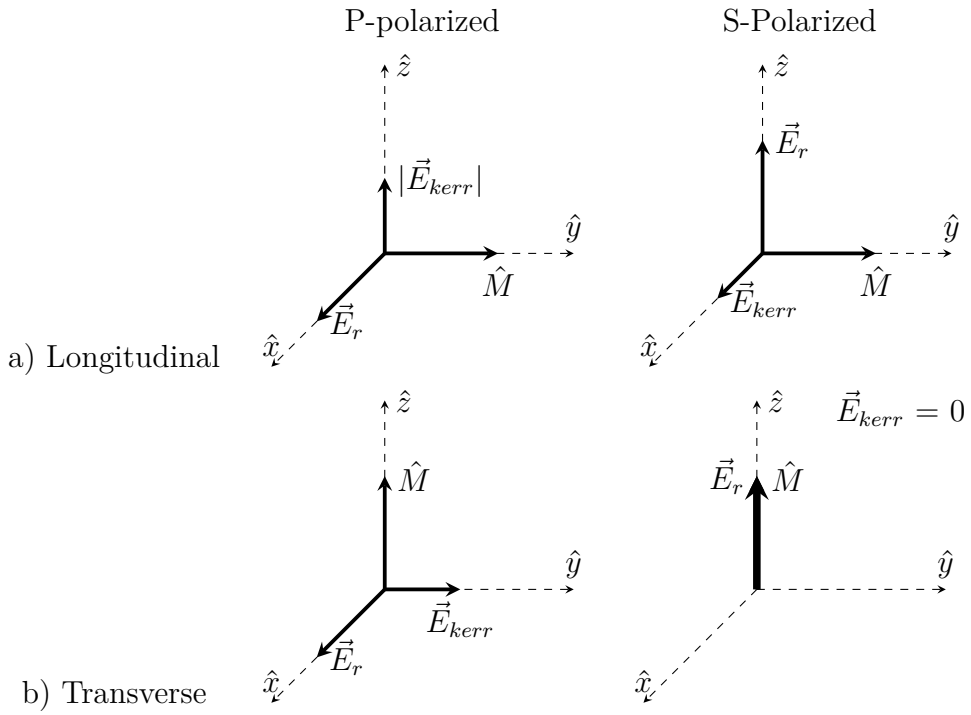

Figure 4.9 Kerr Rotation Diagram: This shows the possibilities for how the light will rotate with $\hat{M}$ being the direction of the magnetization, $\vec{E}_r$ the initial polarization of light, either $\hat{s}$ or $\hat{p}$, and $\vec{E}_{Kerr}$ the induced Kerr rotation. The new polarization is a linear combination of $\vec{E}_r$ and $\vec{E}_{Kerr}$. The Kerr rotation is deduced by taking the cross product of the incident polarization and the direction of the samples magnetization.

Now to mathematically describe this change, I will use Stokes vectors and Mueller matrices. Fundamentally, this formalism works using basic matrix multiplication to find the final state of a wave, where light is represented as a vector($\vec{S}$) and optical

elements are matrices(M). Thus for a generalized setup, if you want to find the final state of polarization then the following happens,

$$\vec{S}_f = M_3(M_2(M_1\vec{S}_i)),$$
$$\vec{S} = \begin{pmatrix} I \\ Q \\ U \\ V \end{pmatrix}, \tag{4.3}$$

where $\vec{S}_f$ is the final state, M_n is an optical element, $\vec{S}_i$ is the initial polarization, and I, Q, U, and V define the state of polarization. The Stokes parameters are defined as follows,

$$\begin{aligned} I &= \text{Total Intensity of Light} && = \langle E_x\rangle^2 + \langle E_y\rangle^2, \\ Q &= \text{Difference in Intensity of Linearly Polarized Light} && = \langle E_x\rangle^2 - \langle E_y\rangle^2, \\ U &= \text{Difference in Intensity of Linearly Polarized Light at } 45^\circ && = \langle E_a\rangle^2 - \langle E_b\rangle^2, \\ V &= \text{Difference in Intensity of Circular Polarized Light} && = \langle E_l\rangle^2 - \langle E_r\rangle^2, \end{aligned} \tag{4.4}$$

where $\langle E_n\rangle^2$ is the intensity of light, and the subscripts denote the coordinate system: Cartesian basis$(\hat{x}, \hat{y})$, Cartesian but rotated $45^\circ(\hat{a}, \hat{b})$, and circular basis$(\hat{l}, \hat{r})$ [43]. For $\hat{p}$ polarization Q equals 1 and $\hat{s}$ polarization happens when Q equals -1, assuming I equals 1. U is related to the off axis rotation of linearly polarized light from $\hat{s}$ and $\hat{p}$, i.e. Kerr rotation. V is related to the ellipticity if the light becomes circularly polarized, i.e. Kerr ellipticity [43].

I know the incident light is linearly polarized, for simplicity $\hat{p}$ polarized and that the reflected light rotates by some small degree. This quantity can be approximated using the ellipticity and rotation equations in Kliger, Lewis, and Randall along with a small angle approximation [43],

$$\begin{aligned} \epsilon = tan(\frac{1}{2}sin^{-1}(\frac{V}{I})) &\approx \frac{1}{2}\frac{V}{I} \rightarrow \frac{V}{I} = v = 2\epsilon_k \\ \theta = \frac{1}{2}tan(\frac{U}{Q}) &\approx \frac{1}{2}\frac{U}{Q} \rightarrow \frac{U}{Q} = u = 2\theta_k \end{aligned} \tag{4.5}$$

where ϵ is the ellipticity, θ is the Kerr rotation, and I and Q equal 1 due to the polarization state. The Kerr rotation and ellipticity are $\pi/2$ out of phase, so to account for this the ellipticity picks up a negative sign. This makes our incident and reflected light equal to the following,

$$\begin{aligned} \vec{S}_{incident} &= \begin{bmatrix} 1 \\ 1 \\ 0 \\ 0 \end{bmatrix} \\ \vec{S}_{reflected} &= \begin{bmatrix} 1 \\ 1 \\ 2\theta_k \\ -2\epsilon_k \end{bmatrix}. \end{aligned} \tag{4.6}$$

After the light is reflected off of the sample, it will pass through a Photoelastic Modulator(PEM) which retards the phase of the light at a set frequency such that the polarization state oscillates between circularly polarized to linearly polarized. By adjusting the type of retardation, for us it is half-wave retardation, one can use a lock-in amplifier to measure either circularly polarized light or linearly polarized light. For my setup, this means that I can use the PEM as a higher frequency(2f=84kHz) optical chopper. After passing through the PEM, the light passes through a polarizer which for these calculations is set at +45 degrees. The Mueller matrices for our optical elements are as follows,

$$M(A)_{PEM} = \begin{bmatrix} 1 & 0 & 0 & 0 \\ 0 & 1 & 0 & 0 \\ 0 & 0 & cos(A) & sin(A) \\ 0 & 0 & -sin(A) & cos(A) \end{bmatrix} \tag{4.7}$$

$$M_{pol} = 0.5 \begin{bmatrix} 1 & 0 & 1 & 0 \\ 0 & 0 & 0 & 0 \\ 1 & 0 & 1 & 0 \\ 0 & 0 & 0 & 0 \end{bmatrix}. \tag{4.8}$$

With these equations, the final state of the polarization can be calculated and thus predict the measured voltages that I can expect to observe. Note, $M(A)_{PEM}$ is time dependent, where A is equal to $A_0 sin(\omega t)$.

$$S_f = M_{pol}(M(A)_{PEM}\vec{S}_{reflected}) = \begin{bmatrix} 0.5 + cos(A)\theta_k - sin(A)\epsilon_k \\ 0 \\ 0.5 + cos(A)\theta_k - sin(A)\epsilon_k \\ 0 \end{bmatrix} \tag{4.9}$$

The first line of the vector is what can be measured and with simple rearrangement and small angle approximation the following can be said about the signals,

$$\begin{aligned} \theta_k &= \frac{\sqrt{2}}{4J_2}\frac{V_{2f}}{V_{DC}} \\ \epsilon_k &= \frac{\sqrt{2}}{4J_1}\frac{V_{1f}}{V_{DC}}, \end{aligned} \tag{4.10}$$

where V_{DC} is the DC signal, V_{1f} is the signal from the set frequency of the PEM, V_{2f} is voltage at the second harmonic frequency, and J_n is a Bessel function. It is evident from this that to measure the Kerr rotation signal I must measure the second harmonic frequency. The big advantage of using a PEM is that it allows for the measurement of both the ellipticity and Kerr rotation simultaneously. The PEM also

reduces noise that is sometimes observed when using a regular optical chopper. It also allowed me to measure at a frequency well beyond any resonance points. For a complete explanation of MOKE, see the following references [41, 44, 42].

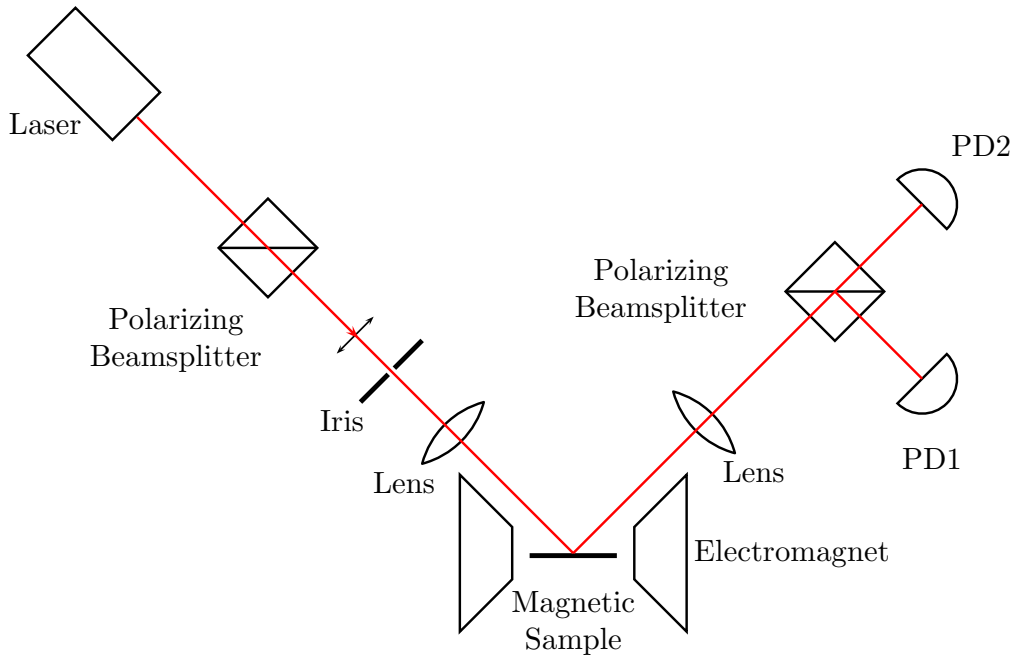

Figure 4.10 Basic LMOKE setup: Starting with the laser, the light is polarized then focused onto a sample between the poles of an electromagnet. The light reflected from the sample is focused again and split with a polarizing beamsplitter allowing for differential detection with two photodetectors. An optical chopper or PEM is also typically incorporated into a MOKE setup for phase sensitive detection.

In practice, to set up a MOKE experiment, the basic way to measure changes in polarization involves measuring the signal from two cross polarizers, i.e. 90 degrees rotated from each other. If the polarizers are perfectly crossed, then the detector will pick up a signal if the polarization rotates due to the sample. To do this, the laser light is first polarized and then reflected from a magnetic sample that is sitting in an electromagnet. When the polarized light is reflected, it will rotate as the electromagnet sweeps the external magnetic field to magnetize the samples. Either a PEM or an optical chopper can be used to modulate the light. Typically, two

photodetectors are also used so that differential detection and better signal-to-noise ratio can be obtained [45]. Figure 4.10 shows a basic MOKE setup.

4.4 Scattered MOKE (ScMOKE)

Scattered MOKE (ScMOKE) is a technique that was developed in collaboration with my colleague Dr. Cory Dolbashian [46, 47]. Here I will give a brief overview of the technique. ScMOKE takes advantage of the fact that our samples produce off-specular light. The polarization of the off-specular light can be measured at set fixed angles. For the typical aggregate diameter of 1-5 μm, the scattered light is Mie scattering instead of Rayleigh. When the wavelength of light(794 nm) is similar to the diameter of a cylinder(1 μm), the regular specular law of reflection does not apply, and Mie formalism is needed [48]. Dolbashian found the MOKE signal to likely be an admixture of both LMOKE and PMOKE due to whole fiber illumination, as shown in Figure 4.11.

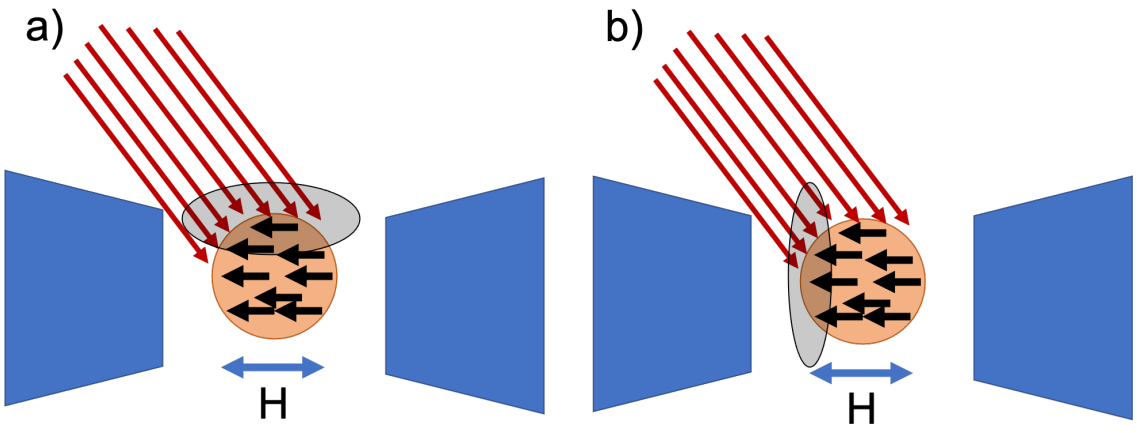

Figure 4.11 Top Down View of ScMOKE Setup: a) LMOKE contribution and b) PMOKE contribution [47].

Only off-specular, scattered light is detected, which reduces the background signal from the substrate that can obscure the MOKE signal. Using the Mie scattering formalism, we find that over our angle measurement range (40-60° from the normal)

there is a nonzero Mie scattering amplitude [46]. In the specular MOKE geometry, the MOKE signal is only nonzero at one angle, i.e. law of reflection, whereas the Mie signal is nonzero at most angles which allows us to measure MOKE with the Mie signal [46].

Much of the ScMOKE setup is the same as the typical MOKE, with a few exceptions. The collection lens collimates the off-specular light, and a quarter-wave plate balances the signals for differential detection. Additionally, a HINDS PEM is used instead of an optical chopper. Finally, since I am measuring how an applied voltage changes the MOKE signal, I have to monitor the voltage continuously. A complete diagram of my setup can be seen in Figure 4.12. The data are taken using a lock-in amplifier and then recorded using an oscilloscope, which significantly increases the number of averages that could be done. The oscilloscope also significantly reduced the time to collect data.

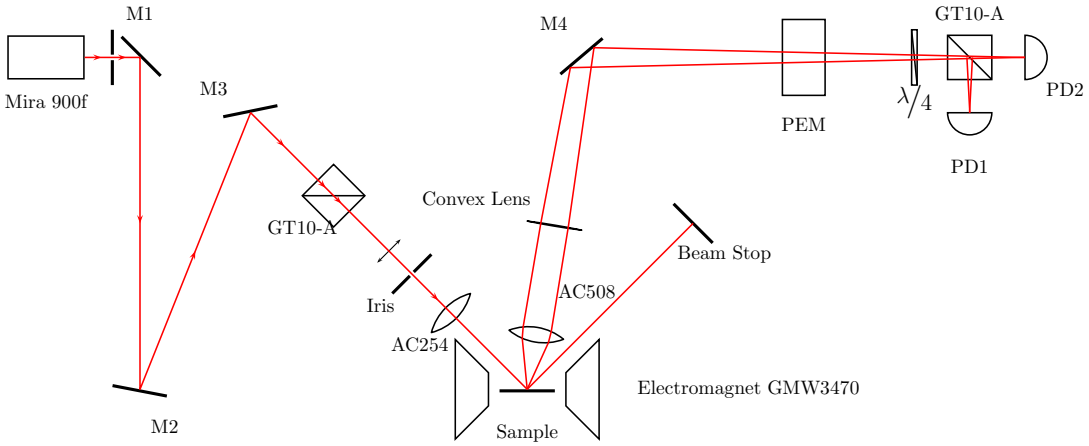

Figure 4.12 ScMOKE Optical Schematic: ScMOKE setup which was used to take all the data in this section. Note for the Parallel-plate capacitor data an optical chopper was used in place of Photoeleastic Modulator (PEM). M# are mirrors, GT10-A is a Glan-Taylor polarizing beamsplitter, and PD1 & PD2 are photodetectors. The PEM 2nd harmonic frequency is 84kHz.

The MOKE signal needs to be averaged to reduce noise, and typical MOKE runs involved 100-500 averages, which significantly reduced the noise as shown in Figure 4.13. Occasionally, the software that controls the electromagnet would get out of sync with the oscilloscope, a problem solved by measuring the voltage. Therefore, the voltage measurements served the dual purpose of counting the number of runs and monitoring the voltage. The voltage measurement can be seen in Figure 7.1 where each run had an average of 200 runs at a set voltage. The total number of runs was usually reduced by a few runs due to missed triggers or the magnetic fields not lining up from run to run. Shifts in the magnetic field were solved by taking the average of a few good runs and then thresholding out the shifted magnetic field runs if they deviated from the average by more than 2-3 standard deviations. Some typical averaged ScMOKE runs can be seen in Figure 4.14

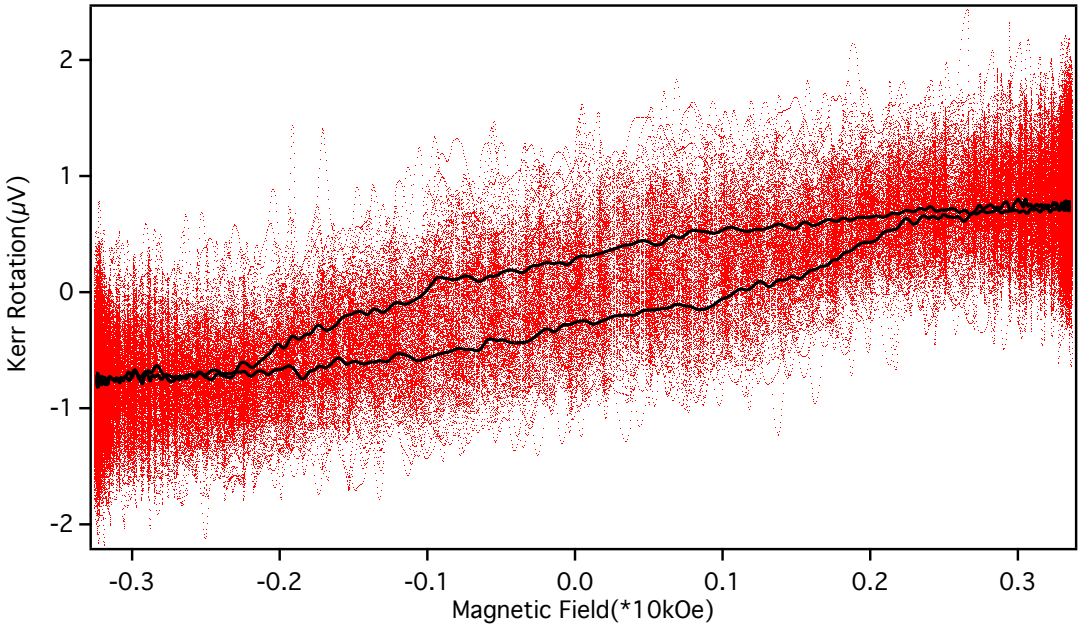

Figure 4.13 ScMOKE Run: This is a test run on a nanofiber with 200 averages. The black line is the averaged run and the red dots are data from individual runs demonstrating significant reduction in noise by averaging, as expected.

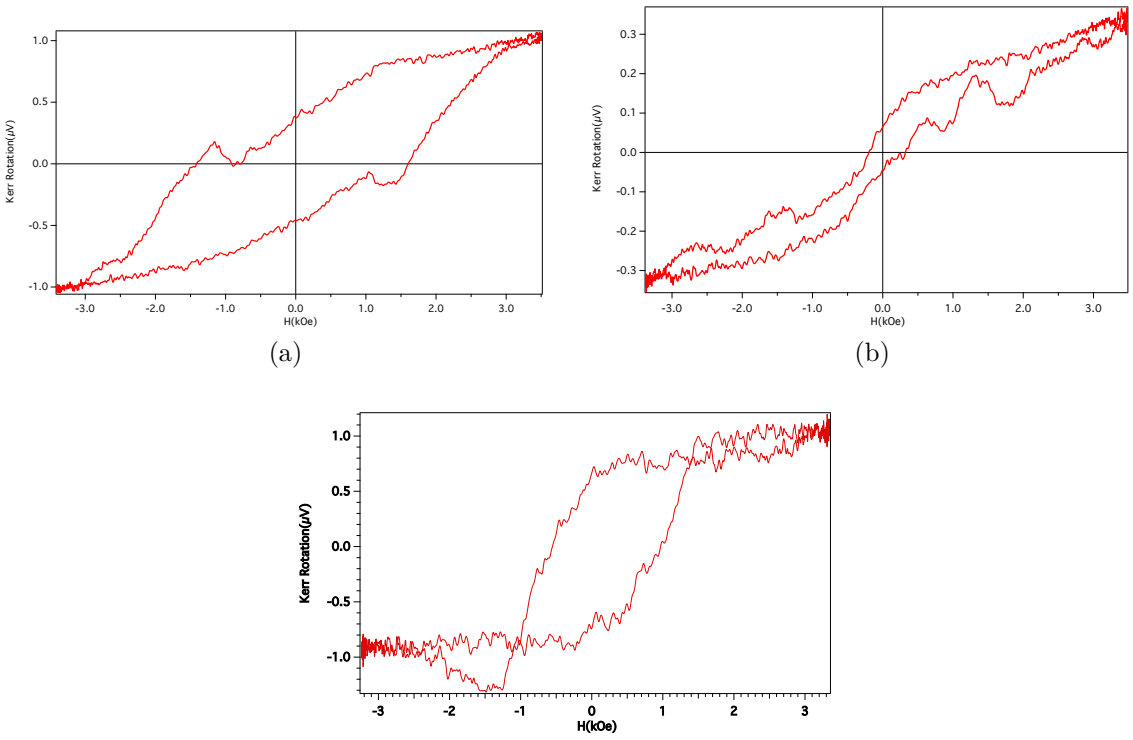

Figure 4.14 Typical ScMOKE Loops: all samples are aggregate chains with fibers oriented parallel to the substrate surface and pointed along the $\hat{s}$ direction with respect to the incident plane. a) and b) show pinched hysteresis loops common in CFO, suggesting these are good candidates for a FORC study. The pinching indicates phase mixing between the ferroic phases due to the synthesis method, c) is another typical loop that is more square [49].

It was originally hypothesized that ScMOKE could only be measured if the fibers were oriented in the $\hat{s}$ direction because it produced the most amount of scattered light. I distrusted this hypothesis, so I measured a fiber oriented in the $\hat{p}$ direction, i.e. parallel to the table, to confirm that the fibers needed to be oriented in a specific way. As can be seen in Figure 4.15b, this hypothesis was incorrect, and as a result, Dr. Dolbashian went back and found from the Mie scattering equation that there was not a significant difference between the two orientations [46]. The overall loop shape is more square in the $\hat{p}$ orientation, suggesting that the easy axis is along the nanofibers' length as we believed. To confirm that the PEM was working as expected,

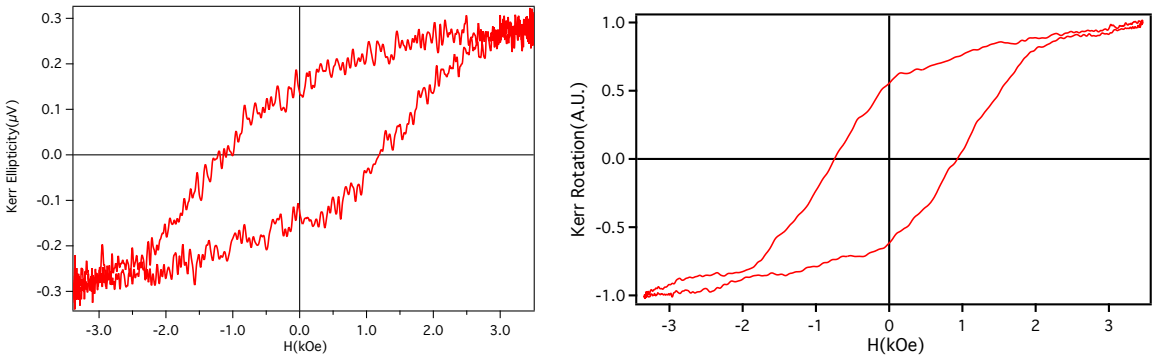

(a) (b)

Figure 4.15 ScMOKE Ellipticity and Rotation for a $\hat{p}$ direction nanofiber: a) Ellipticity component of a nanofiber agglomerate that is oriented parallel to the substrate surface and pointed along to the $\hat{s}$ direction with respect to the incident plane, b) ScMOKE for a nanofiber agglomerate pointed in the $\hat{p}$ direction with respect to the incident plane. It shows a slightly more rectangular magnetization curve, suggesting a possible easy axis exists along the fibers' long axis.

the ellipticity of a regular agglomerate was measured and is shown in Figure 4.15a. Data obtained using ScMOKE is shown in Chapter 7, and the analysis code is shown in Appendix F. Some reference MOKE and Janus data is in Appendix A, including a voltage frequency test which showed some promise.

4.5 Vibrating Sample Magnetometry (VSM)

Vibrating Sample Magnetometry (VSM) is a common way to measure typical magnetic parameters, including magnetic saturation, coercivity, remanence, and blocking temperature. A VSM works by measuring the *emf* induced in pick-up coils by vibrating a sample between them. Figure 4.16 shows the basic setup for a VSM [1]. The amplitude of the induced voltage can be used to extract a sample's magnetic moment when compared to a known sample. Hysteresis curves can be obtained as well as the temperature dependence of the sample's magnetization. The major limitation of VSM is the samples need to be small and in some nonmagnetic carrier. A Quantum Designs PPMS® with a VSM attachment was used to perform these measurements.

The samples for this were fiber samples immobilized in a polymer, which was done by a student in Dr. O. Thompson Mefford's lab at Clemson University. The sample and brass sample holder can be seen in Figure 4.17. VSM was used for the Janus fiber samples to answer two questions: 1) What are the fiber's magnetic saturation, coercivity, and remanence; and 2) What does the magnetization versus temperature curve look like. I am interested in the temperature curve because, as will be shown later in Chapter 5, BTO undergoes a structural phase change at a set temperature that causes a stress-induced shift in the magnetization of the CFO.

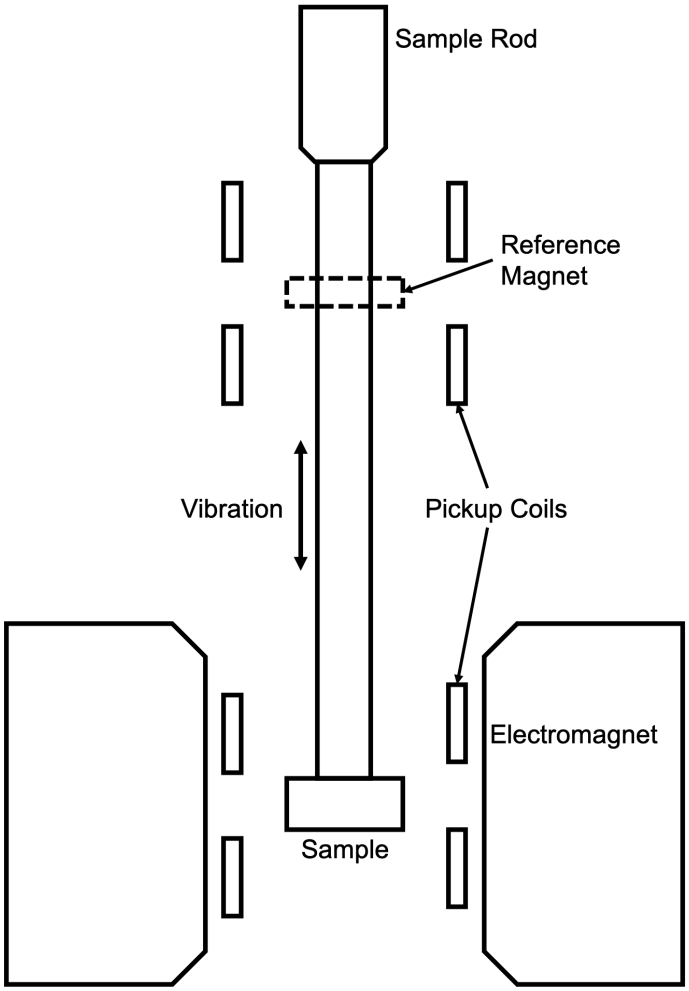

Figure 4.16 VSM Setup: This shows a basic VSM diagram [1].

(a) (b)

Figure 4.17 VSM Samples: a)VSM sample next to a diamond scribe and b) sample placed in the brass VSM sample holder.

4.6 First Order Reversal Curve (FORC)

Before FORC was widely used, an experiment was performed by Ferenc Preisach to study the magnetic after-effect, which is the delay between the measured magnetization strength and the external magnetic field. This experiment laid the foundation for FORC [50, 51]. He treated the system as consisting of single domain, square hysteresis loops with a distribution of coercivities, and non-zero loop centers. The magnetization is then measured while sweeping out a major hysteresis loop (MHL) from $\pm$ H_{max} and minor loops at evenly spaced intervals (ΔH_r), as shown in Figure 4.18a. From this data, Mayergoyz was able to obtain "Preisach Diagrams" by taking the mixed derivative shown in Equation 4.11 [52]. This type of analysis is predicated on two conditions: the congruency of minor loops and the "wiping-out" property, i.e. minor loops should perfectly close after one cycle. Multiparticle magnetic nanoparticle systems typically violate these conditions due to inhomogeneities in their interparticle spacing, variable sizes, inconsistent coercivities, or different interaction field strengths.

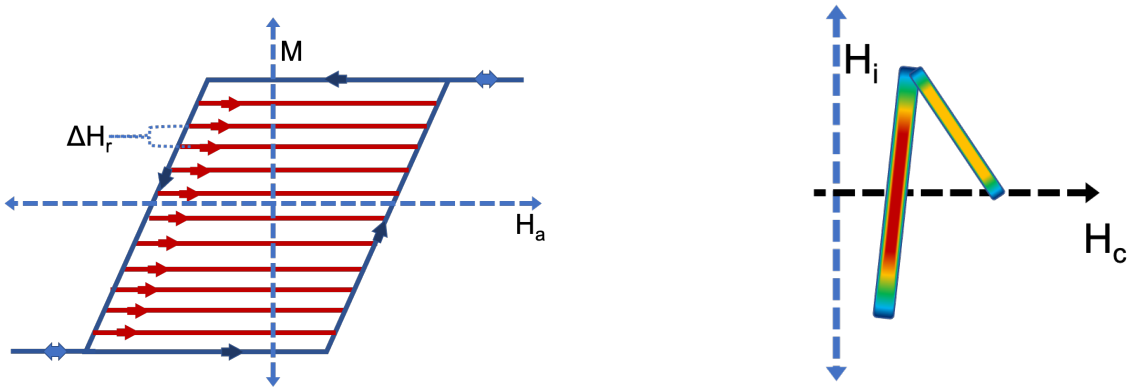

(a) FORC Curve (b) FORC Diagram

Figure 4.18 FORC Curve and Diagram: a) family of FORC curves obtained with either MOKE or VSM, b) characteristic "wishbone" often seen in FORC diagrams of arrays of magnetic materials. This is similar to what Dr. Cory Dolbashian found for our fibers [55, 56, 47].

The modern FORC technique was pioneered by Robert Pike to characterize magnetic rock samples and was extended beyond the limitations placed on the system by Preisach [53]. Pike was able to measure samples with known morphology and predict their corresponding FORC diagrams. This work spurred an expansion of FORC studies in both the geological and magnetics communities.

While typical VSM measurements have the inherent drawback of missing small magnetic changes in the system, FORC tries to remedy this problem by sweeping out minor loops from equally spaced reversal fields (H_r) to $+H_{max}$ [54]. This allows FORC to measure smaller changes in magnetization due to individual interacting particles or fibers. In FORC, a family of minor reversal curves fill in the space encapsulated by the major reversal curve, as shown in Figure 4.18a.

From this family of curves, a FORC diagram can be produced by taking the 2nd derivative of the hysteresis loops to produce a FORC distribution as shown in Figure 4.18b. The FORC distribution is defined as,

$$\rho_{FORC} = -\frac{1}{2}\frac{\partial^2 M}{\partial H_a \partial H_r}, \tag{4.11}$$

where H_a is the applied magnetic field, H_r are the reversal fields, and M is the magnetization [57]. FORC's resolution is limited by the number of reversals performed and the time it takes to measure them. For example, in my FORC runs I did 150 reversals. If the data varies smoothly, this ends up being a relatively simple double partial derivative. However, real systems must contend with noise that is amplified by the 2nd derivative. For MOKE FORC, this necessitates averaging each reversal many times to reduce noise before data processing and smoothing can proceed.

The interaction field (H_i) causes shifts in the center of the peak, which allows us to see how changes in the physical system affect the magnetic distribution. The coercivity field axis (H_c) shows us how the coercivity, half the width of the hysteresis loop, changes through the system of different Janus nanofibers due to particle size and mean-field interactions. The interaction and coercive fields, as labeled in Figure 4.18b, are defined as,

$$H_i = \frac{1}{2}(H_a + H_r) \tag{4.12}$$

$$H_c = \frac{1}{2}(H_a - H_r), \tag{4.13}$$

where H_i is the interaction field, H_c is the coercive field, H_a is the applied field, and H_r is the reversal field. FORC formalism dictates this coordinate transformation from H_a and H_r to H_i and H_c. While I have not finished the FORC diagram analysis, two families of curves were obtained on a fiber at two different voltages(0, 25 V). The noise hindered my ability to render a FORC diagram. While the 25 V FORC curves show a splitting in the reversal curves shown in Appendix B, a future FORC study of these fibers at multiple applied voltages is needed.

Chapter 5

Vibrating Sample Magnetometer Data

To confirm the coupling between the BTO and CFO phases, their magnetization was measured as a function of temperature in a VSM. Above 120°C (393.15 K), BTO is stable in a cubic phase but, when cooled, it undergoes a structural phase change to tetragonal. Below 5°C (278.15 K), BTO's crystal structure is orthorhombic and then rhombohedral below -90°C (183.15 K) [58]. These structural phase changes provide a basic route to confirm that the Janus nanofibers are coupled before doing other measurements. The Janus nanofibers were suspended and cured in polystyrene-divinyl benzene, which cures as a hard polymer similar to glass. The samples are cut to fit into the brass VSM sample holder and held in place with double-sided Kapton tape. The sample is then placed in the VSM attached to a Quantum Design PPMS®. First, a major hysteresis loop(H_{max}=± 4 Tesla) is taken, and then the sample is heated to 400 K and slowly cooled while measuring the magnetization. Figure 5.1 shows a smooth temperature dependence.

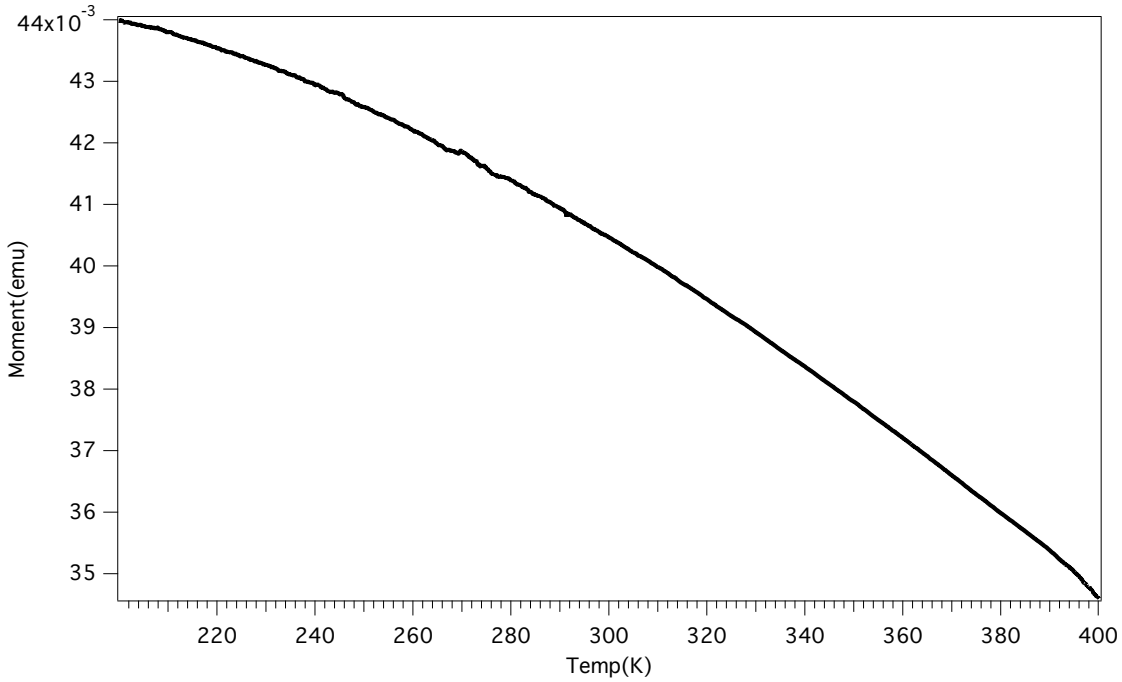

Figure 5.1 MvsT on Janus Nanofibers: Magnetic moment dependence vs. temperature to detect shifts in the moment arising from phase transitions.

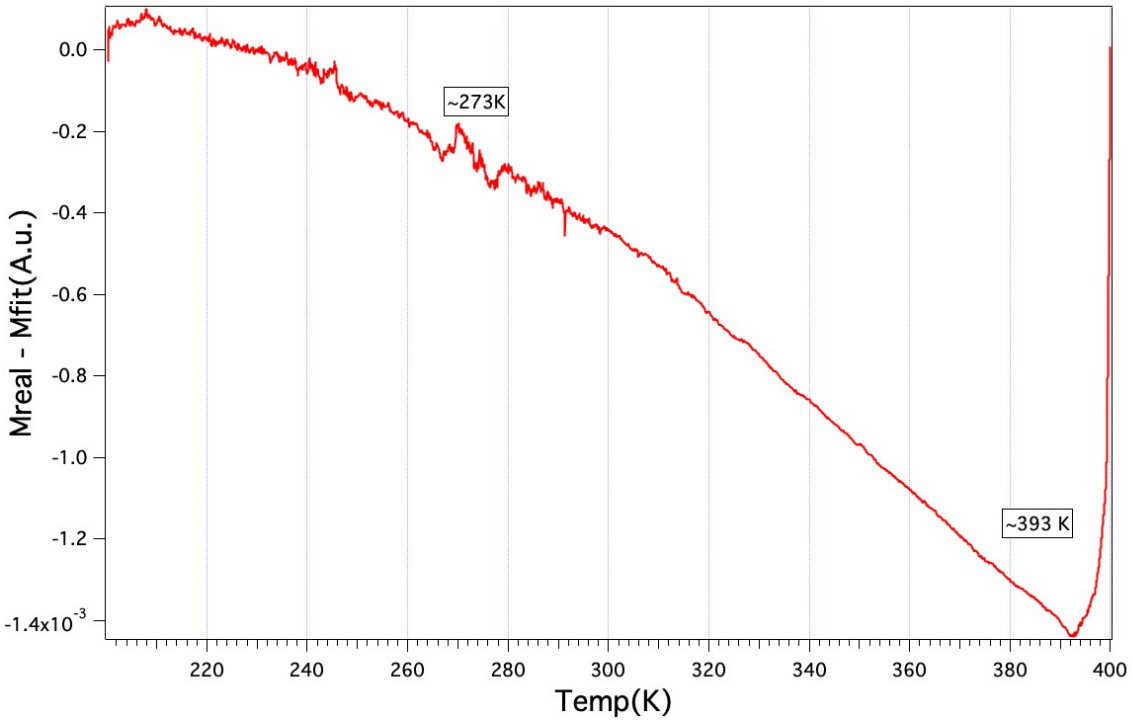

Figure 5.2 Magnetization Shift of Janus nanofibers: Magnetic moment subtracted from the 10^{th} order polynomial fit line to look for discontinuities in the slope.

To look for small deviations in the moment, the data was modeled with a 10^{th} order polynomial to get an average fit through the system. The measured and fit data was subtracted to look for discontinuities due to the structural phase changes. By doing this, two points of interest come to light in Figure 5.2. First, at $\sim$393 K there is an apparent discontinuity which correlates with the expected structural phase change for BTO going from cubic to tetragonal. There appears to also be a shift at around $\sim$273 K which would correlate with the BTO going from tetragonal to orthorhombic, but it is not as clear. This measurement confirms that the nanofiber samples we have are multiferroic.

Chapter 6

Janus Nanofiber Chaining Data

6.1 Magnetic Field Driven Data

In this section, I will review the magnetic chaining data. Figures 6.1a-b show representative images of chaining for the highest and lowest concentrations used, highlighting the significant difference in chain length for the two cases. Figure 6.2 plots average chain length for the three concentrations with respect to magnetic field. For the weakest concentration, the increase in chain length follows the same 4/3 power law that Fermigier *et al.* observed for nanoparticle chaining(dashed line). At twice and three times the concentration, chain length increases rapidly at low fields, but above 100 Oe also follows the chaining power law(dash-dot and solid lines) [9]. I hypothesize that the rapid increase in chain length at higher fiber concentration is a field-driven homogenization process where shorter fibers aggregate to form long fibers, then chain together in dipolar or tip-tip fashion at higher magnetic fields. The difference in average chain length for different concentrations is attributed to the increase in the amount of nanofibers available to form the chains.

Figure 6.3 shows that as the magnetic field increases, the angular dispersion decreases. The longer the average chain length, the more well-aligned the sample is at higher magnetic fields. Below 100 Oe, the dispersion is flat while the chain length increases rapidly and then starts to decrease monotonically as the field increases. It should also be noted that the dispersion does not show drastically different dynamics as the concentration increases.

(a)

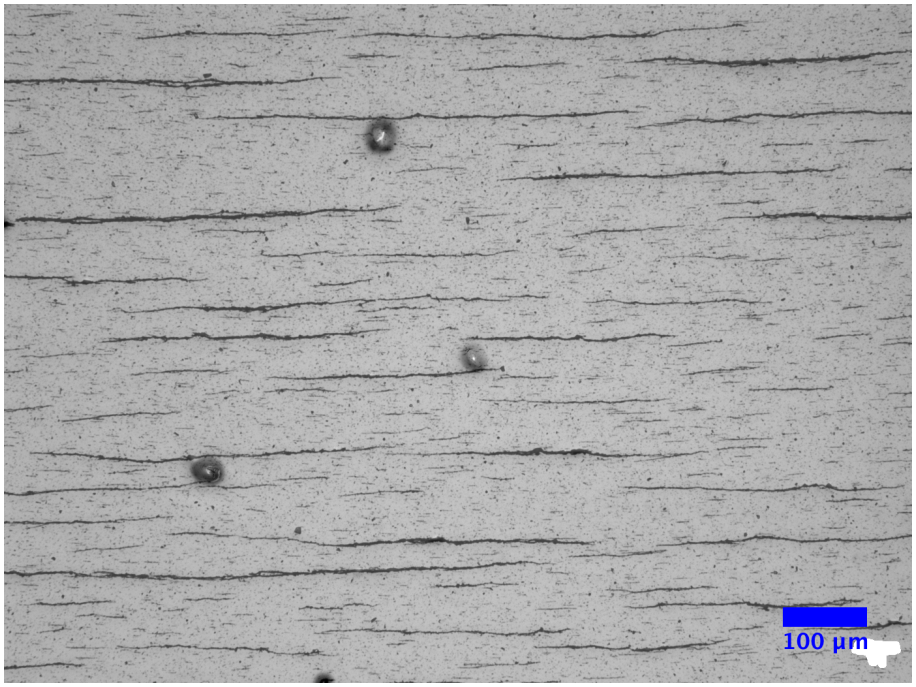

(b)

Figure 6.1 Low, High Concentration Chaining: Sample Images at H = 1kOe: a) lowest concentration, b) highest concentration sample, Scale bar is 100 μm.

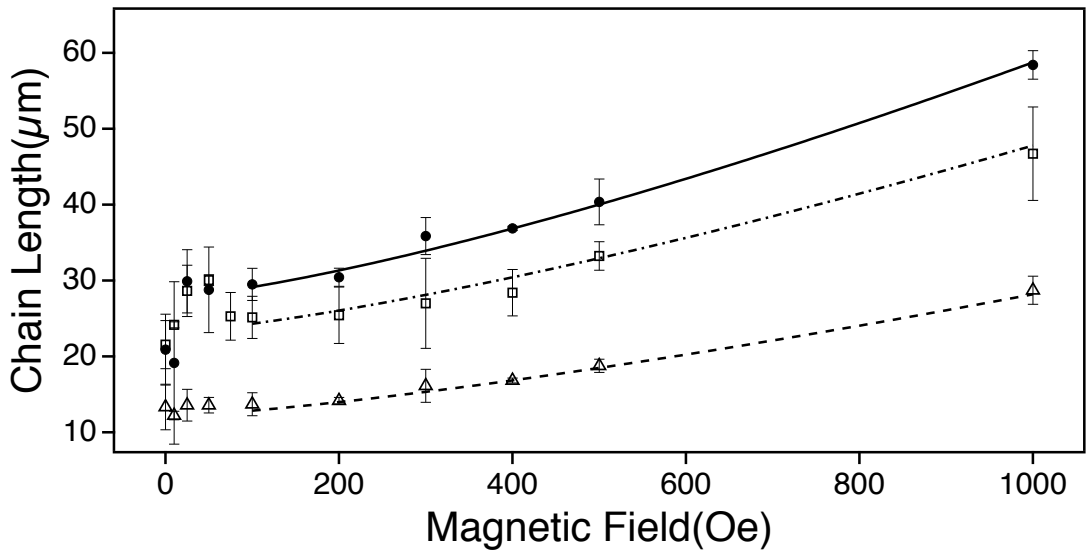

Figure 6.2 Average Chain Length vs Magnetic Field: Δ are the base sample with the lowest concentration of fibers, $\square$ are two times as concentrated, $\bullet$ are three times as concentrated, the fitted lines are, - - -, - · -, —, respectively.

Chain length versus time is shown in Figure 6.4 for the middle concentration (volume fraction $3.0 * 10^{-5}$) and a range of magnetic fields to obtain the dynamic parameters. At long time, the growth should be linear according to dynamic scaling theory, $log_{10}(\langle L \rangle) \sim z' * log_{10}(t)$. The data are transformed and fitted to a line where the slope is the dynamic exponent. As discussed in Chapter 2.3, to obtain w, n_s is fitted at long times in the same way as for average chain length and $\langle S(t) \rangle$ to extract their scaling exponents, respectively. Figure 6.5 shows a representation of the data for obtaining a z′ scaling parameter.

To obtain n_1, we used ImageJ to extract the number of "individual" fibers by picking out the chains with aspect ratios of 2 or less [11]. ImageJ's circularity limits are used to count these objects. Chains will form from the smallest fibers, but I assume that if a chain has an aspect ratio larger than 2, it is not an individual fiber. This is reasonable because when n_1 is plotted, I find a negative slope as expected for w. The crossover exponent, Δ, is then calculated by dividing w by z [20, 13, 7].

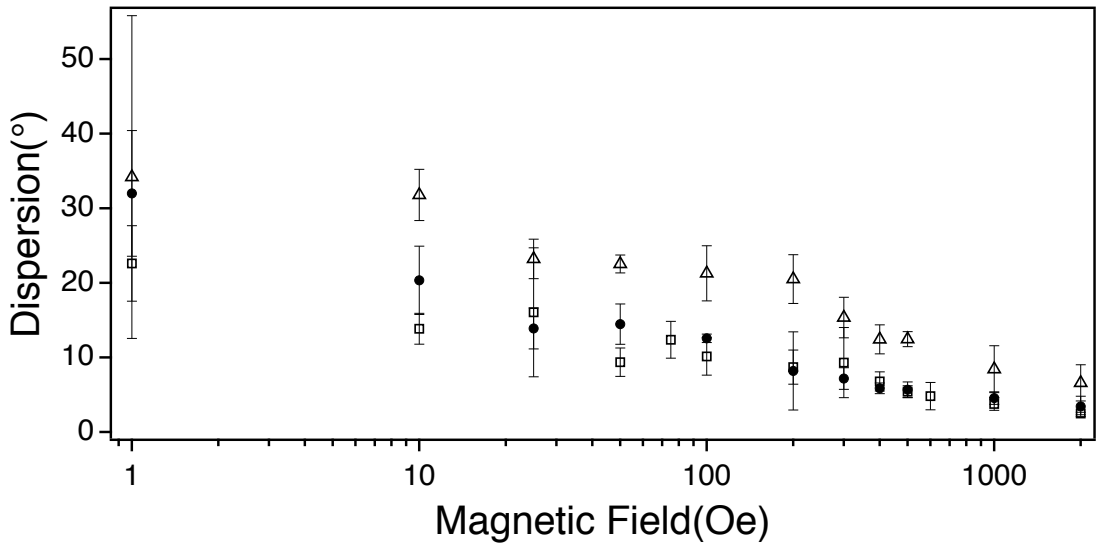

Figure 6.3 Dispersion vs Magnetic Field: Δ are the base samples with the lowest concentration of fibers, $\square$ are two times as concentrated, $\bullet$ are three times as concentrated. Note that 0 Oe has been shifted to be included.

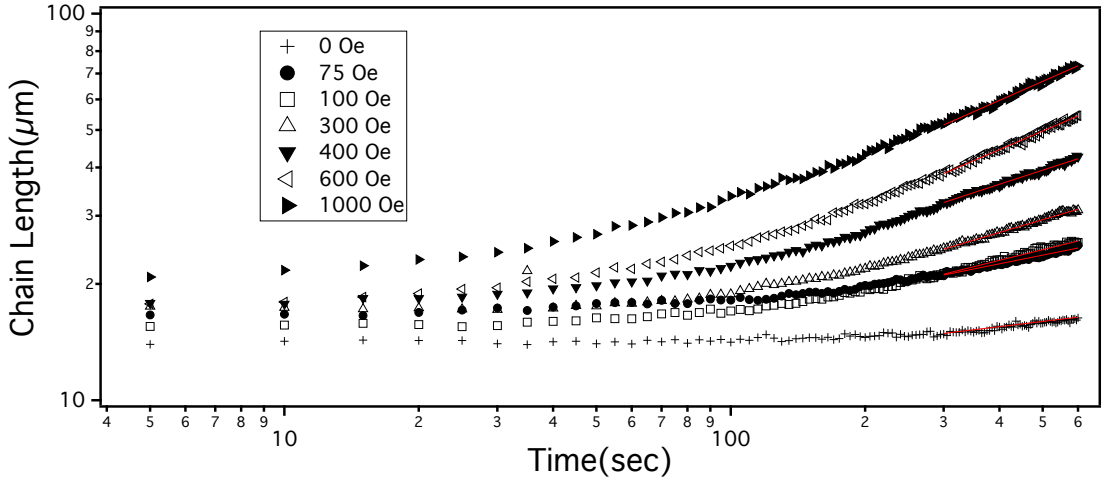

Figure 6.4 Chaining vs Time: average chain length for 0.18 mg/mL concentration over a range of magnetic fields. Each point is the average of 3 samples and the red lines are the power law fits using the scaling parameter obtained form the log plots.

As explained earlier in Chapter 2.3, Δ is a measurement of how the fibers chains are growing.

Table 6.1 summarizes the dynamic parameters. At low fields, the scaling parameter z' does not follow either mass or diffusion-limited aggregation, implying a change

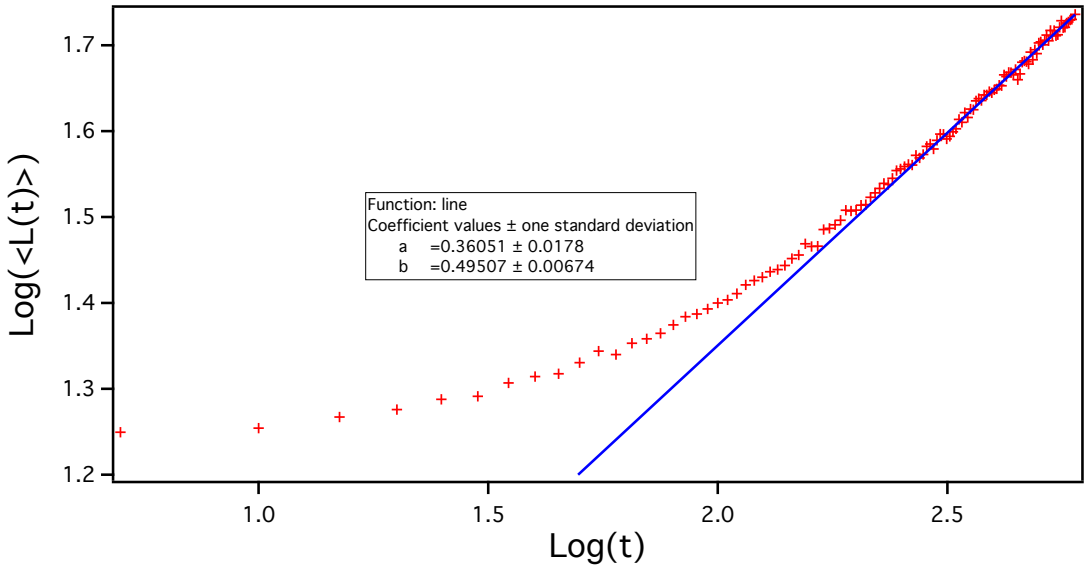

Figure 6.5 Chain Length Fitting Data: Transformed chain length and the fitted line at long times for the corresponding data.

in diffusion dynamics. The scaling parameter(z′) does approach the ideal diffusion-limited state at higher fields, and field dependence is also observed for w and z.

The crossover exponent(Δ) does show diffusion-limited chaining in the regime where the fiber and chains are expected to aggregate simultaneously. z and z′ show large deviations in their values even when $\Delta > 1$ as do w and z′ when $\Delta < 1$. The fluctuations in w and Δ indicate that nanofiber chaining is not fully described by diffusion-limited chaining. This may be due to the fibers' various sizes, with the smallest experiencing Brownian motion and the largest not.

Table 6.1 Scaling Parameters

Magnetic Field(Oe)	0	75	100	300	400	600	1000
z′ (±0.01)	0.12	0.23	0.28	0.34	0.38	0.49	0.51
z(±0.01)	0.26	0.20	0.39	0.39	0.48	0.64	0.68
w	0.19	0.26	0.33	0.36	0.55	0.44	0.38
Δ	0.73	1.29	0.85	0.92	1.16	0.68	0.54

6.2 Magnetoelectric Microscope Chaining Data

In this section, I will outline how I attempted to extract the coupling between the CFO:BTO phases by looking at the chaining data. The real-time chaining data shows that there is a magnetic field dependence for the scaling parameters. This is shown in Table 6.1 as well as Figure 6.6. Due to the magnetic field dependence, it was logical to probe if applying an electric field would also affect the chaining dynamics. The hypothesis was that for an electric field, the scaling parameter would change and thus be both magnetic and electric field dependent. If measurable, then a coupling constant for the fiber sample could be extracted.

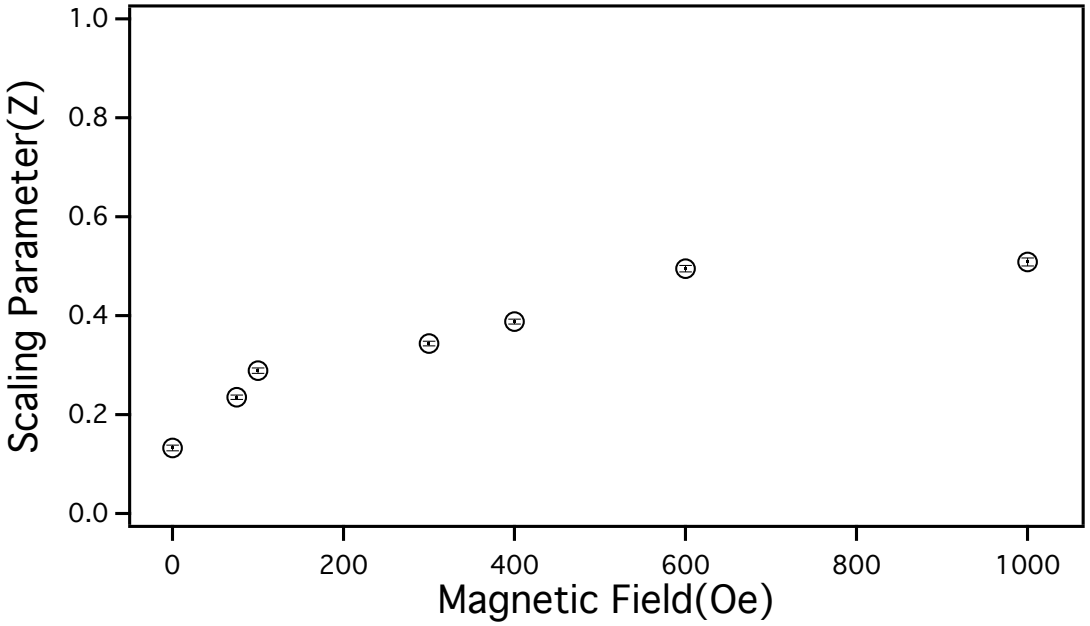

Figure 6.6 z′ vs Magnetic Field: Shows field dependence of z′ which will be used to extrapolate the magnetoelectric coupling.

Phenomenologically, this would mean replacing the stress tensor in Equation 3.1 with a scaling parameter. The average chain length's $\langle L(t) \rangle$ scaling parameter(z′) will be used to define this magnetoelectric chaining coupling (MECC). Using Equation 3.1 and Equation 2.7a where z′ goes to z′(H,E) a simple formulation of magnetoelectric chaining coupling can be developed as follows,

$$\alpha_{z'} = \frac{dz'(H,a)}{dH} \times \frac{1}{\frac{dz'(b,E)}{dE}} = \frac{dz'}{dH} \times \frac{dE}{dz'} = \frac{dE}{dH}, \tag{6.1}$$

where $\alpha_{z'}$ is the magnetoelectric chaining coupling constant, $\frac{dz'(H,a)}{dH}$ and $\frac{dz'(b,E)}{dE}$ are the slope of z′ versus magnetic field and electric field respectively, at constant electric field(a) and constant magnetic field(b). Since a DC magnetic field is being used, MECC should be non-linear and is expected to follow the butterfly shape of CFO's magnetostriction curve [4].

The non-linearity is also assumed because of the magnetic dependence of the scaling parameters. Figure 6.6 shows three regions: below 100 Oe, there is a sharp increase in z′, between 100 Oe and 600 Oe it increases more slowly, and above that it flattens out.

In the first test, a Hele-Shaw fluid cell is built with conductive indium tin oxide(ITO) coated glass, which applied an electric field perpendicular to the plane of magnetic chaining. The PVA/water/fiber solution is sealed in a 120 μm hydrophobic well with a diameter of 9 mm. Once the sample is sealed, it is placed in a static magnetic field (200 Oe) produced by two bar magnets. The fibers chain for five minutes and the voltage is increased in one volt increments every five minutes until a maximum of six volts. The experimental sample setup is shown in Figure 6.7. The average chain length from this experiment is shown in Figure 6.8. The measurement seems to indicate magnetoelectric coupling, and subsequent measurements show electroplating of the ITO and electrochemical interaction above 25 kV/m (3 volts). A dielectric coating, Kapton tape, was added to the ITO's surface to mitigate these effects and flush out a magnetoelectric chaining parameter.

The previously described experiment was performed with DC electric fields, and Kapton tape was placed on the ITO to stop electroplating, and the scaling parameter z′ was extracted. When the electric field was applied, z′ decreased by 6% compared to the control. Based on these initial and crude tests, a more controlled setup was

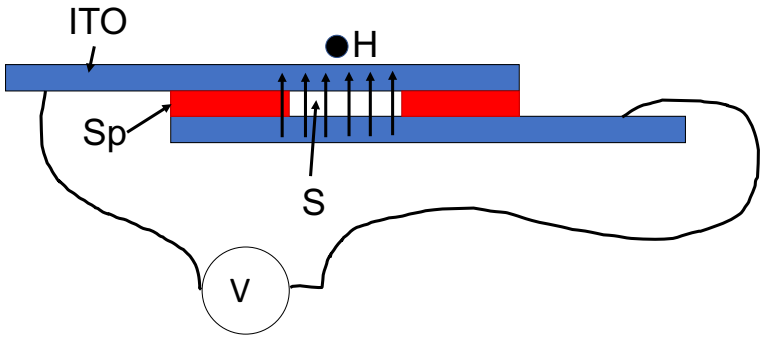

Figure 6.7 Hele-Shaw Setup: the sample(S) is sitting between two ITO glass slides which have a spacer(Sp) of 120 μm. The magnetic field is directed out of the page and the electric field is perpendicular to the magnetic field.

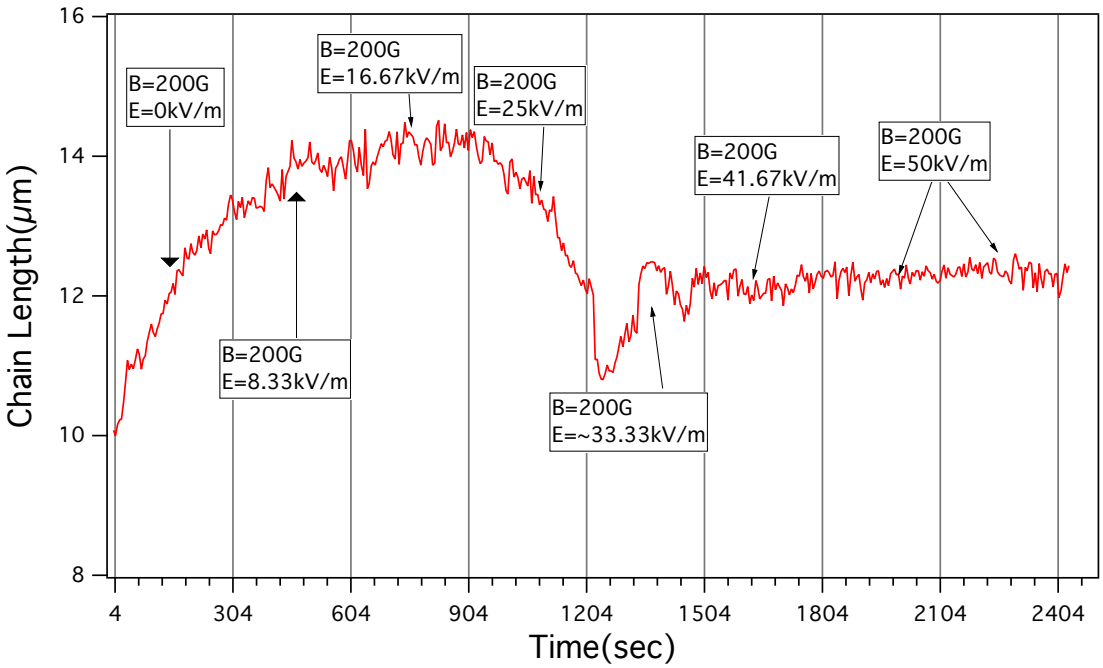

Figure 6.8 Average Chain Length vs Time: The average chain length is measured as the electric field is increased.

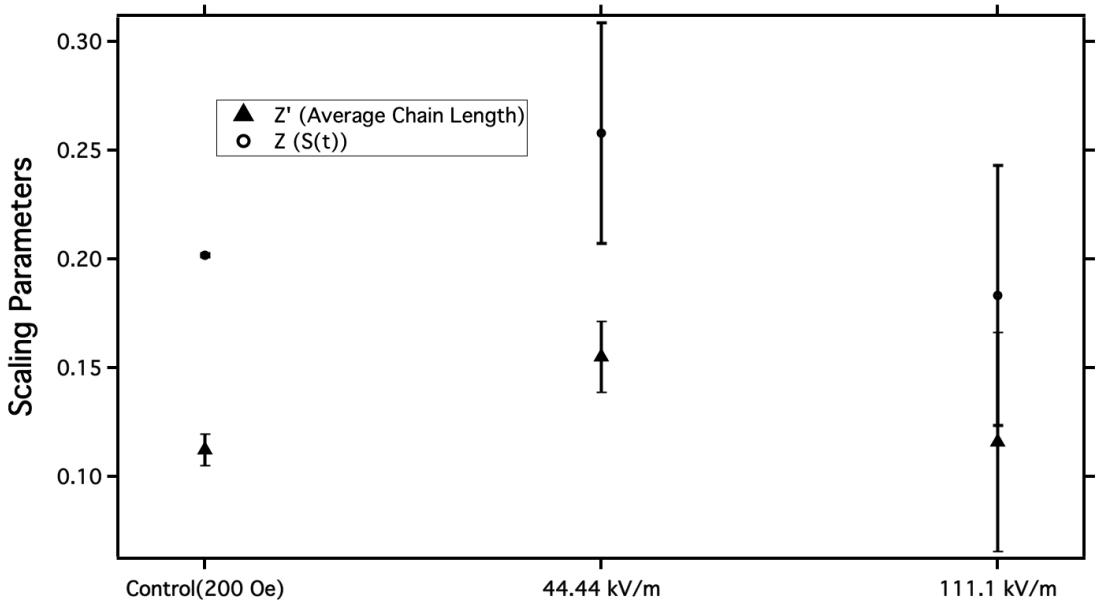

Figure 6.9 Scaling Parameters vs Electric Field: This is a summary of the initial test of magnetoelectric chaining versus electric field. Of particular note is the increase in the standard deviation as the field strength increases.

designed. The data for the first test of magnetoelectric chaining is summarized in Figure 6.9. It shows that the control (200 Oe) chain has a very tight grouping for its scaling parameters. However, the scaling parameters for the control are not the same as the original chaining data because of differences in sample fabrication. This data also shows a significant increase in the standard deviation as the electric field is increased.

The new setup involved building two electromagnet coils using an iron core wrapped with copper wire(15 gauge) and immobilized with silicone epoxy. The original base was made from plastic, but the coils produced enough force to cause the setup to flex and therefore cause the sample to drift out of focus. Therefore, it was replaced with a solid aluminum base. The coils produce a fair amount of heat that can affect our samples due to the water/polymer solution they are suspended in. Two Peltier coolers were attached to the side of the coils to act as a heat sink, and a fan was used to cool them. This worked well to keep the coils and sample area from heating even

at the highest field strength(200 Oe). Due to size limitations, this setup could not reach the field strength that the first setup could. However, this setup's advantages included a better camera, image quality, and videos that could be longer than 10 minutes. A Hall probe was incorporated into the sample holder to constantly measure the applied magnetic field, which had a deviation no larger than 0.5 Oe, during a run, which typically lasted between 45 minutes to an hour. A computer controlled the AC and DC power supplies, which allowed for seamless control of the magnetic field and applied voltage. A plastic platform was made, and a vacuum line was hooked up to keep the sample in place throughout. The videos were taken on with an Exi Aqua QImaging Camera attached to the microscope, and a 10x dark-field object was used. Dark-field microscopy was used in this setup because transmission microscopy could not be used as in the straight magnetic chaining setup. The full setup is shown in Figure 6.10.

Data was taken at six different magnetic fields ranging from 25 Oe to 150 Oe and three different voltages. Each data point in Figures 6.11 and 6.12 represents at least three chaining videos that lasted 45 minutes each. As before, the chaining data was extracted using ImageJ. Only the z' and z scaling parameters were measured because of how I defined the magnetoelectric chaining effect. Figure 6.11 and Figure 6.12 summarize the data that were collected. It is clear that if there is a magnetoelectric chaining effect, we do not have the sensitivity to detect it. Although I could not extract a coupling constant from this data, the Hele-Shaw sample fabrication proved useful for measuring changes using MOKE.

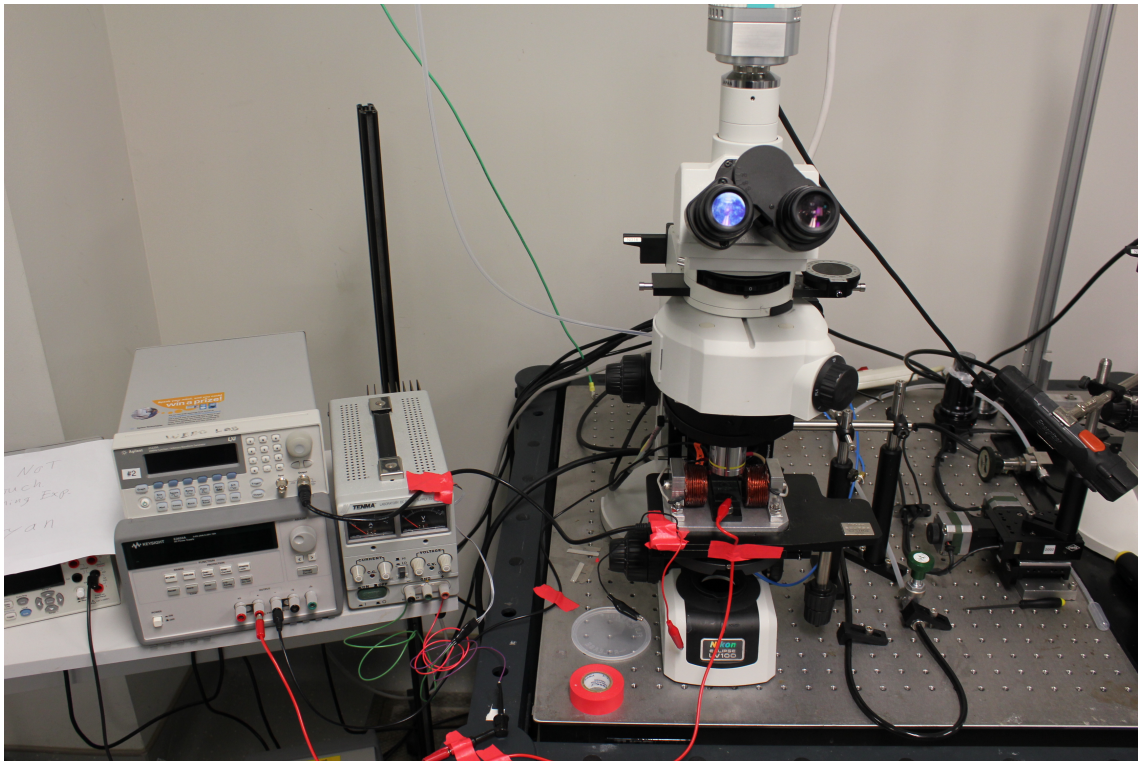

Figure 6.10 ME Microscope setup: Full ME Microscope setup, note this is without the Peltier coolers.

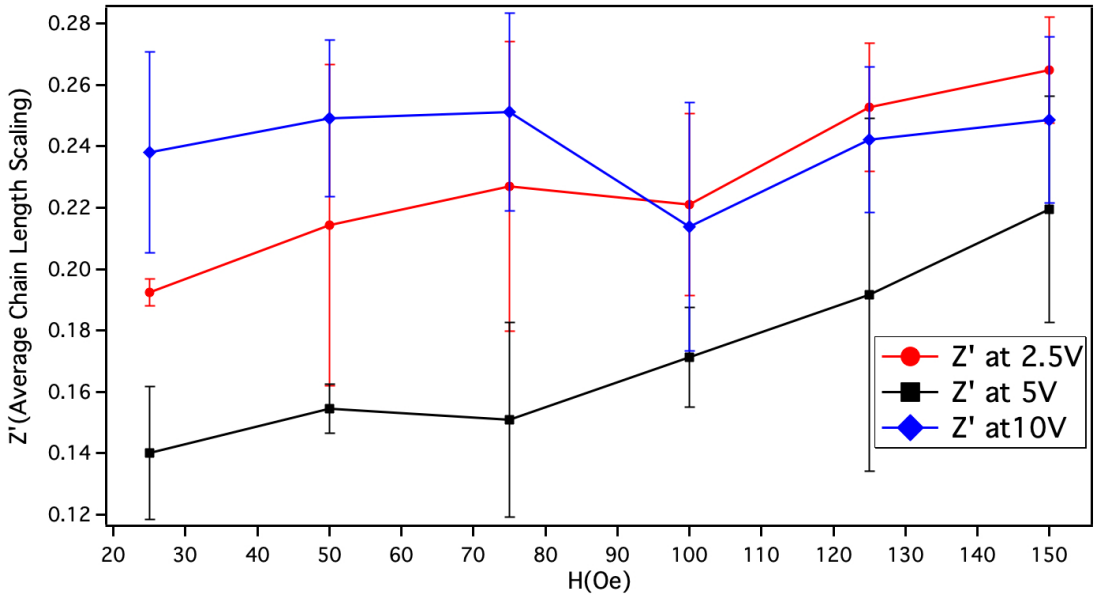

Figure 6.11 Magnetoelectric z′(Chain length) Scaling Parameter: This shows some splitting of the scaling parameters but the standard deviations are too large to make any statements about a magnetoelectric chaining effect.

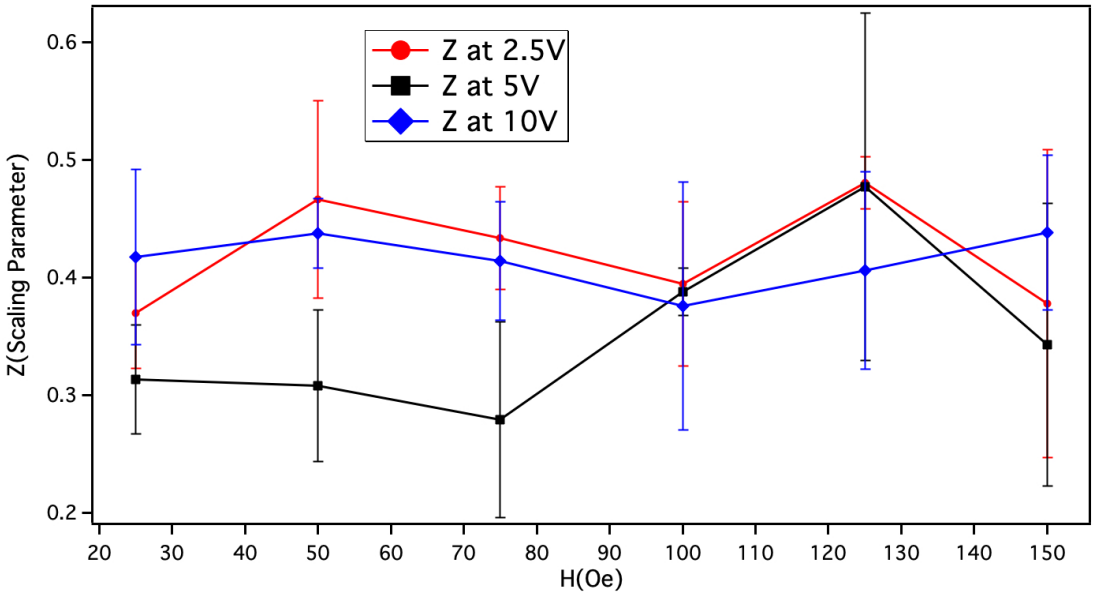

Figure 6.12 Magnetoelectric z Scaling Parameter: This shows that there is no electrical effect on the chaining data or that it is hidden behind noise that I was not able to reduce.

Chapter 7

Magnetoelectric ScMOKE

In this chapter, I will go over the data collected using Scattered MOKE to measure the magnetoelectric coupling. Figure 4.12 shows the modified ScMOKE apparatus used for most of the data taken in this section. The only difference is for the parallel plate capacitor setup, which used an optical chopper instead of a Photoelastic Modulator (PEM). A PEM was substituted because it reduced the signal noise, namely an anomalous sine wave signal that was sometimes observed in the system, and it allowed me to measure both the Kerr rotation and ellipticity of the polarized light as explained in Chapter 4.3. By applying both an electric field (voltage) and a magnetic field to the sample, I probed the coupling effects. To quantify the changes to the sample, I looked at coercivity, remanence, and Kerr rotation. For multiferroic materials, researchers typically look at these three quantities with the ultimate goal of seeing an electric field-dependent hysteresis loop in one of them or a "collapse" of the magnetic hysteresis loop [59, 60, 61, 62, 63]. I will use two abbreviations in this discussion: MOKE run and MEMOKE run. A MOKE run is a sweep of the magnetic field($\pm H_{max}$) while measuring the MOKE signal with multiple averages, typically at least 150. A MEMOKE run is the same thing, except the applied voltage is different during each MOKE run. Figure 7.1 shows the step in the voltage during a MEMOKE run. Figure 7.2 defines the directions used in explaining the geometry of the fiber chains, magnetic field, and electric field. Table 7.1 defines the resolution obtained in these experiments. The resolution was obtained by running 20 individual MOKE runs, 200 averages, at no applied voltage to see if there was significant variance between

consecutive runs. I observed very little difference between consecutive runs, and of note for the coercivity, the resolution was below what the Gauss probe was rated for. Due to limitation with the probe, I will use the probe's resolution as the standard deviation for the coercivity. I will start by discussing the parallel-plate capacitor setup.

Table 7.1 MOKE Resolution

	H_c(Oe)	M_r(A.U.)	Kerr Rotation(nV)	Gauss Probe(Oe)
Standard Deviation	±18	±0.026	±33	±25

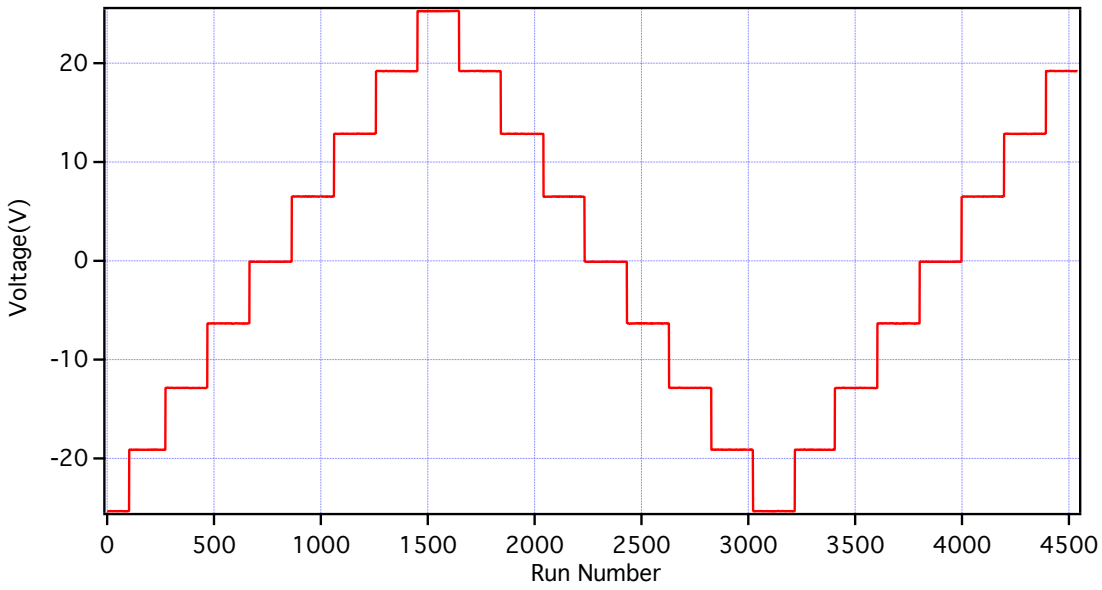

Figure 7.1 Measured Voltage: Voltage measured during MOKE runs with 200 averages.

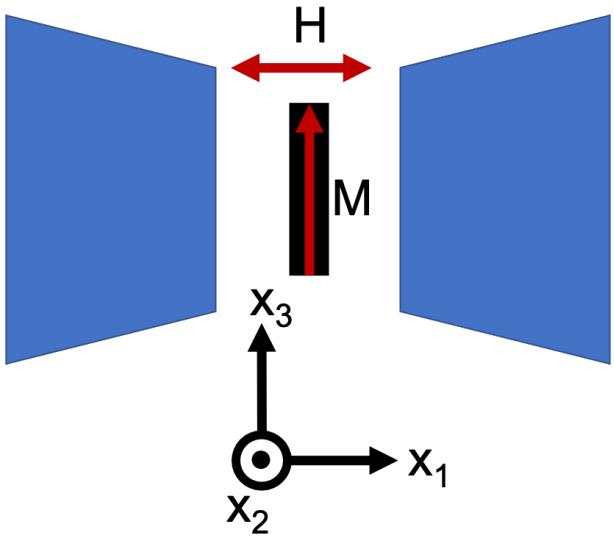

Figure 7.2 Janus Fiber MOKE Orientation: The fiber chains are aligned with their long axis along x_3 unless otherwise stated, same as the $\hat{s}$ polarization direction. The external magnetic field(H) is always applied in the x_1 direction, which is the same as the $\hat{p}$ polarization direction. The electric field can be applied in all three directions: parallel plate samples(x_2) and coplanar samples(x_1, x_3).

7.1 Parallel Plate Capacitor Data

As explained earlier, these samples involved aligning the Janus nanofibers on top of an ITO glass slide and sandwiching them with another ITO glass slide on top, thus producing a parallel plate capacitor. This allows for the electric field to be applied perpendicular to the external magnetic field and in the x_2 direction. Although this is not the most advantageous geometry for measuring the ME coupling, ideally both the $\vec{E}$ and $\vec{H}$ would be applied along the length of a fiber(x_3), it does allow me to apply a higher electric field to the fibers with lower voltages. The first attempt is shown in Figure 7.3. This is the first promising indication that applying an electric field to the fibers can produce measurable changes in MOKE.

Figure 7.3 shows both a shift in coercivity and changes in the loop shape. There is an evident increase in the coercivity as the voltage is increased from 0 to 18 volts. In subsequent measurements, a bi-polar power supply was used to apply the voltage

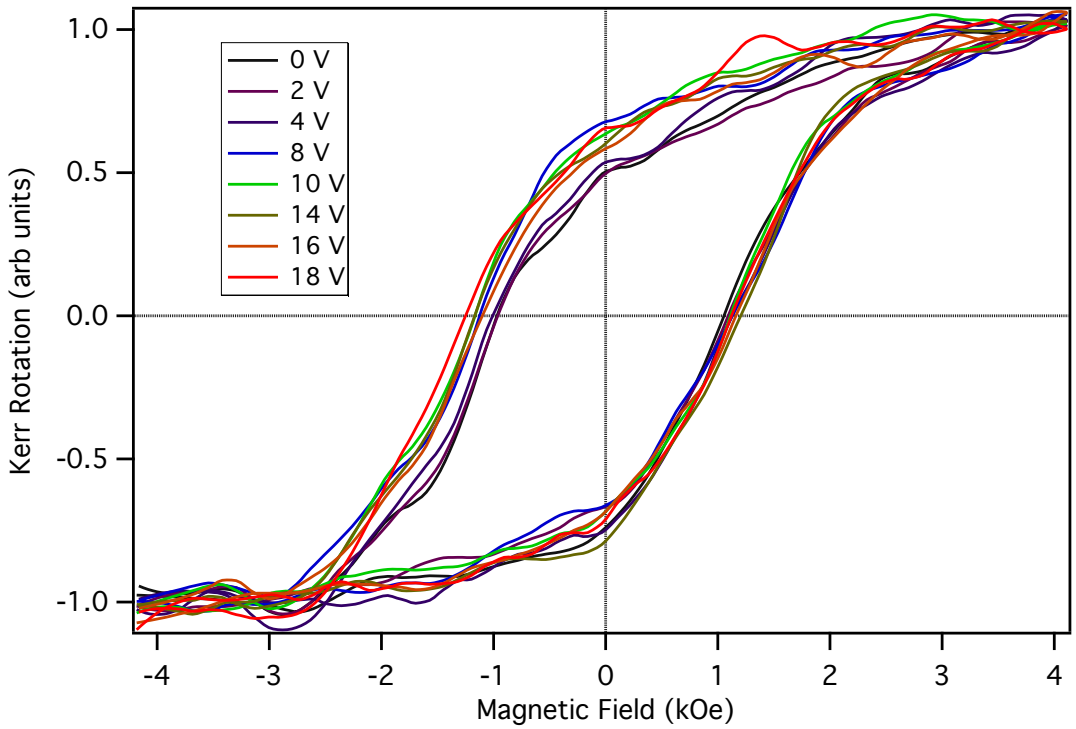

Figure 7.3 First MEMOKE Run: MOKE measurements of Janus fibers at various voltages(0-18 V). This is measured with our old setup which did not include fast acquisition with an oscilloscope or a PEM.

to probe if there was hysteresis in the coupling. Figure 7.4 shows remanence from two successive ME runs. On the second run (dashed lines), the change in the remanence is not as pronounced as in the original run. This became a common theme in these measurements, i.e. the more I measured a fiber/sample the less it would respond to the electric field. This is also shown in Figure 7.5 where during the first pass from -50V to +50V and back, the signal shows a clear hysteretic shape that disappears on the 2nd run. I hypothesize that after the first ME run, the system has either been strained so that the domains are pinned or the BTO:CFO interface is no longer coupled. At this point, before beginning a MEMOKE run, the voltage was swept from $\pm V_{max}$ so that the state of electric polarization was known. As seen in Figure 7.5, if the voltage was swept multiple times before the MOKE began, little response was observed.

Furthermore, if an initial "test" MEMOKE run, with fewer averages, was conducted before a longer run, then the response also decreased or was nonexistent. As a result, I stopped sweeping the electric field first and started MOKE runs at zero voltage to account for the initial state of a fiber/sample.

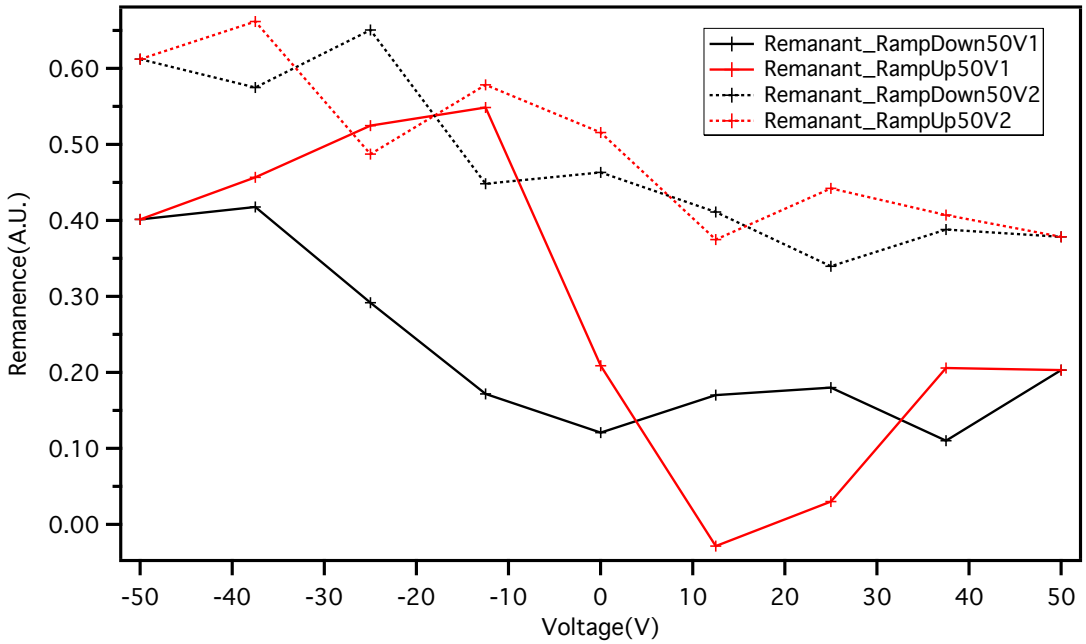

Figure 7.4 Parallel Plate Remanence: Remanence difference showing a decrease in the effectiveness of the electric field. The remanence is measured from normalized MOKE curves.

MEMOKE was also done with fibers aligned parallel to the optical table(x_1). This allowed for the magnetic field to be applied in the same direction as the long axis of the fiber, with the voltage applied perpendicular(x_2). In this geometry, the overall loop shapes were more square, indicating an easy magnetic axis. However, the ME effects in this direction are not as pronounced, which is surprising considering this is typically considered the more advantageous geometry [64]. The MEMOKE run is shown in Figure 7.6. This is important for future studies on multiferroic nanofibers because it shows a reduced response in a geometry previously believed to be advantageous. In this orientation, I did not observe the hysteresis loop collapse, so it appears the applied stress is not moving the domains as significantly.

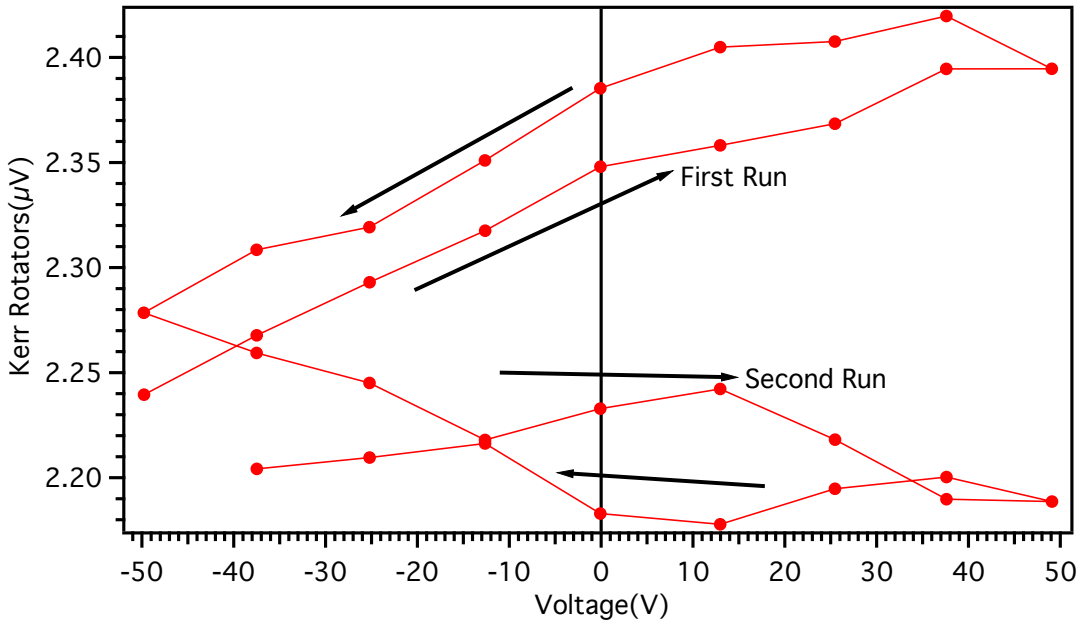

Figure 7.5 Kerr Rotation Voltage Dependence: Dependence of Kerr rotation on the applied voltage in a parallel plate setup.

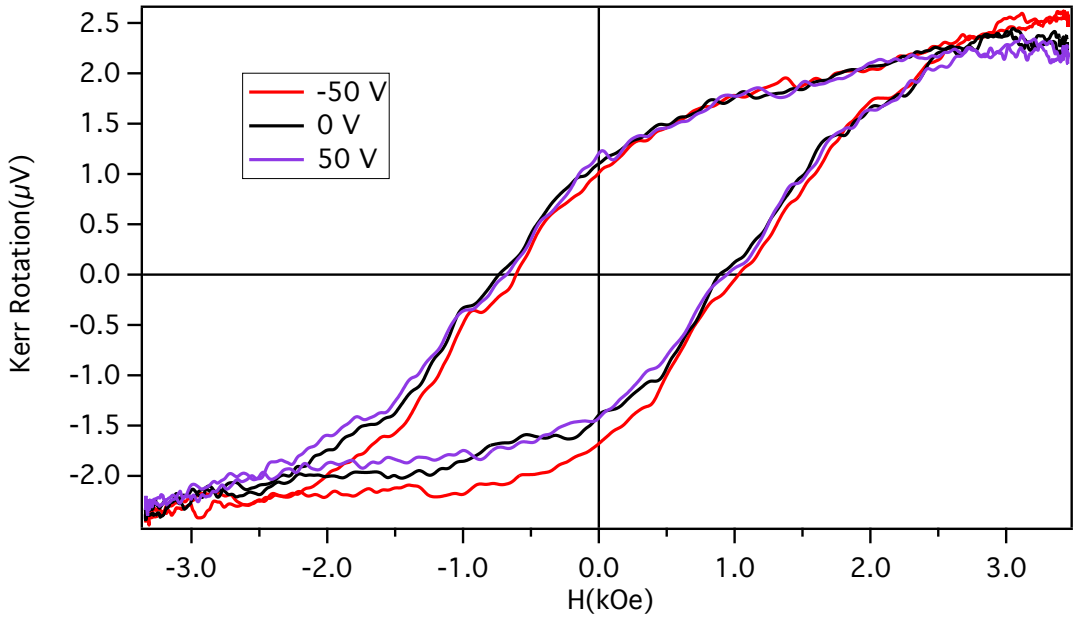

Figure 7.6 Parallel Plate ScMOKE on Rotated Nanofiber: ScMOKE measured on an agglomerate of fibers in the x_1 direction that that shows splitting in the MOKE loops with 200 averages. Though this does not show as dramatic a decrease in the MOKE loop, it does inform us that the nanofibers can be probed in multiple directions.

Figure 7.7a shows a clear increase in the Kerr rotation as the applied voltage is increased. As explained in Chapter 3.1, the magnetoelectric effect depends on the crystal structure and the direction of the applied fields. Therefore, it is difficult to predict how the MOKE loops will change. If the sample is being heated, then the overall Kerr rotation will decrease with time. Care must be taken to make sure this does not happen. It is usually easy to tell if a sample is being heated due to the exponential decay in its Kerr signal, and the fiber disappears or melts [45]. Figure 7.8 shows what typical heating decay from all samples looks like. In conclusion, the parallel plate samples show voltage-induced changes in the coercivity, remanence, and Kerr rotation with indications of a changing hysteresis.

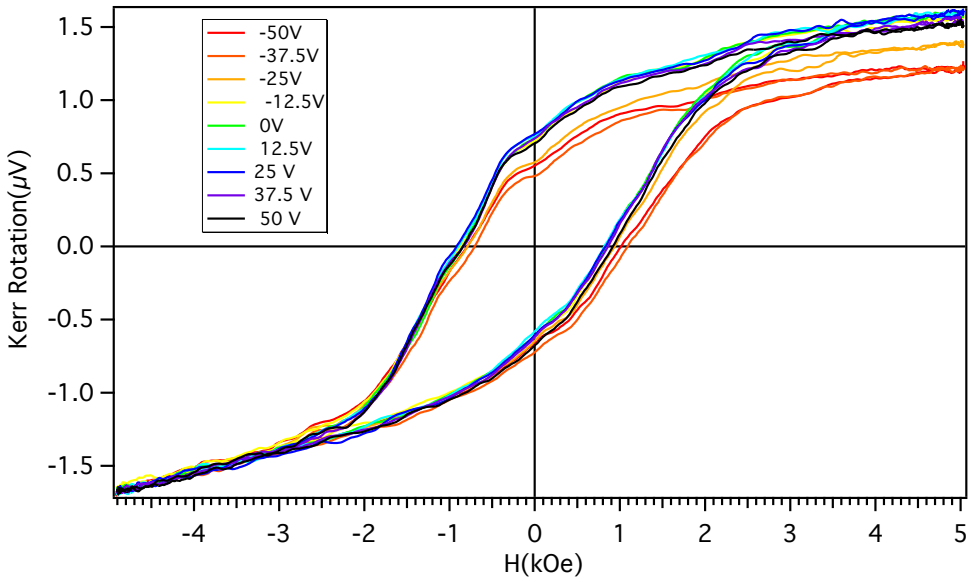

(a)

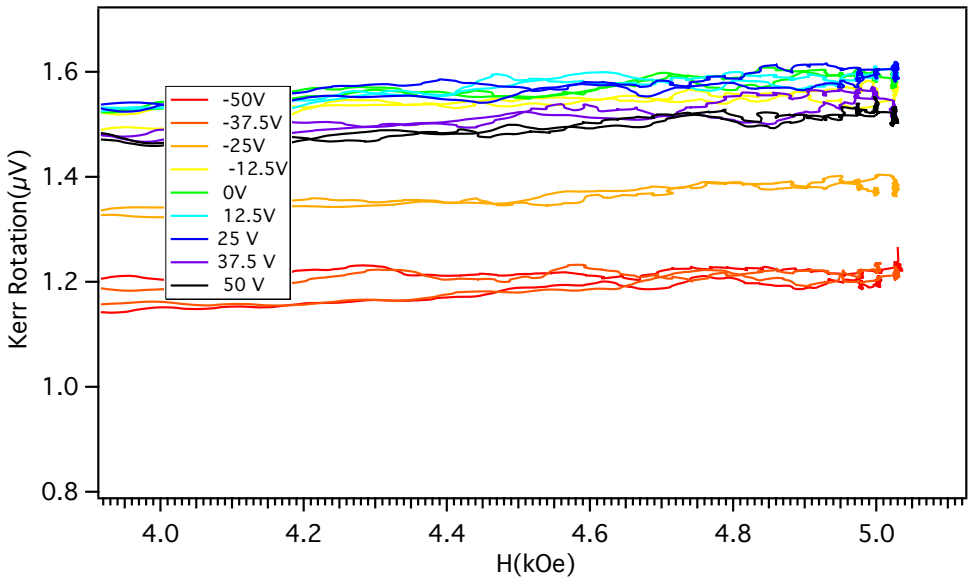

(b)

Figure 7.7 Shifted MOKE Loops: a) Show clear differences in the "height" of the Kerr rotation as the voltage is swept from -50 V to +50 V. b) Close-up of the MOKE loops in a)

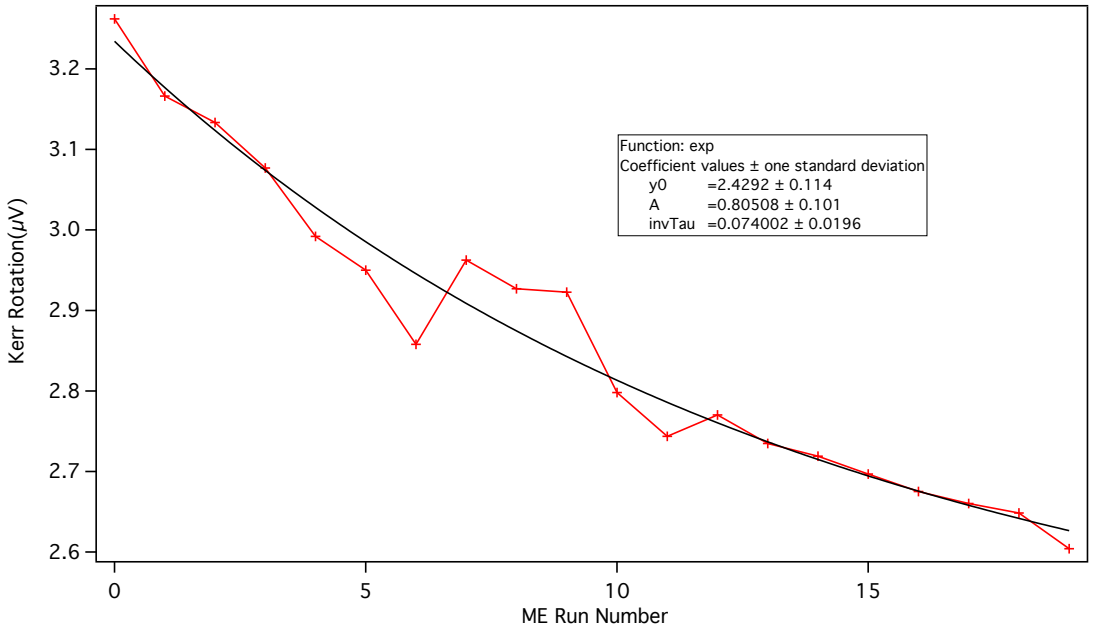

Figure 7.8 Kerr Rotation Signal From Heated Fiber Chain: The Kerr rotation is fit with an exponential decay fit line, typical of heating that has been seen in our fibers. Although there is a small deviation in the middle that could possibly be ME coupling this cannot be confirmed due to heating.

7.2 Coplanar Electrode Data

In this section, I will explain what was seen in the coplanar electrode geometry. These samples were simpler to make than parallel plate capacitors because they just required gold electrodes on glass with wires attached with silver epoxy. The fibers were cured in the same way using bar magnets and then attached to the sample holder using double-sided Kapton tape. In this geometry, a control test was first done on CFO nanofibers to confirm that changes due to the applied voltage only happened in the Janus nanofibers. This can be seen in Figure 7.9 and confirmed that if we were seeing changes in the coercivity, remanence, or Kerr rotation, it was caused by the applied voltage.

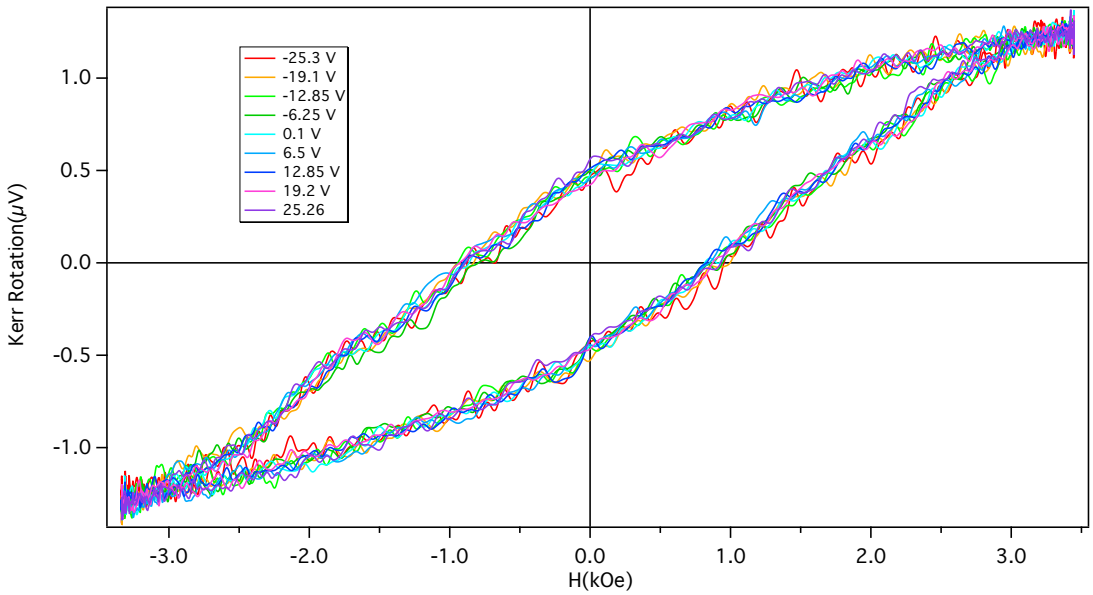

Figure 7.9 Multiple CFO MOKE Nanofibers Curves: This shows stacked CFO MOKE loops, displaying no change in the Kerr rotation in contrast to those observed in multiferroic Janus nanofibers. MOKE loops are measured in a coplanar electrode setup and with an optical chopper.

In the coplanar geometry, I measured distinct changes to the ScMOKE loop shape that were not seen in the parallel plate geometry. This is attributed to the voltage now being along the length of the fiber(x_3) instead of perpendicular(x_2). Observations include the hysteresis loop collapsing in on itself as seen in Figure 7.10a-b. This collapse was more common in the coplanar geometry than in the parallel plate geometry, indicating that the BTO is transferring more stress to the CFO in this geometry.

The most dramatic collapse in the ScMOKE signal can be seen in Figure 7.11. Collapsing hysteresis loops are commonly seen ME effects in composite multiferroics as well as changes in coercivity and remanence [59, 60, 61, 62, 63]. This is also the most dramatic change I have seen in the coplanar geometry. While I cannot currently extract a coupling constant from this, I am confident that ScMOKE can be used to probe non-thin film nanostructures. With a few modifications, I believe the current setup could extract a ME coupling constant for a fiber chain.

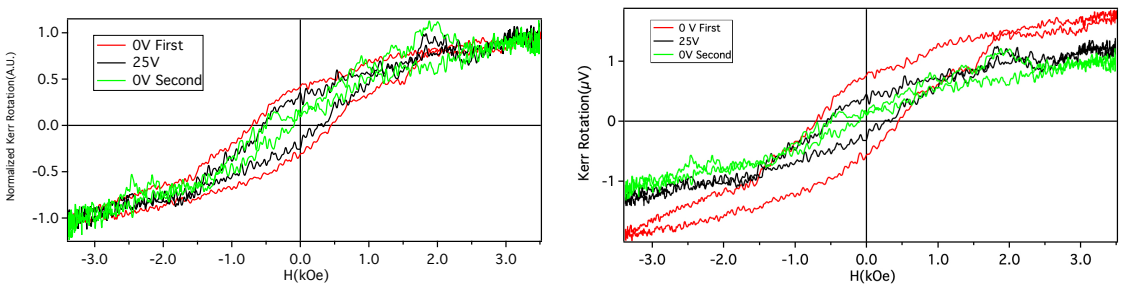

Figure 7.10 ScMOKE Collapsing Loops: This sample is aggregate chains measured with ScMOKE with fibers oriented in the x_3 direction. a) and b) Collapsing hysteresis loops in the same sample with application of an electric field [62, 63].

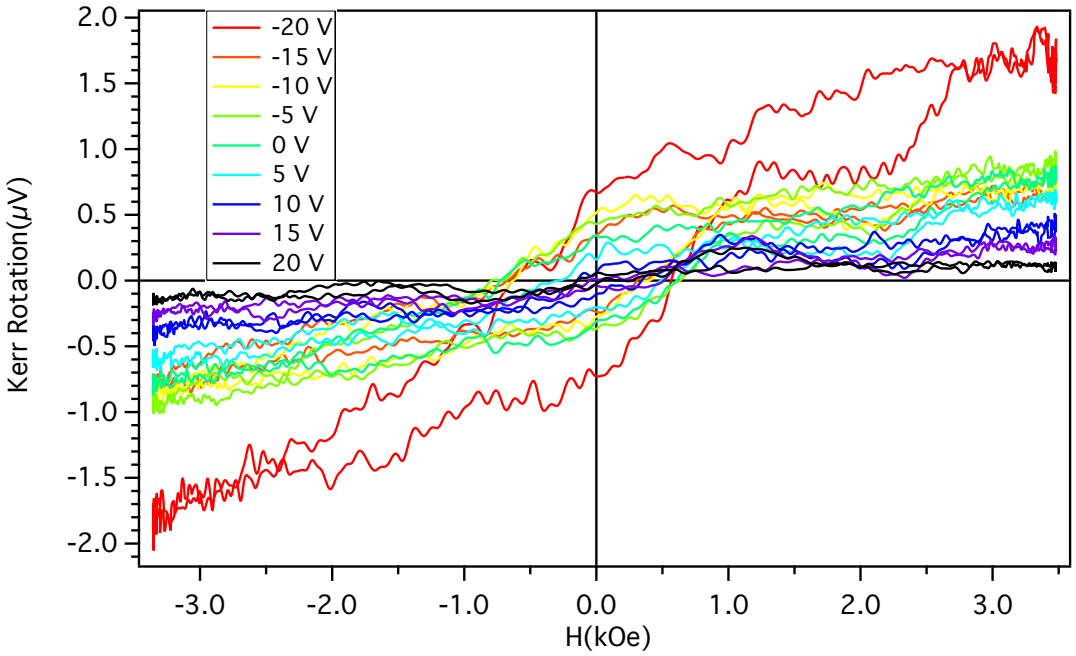

Figure 7.11 ScMOKE measured for a chain of fibers aligned in the typical x_3 orientation shows a complete collapse in the Kerr signal, similar to what was observed in Figure 7.10b. This type of behavior has been seen many times in MOKE studies of thin film multiferroic heterostructure.

Figure 7.12 shows for the coplanar setup a clear splitting of coercivity as the voltage changes, ∼100-200 Oe. This proves that there can be a significant change in the coercivity across samples, even when they have vastly different initial coercivity.

It can be inferred from these graphs that the stress produced by the BTO is large enough to change the coercivity of the CFO phase.

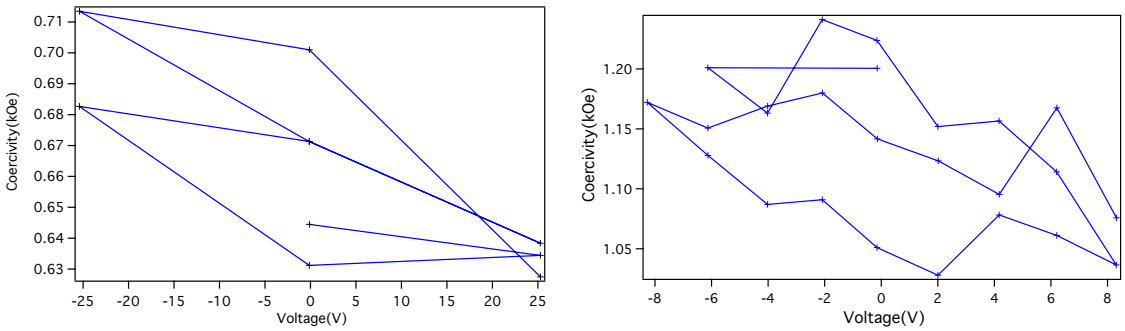

(a) (b)

Figure 7.12 Coercivity vs Voltage: Two different samples showing splitting in their coercivity that is greater than the resolution of the probe. For the coplanar they typically showed this open loop. Note: each run starts at 0 voltage.

Furthermore, voltage-induced changes in all three CFO magnetic parameters are shown in all three Figures 7.13,7.14 and 7.15. Figure 7.13 is the response seen in a fiber chain with large gaps (1mm) between the coplanar electrodes while the other two had a 240μm gap. Each set of graphs shows changes in the coercivity, remanence, and Kerr rotation. The Kerr rotation is the "height" of the hysteresis loop and can be thought of as a corollary to the magnetic saturation. Qualitatively, each shows interesting dynamics, of particular note the hysteretic loops in each measured value, i.e. Figure 7.14c resembles an oval. Figures 7.13c and 7.15c show a diamond-like shape.

The remanence appears to be affected by the applied voltage, but there is no clear trend. Although the changes in Figures 7.14b and 7.15b are from the same fiber, more runs are needed to confirm changes. The Kerr rotation does show hysteretic behavior in all samples, which is especially important because it lets us rule out heating effects. All these observed changes are from chained fibers and not from single fibers.

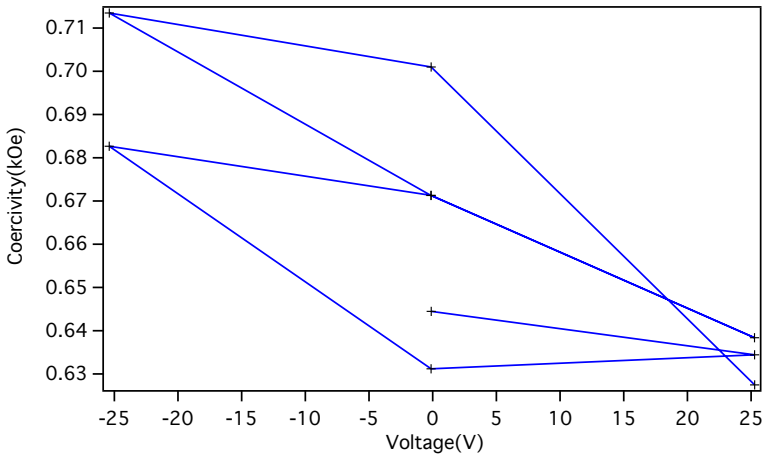

(a)

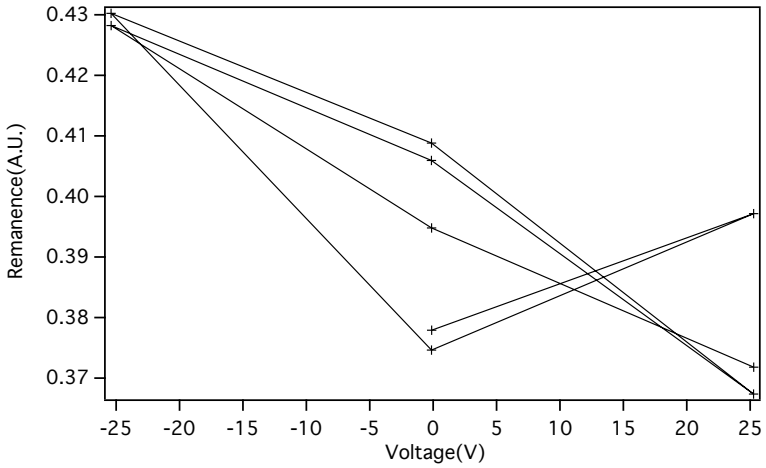

(b)

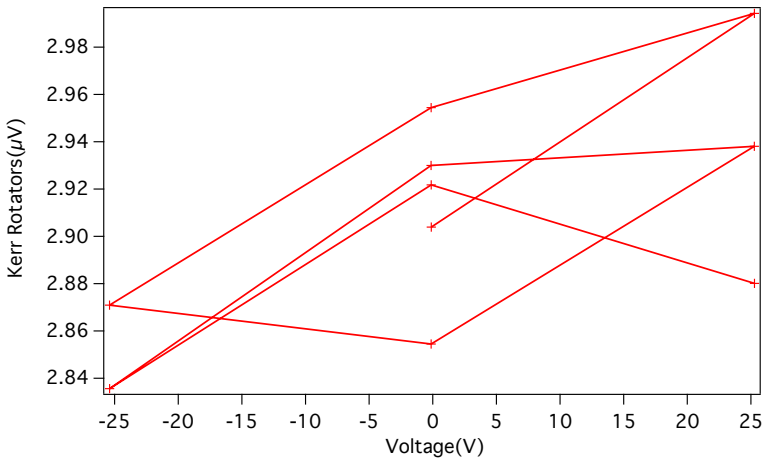

(c)

Figure 7.13 Coercivity, Remanence, and Kerr Rotation vs. Voltage: From a single sample shows coercivity and remanence follow similar changes, whereas the Kerr rotation is opposite. All are from 200 MOKE loops averaged.

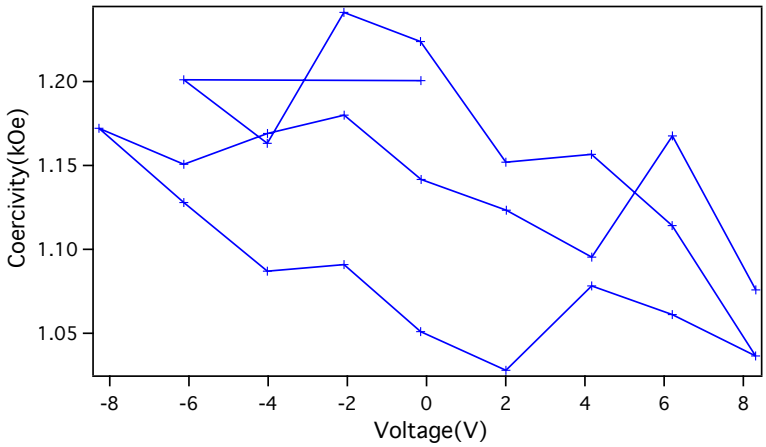

(a)

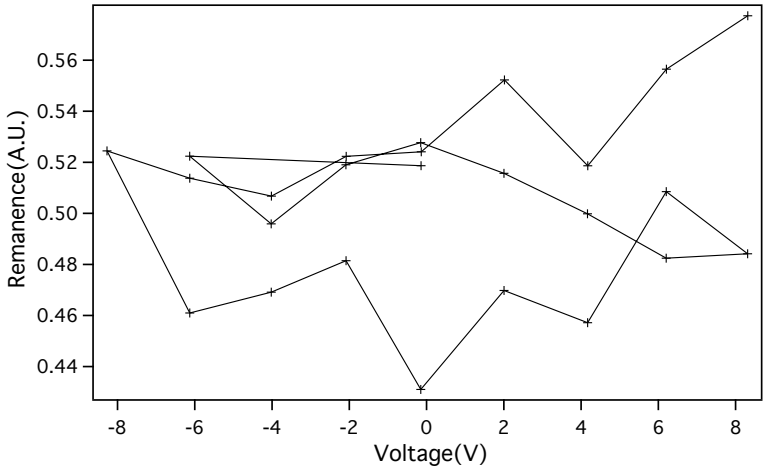

(b)

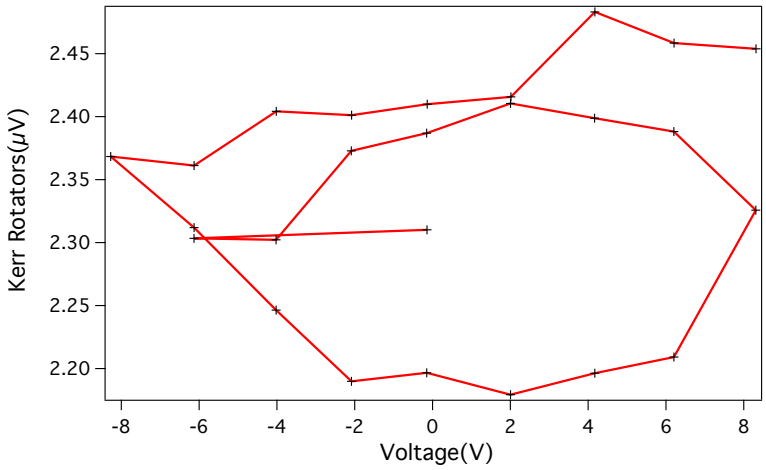

(c)

Figure 7.14 Coercivity, Remanence, and Kerr Rotation vs Voltage: For the smallest coplanar setup with a gap of 240μm between the gold contacts. These runs are for 300 averages and a linear fit shows a 110 Oe/V slope.

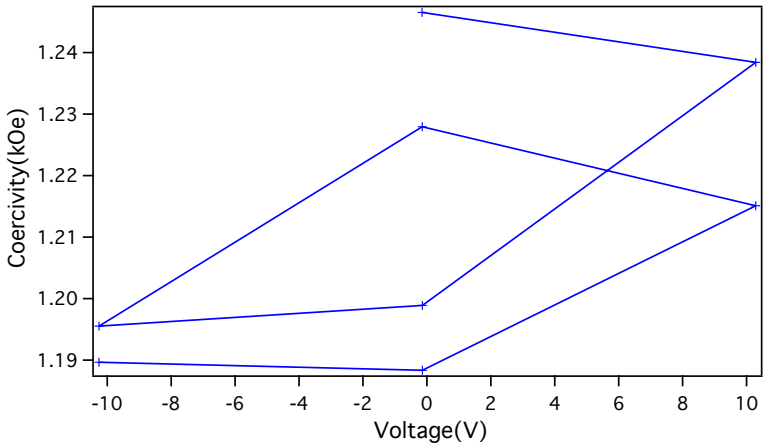

(a)

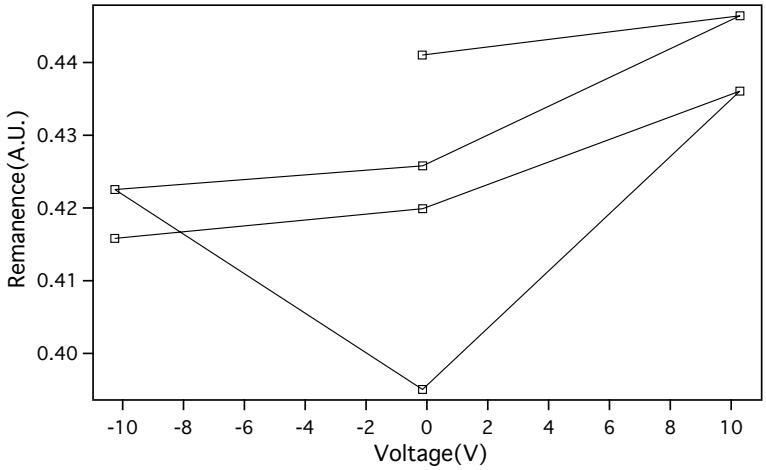

(b)

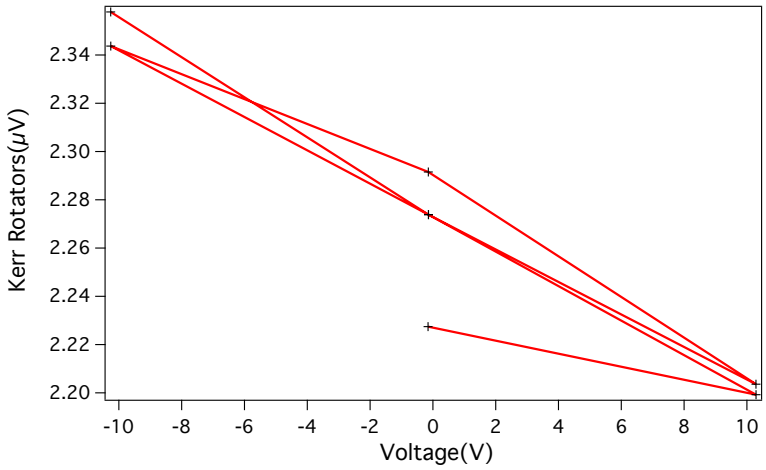

(c)

Figure 7.15 Coercivity, Remanence, and Kerr Rotation vs Voltage: For the smallest coplanar setup with a gap of 240μm between the gold contacts. These runs are for 200 averages.

The fibers' long axis is now aligned parallel to the magnetic field(x_1), allowing for the applied voltage and magnetic field to be in the same direction. Similar to when this was done with the parallel plate setup(Figure 7.6), the effect on the coercivity and remanence was not as pronounced. At the same time, the Kerr rotation shows a more dramatic non-hysteretic change. I hypothesize that since I am probing the easy axis in this geometry, the domains do not need to rotate as much; therefore, they cannot increase or decrease as much. Comparatively, when the fibers are orientated in the x_3 direction, I am probing the hard axis, and the measured magnetization can rotate more. This orientation shows the same non-hysteretic behavior, which is most dramatically demonstrated in Figure 7.16.

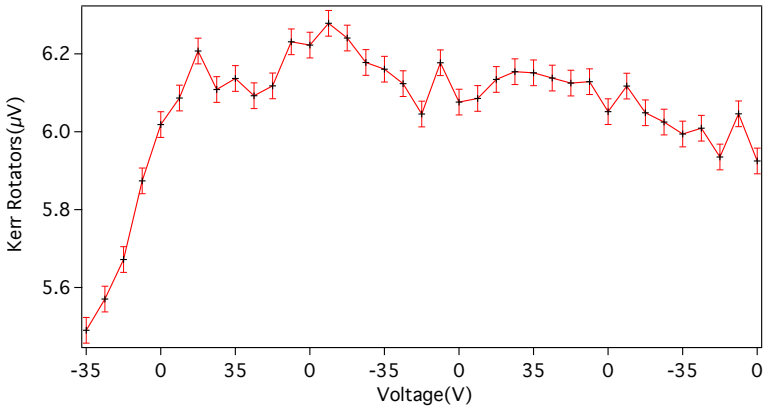

Figure 7.16 Kerr Rotation vs. Voltage: The Kerr rotation is plotted point-wise with the run number replaced with the applied voltages. After the sample has gone from -35 V to +35 V, it shows no more change in the rotation, as if the stress has pinned the domains. A MOKE for this sample is shown in Figure 4.15b.

Moving back to the fibers oriented in the x_3 direction, the stress-induced changes in all samples are the most dramatic when looking at the Kerr rotation. To see this, look at Figure 7.17. This shows the difference in Kerr saturation at different applied voltages. Note it is plotted with respect to the point number instead of the field to make it easier to see. The overall shape is similar to the inverse magnetostriction in Figure 2.3. Based on this, for Figure 7.17b the 0V, middle line, is the no stress

in the system; -20V would be the positive applied stress, and +15V would be the negative applied stress. Note that the applied stress is not symmetric with respect to voltage. It is evident from this that I can apply stress by applying a voltage that can be correlated to applied stress. To see the hysteresis loops for this sample, look at Appendix A.

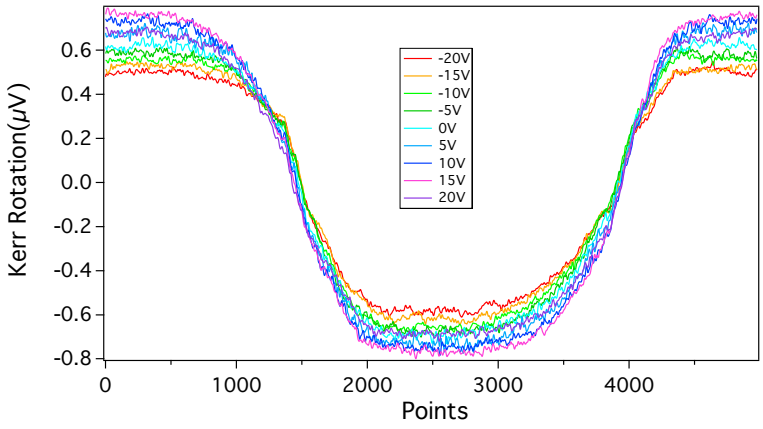

(a)

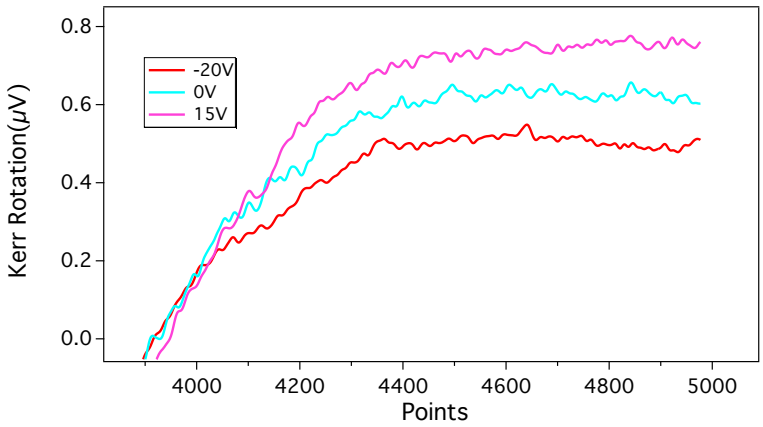

(b)

Figure 7.17 Kerr Rotation vs. Points: a) This shows the Kerr rotation at different applied voltages. b) show three different voltages and the max differences in the Kerr rotation signal. The middle line 0 V is the no applied stress situation, -20 V is the positive applied stress, and -15 V would be the negative applied stress. Each run is the average of 300 MOKE runs.

In summary, I measured voltage-induced changes in coercivity, remanence, and Kerr rotators in multiferroic Janus nanofibers. This is the first time that ScMOKE has been used to measure such changes in these nanofibers. The fibers show apparent changes in their magnetic properties, and I have taken the first step in measuring the magnetoelectric coupling in Janus nanofibers. In the current setup, changes in the Kerr rotations are the best indications of the coupling, especially until a better gaussmeter is obtained. Since I am measuring a chain of fibers, all the magnetic properties need to be looked at to understand the effect. In conclusion, the coplanar MEMOKE data does show stress-induced changes to the MOKE loops, but more studies are needed to quantify the changes.

Chapter 8

Results

8.1 Chaining Data

8.1.1 Magnetic Field Driven Chaining Results

I investigated the chaining dynamics in multiferroic nanofibers and found significant deviations from the conventional diffusion-limited model, especially at higher nanofiber concentration(Figure 6.2). Neither the magnetic field dependence of the dynamic scaling parameters(Figure 6.6), nor the rapid increase in chain length at low fields is expected from standard chaining models. In particular, the rapid increase in chain length at low fields and high concentrations suggests a field-driven homogenization of chain length occurs prior to a transition to a standard chaining process at higher fields. Additional modeling, modified to address the polydispersity in electrospun nanofibers, taking into account size and aspect ratio, is required to explain our observed assembly dynamics.

8.1.2 Magnetoelectric Chaining Results

By simultaneously applying an electric field perpendicular to the magnetic field, I observe changes in the length of the fiber chains and an increase in the dispersion of chain length across a multi-chain sample. I used video imaging to initially monitor the chaining process at 200 Oe magnetic field alone and with electric fields of 44.44 and 111.1 kV/m, respectively. This initial study showed promise that there was a magnetoelectric chain interaction, although with further studies this proved not to be

true. By avoiding electroplating on the ITO with a layer of PMMA and measuring three different electric fields and six different magnetic fields, the scaling parameters did not show a clear trend.

As seen in Figure 6.12, even though the three different electric fields do shift the average z, the standard deviations for most are large enough to make differentiating them impossible. z' does show a more convincing trend that there may be a magnetoelectric chaining effect, but the standard deviations are still too large. The electric field does increase the standard deviation for a scaling parameter compared to the pure magnetic chaining system. If there is a magnetoelectric chaining effect, it does not appear to change coherently.

There is also significant screening from the water in the system, so the electric field may not be fully poling the BTO. In that case, a stress is not significantly transferred to the CFO. As the carrier solution is optimized to immobilize and self-assemble the fiber, it may not have been the most advantageous for this type of measurement. The coupling could also be small enough that this type of measurement would not have been possible either way. Since the fibers are not immobilized(i.e., clamped), the BTO could be rotating so that it is not stressing the CFO. While the issue could be a combination of these, I do believe that further studies should be done with new nanofibers and a different carrier solution(i.e., oil). Although this measurement did not end up with a conclusive answer, it did provide me with insight into making samples for measuring the fibers with ScMOKE.

8.2 Magnetoelectric MOKE Results

After comparing all the MOKE data, I gleaned a few results; most notably, the Janus nanofibers show a magnetoelectric effect. The magnetoelectric coupling is not hysteretic except in a few special cases. As this is the first study using MOKE to probe multiferroic nanofibers, we have made great leaps in understanding how to

measure these types of materials. This experience will be invaluable for future work to expand how nanofiber and nanoparticle multiferroics can be characterized.

For the parallel plate capacitor setup, I measured clear changes in the hysteresis loops of Janus nanofibers. The hysteresis loops' changes were not consistent across a single fiber sample, i.e. different fiber chains in the same sample or different parallel plate setups. The parallel plate capacitor samples also presented their own difficulties due to the sample's glass thickness compared to the coplanar samples. This setup produced evidence of a non-hysteretic coupling between the BTO and CFO phases that decreased with multiple voltage applications. The parallel plate capacitor setup was able to show coupling between Janus nanofibers, even though a coupling constant could not be extracted. With improvement to the sample holder, a new gaussmeter with better resolution, and systematic noise reduction, this method should be able to extract a coupling constant.

The coplanar electrodes applied the electric field along the length of the nanofiber, which according to the literature, is more advantageous for measuring the ME coupling. However, this setup's inherent drawback is that the electrodes are farther away from the fiber than the parallel plate, either 1 mm or 240 μm. Closer electrodes or connected electrodes could be made in the future with the new NanoFrazor, that the Smart State Center for Experimental Nanoscale Physics acquired in 2020, but this was beyond the time constraints of this work. The coplanar setup confirmed that the Janus nanofibers' changes are not observed in pure CFO nanofibers. CFO nanofibers never showed changes in Kerr rotation and coercivity that were outside of the setup's noise limit.

The Janus nanofibers measured with their long axes parallel to the external magnetic field (x_1) showed more square hysteresis loops, indicative of an easy magnetic axis.The magnetoelectric coupling in this geometry was weak, but it was greater than the noise. The Kerr rotation in this geometry did show a large non-hysteretic

increase. It should be noted that measuring MOKE in this direction produced less in-plane scattered light, making it more challenging to measure than the typical geometry. Future work should be done to further confirm that the coupling in this geometry is less than the perpendicular geometry.

The coplanar setup did show some interesting dynamics in a handful of fibers, the most interesting being the collapse of the hysteresis loop. The collapse happened in a few samples, and although repeatable in the same sample, it was a rare effect. Of note, these fibers were typically closer to one of the electrodes. With smaller coplanar electrodes and a smaller gap, this effect should become more likely. The coplanar geometry produces a non-uniform electric field, so it is difficult to make concrete statements about the electric field a fiber chain is experiencing. Still, it is clear that there is a stress-induced magnetoelectric effect. Unlike the parallel plate capacitor, the electric field in the coplanar geometry can change over the length of a fiber chain. It is, therefore, surprising that coherent changes in the chain's magnetization could be observed.

8.3 Conclusion

In conclusion, multiferroic Janus nanofibers were probed using VSM, magnetic-driven chaining, and MOKE to confirm that they exhibit a magnetoelectric effect. First, using a VSM, the magnetization temperature dependence proved a good initial test to verify that the BTO and CFO are coupled. The magnetic chaining results showed that these fibers do not follow diffusion-limited chaining models like nanoparticles and have magnetic-dependent scaling parameters. The magnetoelectric chaining data showed that the ME coupling was too small to be observed in the chaining dynamics. ScMOKE has proved to be a versatile way to probe multiferroic nanofibers' magnetics, but further modifications will need to be made to obtain a clear ME coupling value. The most obvious next step for those measuring multiferroic nanofibers with MOKE

is to make direct electrical contacts. FORC showed a split in the reversal curves, but the two runs are too noisy to obtain a FORC diagram at the moment. Further studies will show how the voltage affects the interparticle interactions that FORC can measure. This project has laid the groundwork for further studies of composite multiferroic nanomaterials that moves beyond the need for thin-film heterostructures.

Bibliography

[1] B.D. Cullity and C.D. Graham. *Introduction to Magnetic Materials*. Wiley, 2009.

[2] John David Jackson. *Classical electrodynamics*. Wiley, New York, NY, 2nd edition, 1975.

[3] D.J. Griffiths. *Introduction to Electrodynamics*. Prentice Hall, 1999.

[4] R. M. Bozorth, Elizabeth F. Tilden, and Albert J. Williams. Anisotropy and magnetostriction of some ferrites. *Physical Review*, 99(6):1788–1798, 1955.

[5] Chinchun Ooi and Benjamin B. Yellen. Field Gradients Can Control the Alignment of Nanorods. *Langmuir*, 24(16):8514–8521, aug 2008.

[6] Carlos M. Hangarter and Nosang V. Myung. Magnetic alignment of nanowires. *Chemistry of Materials*, 17(6):1320–1324, 2005.

[7] Randall M. Erb, Melissa D. Krebs, Eben Alsberg, Bappaditya Samanta, Vincent M. Rotello, and Benjamin B. Yellen. Beyond diffusion-limited aggregation kinetics in microparticle suspensions. *Physical Review E - Statistical, Nonlinear, and Soft Matter Physics*, 80(5):1–7, 2009.

[8] Joanne H. E. Promislow, Alice P. Gast, and Marc Fermigier. Aggregation kinetics of paramagnetic colloidal particles. *The Journal of Chemical Physics*, 102(13):5492–5498, apr 1995.

[9] Marc Fermigier and Alice P. Gast. Structure Evolution in a Paramagnetic Latex Suspension. *Journal of Colloid and Interface Science*, 154(2):523–539, 1992.

[10] Jozef Černák, Geir Helgesen, and Arne T. Skjeltorp. Aggregation dynamics of nonmagnetic particles in a ferrofluid. *Physical Review E - Statistical, Nonlinear, and Soft Matter Physics*, 70(3 1):1–8, 2004.

[11] P. Domínguez-García, Sonia Melle, J. M. Pastor, and M. A. Rubio. Scaling in the aggregation dynamics of a magnetorheological fluid. *Physical Review E - Statistical, Nonlinear, and Soft Matter Physics*, 76(5):1–13, 2007.

[12] Jordi Faraudo, Jordi S. Andreu, Carles Calero, and Juan Camacho. Predicting the Self-Assembly of Superparamagnetic Colloids under Magnetic Fields. *Advanced Functional Materials*, 26(22):3837–3858, jun 2016.

[13] Paul Meakin, Tamas Vicsek, and Fereydoon Family. Dynamic cluster-size distribution in cluster-cluster aggregation: Effects of cluster diffusivity. *Physical Review B*, 31(1):564–569, 1985.

[14] Colin P. Reynolds, Kira E. Klop, François A. Lavergne, Sarah M. Morrow, Dirk G A L Aarts, and Roel P A Dullens. Deterministic aggregation kinetics of superparamagnetic colloidal particles. *The Journal of Chemical Physics*, 143(21):214903, dec 2015.

[15] Robert M. Ziff, E. D. McGrady, and Paul Meakin. On the validity of Smoluchowski's equation for cluster–cluster aggregation kinetics. *The Journal of Chemical Physics*, 82(11):5269–5274, jun 1985.

[16] Rui Cheng, Lu Zhu, Weijie Huang, Leidong Mao, and Y.-P. Zhao. Dynamic Scaling of Ferromagnetic Micro-rod Clusters under a Weak Magnetic Field. *Soft Matter*, 12:8440–8447, 2016.

[17] M.-Carmen Miguel and R. Pastor-Satorras. Kinetic growth of field-oriented chains in dipolar colloidal solutions. *Physical Review E*, 59(1):826–834, jan 1999.

[18] JitKang Lim, David X. Tan, Frederick Lanni, Robert D. Tilton, and Sara A. Majetich. Optical imaging and magnetophoresis of nanorods. *Journal of Magnetism and Magnetic Materials*, 321(10):1557–1562, may 2009.

[19] Miyazima, Meakin, and Family. Aggregation of oriented anisotropic particles. *Physical review. A, General physics*, 36(3):1421–1427, aug 1987.

[20] Tamás Vicsek and Fereydoon Family. Dynamic scaling for aggregation of clusters. *Physical Review Letters*, 52(19):1669–1672, 1984.

[21] Ce Wen Nan, M. I. Bichurin, Shuxiang Dong, D. Viehland, and G. Srinivasan. Multiferroic magnetoelectric composites: Historical perspective, status, and future directions. *Journal of Applied Physics*, 103(3), 2008.

[22] G Lawes and G Srinivasan. Introduction to magnetoelectric coupling and multiferroic films. *Journal of Physics D: Applied Physics*, 44(24):243001, 2011.

[23] Jennifer S. Andrew, Justin D. Starr, and Maeve A K Budi. Prospects for nanostructured multiferroic composite materials. *Scripta Materialia*, 74:38–43, 2014.

[24] Manfred Fiebig. Revival of the magnetoelectric effect. *Journal of Physics D: Applied Physics*, 38(8):R123–R152, 2005.

[25] C. L. Zhang, W. Q. Chen, S. H. Xie, J. S. Yang, and J. Y. Li. The magnetoelectric effects in multiferroic composite nanofibers. *Applied Physics Letters*, 94(10), 2009.

[26] Bi Fu, Ruie Lu, Kun Gao, Yaodong Yang, and Yaping Wang. Magnetoelectric coupling in multiferroic BaTiO 3 -CoFe 2 O 4 composite nanofibers via electrospinning. *EPL (Europhysics Letters)*, 111(1):17007, jul 2015.

[27] Gollapudi Sreenivasulu, Maksym Popov, Ferman A. Chavez, Sean L. Hamilton, Piper R. Lehto, and Gopalan Srinivasan. Controlled self-assembly of multiferroic core-shell nanoparticles exhibiting strong magneto-electric effects. *Applied Physics Letters*, 104(5), 2014.

[28] Haribabu Palneedi, Venkateswarlu Annapureddy, Shashank Priya, and Jungho Ryu. Status and Perspectives of Multiferroic Magnetoelectric Composite Materials and Applications. *Actuators*, 5(1):9, 2016.

[29] C. Kittel. *Introduction to solid state physics*. Wiley, 1986.

[30] Matthew J. Bauer, Xiao Wen, Prabal Tiwari, David P. Arnold, and Jennifer S. Andrew. Magnetic field sensors using arrays of electrospun magnetoelectric Janus nanowires. *Microsystems & Nanoengineering*, 4(1):37, dec 2018.

[31] M M Vopson, Y K Fetisov, G Caruntu, and G Srinivasan. Measurement Techniques of the Magneto-Electric Coupling in Multiferroics. *Materials*, 10(8):963, aug 2017.

[32] Morad Etier, Vladimir V. Shvartsman, Soma Salamon, Yanling Gao, Heiko Wende, and Doru C. Lupascu. The Direct and the Converse Magnetoelectric Effect in Multiferroic Cobalt Ferrite-Barium Titanate Ceramic Composites. *Journal of the American Ceramic Society*, 99(11):3623–3631, nov 2016.

[33] G. Sreenivasulu, Maksym Popov, Ru Zhang, K. Sharma, C. Janes, A. Mukundan, and G. Srinivasan. Magnetic field assisted self-assembly of ferrite-ferroelectric core-shell nanofibers and studies on magneto-electric interactions. *Applied Physics Letters*, 104(5):052910, feb 2014.

[34] Justin D. Starr, Maeve A K Budi, and Jennifer S. Andrew. Processing-property relationships in electrospun Janus-type biphasic ceramic nanofibers. *Journal of the American Ceramic Society*, 98(1):12–19, 2015.

[35] Avinash Baji, Yiu-Wing Mai, Rattikorn Yimnirun, and Sujitra Unruan. Electrospun barium titanate/cobalt ferrite composite fibers with improved magnetoelectric performance. *RSC Adv.*, 4:55217–55223, 2014.

[36] Jacob L. Jones, Justin D. Starr, and Jennifer S. Andrew. Anisotropy in magnetoelectric composites. *Applied Physics Letters*, 104(24):10–14, 2014.

[37] Giap V. Duong, R. Groessinger, M. Schoenhart, and D. Bueno-Basques. The lock-in technique for studying magnetoelectric effect. *Journal of Magnetism and Magnetic Materials*, 316(2 SPEC. ISS.):390–393, 2007.

[38] H S HELE-SHAW. The Flow of Water. *Nature*, 58(1489):34–36, 1898.

[39] Johannes Schindelin, Ignacio Arganda-Carreras, Erwin Frise, Verena Kaynig, Mark Longair, Tobias Pietzsch, Stephan Preibisch, Curtis Rueden, Stephan Saalfeld, Benjamin Schmid, Jean-Yves Tinevez, Daniel James White, Volker Hartenstein, Kevin Eliceiri, Pavel Tomancak, and Albert Cardona. Fiji: an open-source platform for biological-image analysis. *Nature Methods*, 9(7):676 – 682, 2012.

[40] P. Domínguez-García and M. A. Rubio. JChainsAnalyser: an ImageJ-based stand-alone application for the study of magneto-rheological fluids. *Computer Physics Communications*, 180(10):1956–1960, 2009.

[41] Z Q Qiu and S. D. Bader. Surface magneto-optic Kerr effect. *Review of Scientific Instruments*, 71(3):1243–1255, mar 2000.

[42] Robert P. Hunt. Magneto-optic scattering from thin solid films. *Journal of Applied Physics*, 38(4):1652–1671, 1967.

[43] D. Kliger, J. Lewis, and C. Randall. *Polarized light in optics and spectroscopy.* Academic Press., 1990.

[44] Chun-Yeol You and Sung-Chul Shin. Generalized analytic formulae for magneto-optical Kerr effects. *Journal of Applied Physics*, 84(1):541–546, jul 1998.

[45] DA Allwood, G Xiong, MD Cooke, and RP Cowburn. Magneto-optical Kerr effect analysis of magnetic nanostructures. *J. Phys. D: Appl. Phys.*, 36(18):2175, 2003.

[46] Cory Dolbashian, B L Chavez, Matt Bauer, Maeve Budi, Jennifer S Andrew, and Thomas M Crawford. Magnetic properties of aligned multiferroic Janus nanofiber agglomerates measured with the scattered magneto-optical Kerr effect. *Journal of Physics D: Applied Physics*, 53(19):195002, may 2020.

[47] Cory Dolbashian. *What Can Scattered Light Tell you about your favorite Magnetic Material?: A magneto optical investigation of the magnetic properties of aligned Janus Fiber Agglomerates*. PhD thesis, University of South Carolina, 2020.

[48] H C van de Hulst. Light scattering by small particles, 1957.

[49] Hong Guo Zhang, Yu Jie Zhang, Weng Hong Wang, and Guang Heng Wu. Origin of the constricted hysteresis loop in cobalt ferrites revisited. *Journal of Magnetism and Magnetic Materials*, 2011.

[50] L Clime, A Stancu, P Ciureanu, and A Yelon. FIRST ORDER REVERSAL CURVES DIAGRAM DEDUCED BY A SHEPARD METHOD FOR BIVARIATE INTERPOLATION OF SCATTERED DATA. *Journal of Optoelectronics and Advanced Materials*, 6(3):1005 – 1008, 2004.

[51] Edward Della Torre, John Oti, and György Kádár. Preisach Modeling and Reversible Magnetization. *IEEE Transactions on Magnetics*, 26(6):3052–3058, 1990.

[52] I.D. Mayergoyz. Mathematical Models of Hysteresis. *Phys Rev Lett*, 56(15), 1986.

[53] C R Pike, C A Ross, R T Scalettar, and G Zimanyi. First-order reversal curve diagram analysis of a perpendicular nickel nanopillar array. *Physical Review B*, 71(13):134407, apr 2005.

[54] Andrew P. Roberts, David Heslop, Xiang Zhao, and Christopher R. Pike. Understanding fine magnetic particle systems through use of first-order reversal curve diagrams. *Reviews of Geophysics*, 52(4):557–602, dec 2014.

[55] Fanny Béron, Andreas Kaidatzis, Murilo F Velo, Luis C C Arzuza, Ester M Palmero, Rafael P. del Real, Dimitrios Niarchos, Kleber R Pirota, and

José Miguel García-Martín. Nanometer Scale Hard/Soft Bilayer Magnetic Antidots. *Nanoscale Research Letters*, 11(1):86, dec 2016.

[56] F. Beron, Liviu Clime, Mariana Ciureanu, D. Menard, R.W. Cochrane, and Arthur Yelon. First-Order Reversal Curves Diagrams of Ferromagnetic Soft Nanowire Arrays. *IEEE Transactions on Magnetics*, 42(10):3060–3062, oct 2006.

[57] Andrew P. Roberts, Christopher R. Pike, and Kenneth L. Verosub. First-order reversal curve diagrams: A new tool for characterizing the magnetic properties of natural samples. *Journal of Geophysical Research: Solid Earth*, 105(B12):28461–28475, dec 2000.

[58] Franco Jona and G Shirane. *Ferroelectric crystals*. International series of monographs on solid state physics. Oxford, 1962.

[59] Jing Ma, Yuanhua Lin, and C. W. Nan. Anomalous electric field-induced switching of local magnetization vector in a simple FeBSiC-on-Pb(Zr,Ti)O 3 multiferroic bilayer. *Journal of Physics D: Applied Physics*, 43(1):012001, jan 2010.

[60] Yi Zhang, Jing Liu, X. H. Xiao, T. C. Peng, C. Z. Jiang, Y. H. Lin, and C. W. Nan. Large reversible electric-voltage manipulation of magnetism in NiFe/BaTiO 3 heterostructures at room temperature. *Journal of Physics D: Applied Physics*, 43(8):082002, mar 2010.

[61] Giovanni Vinai, Barbara Ressel, Piero Torelli, Federico Loi, Benoit Gobaut, Regina Ciancio, Barbara Casarin, Antonio Caretta, Luca Capasso, Fulvio Parmigiani, Francesco Cugini, Massimo Solzi, Marco Malvestuto, and Roberta Ciprian. Giant magneto–electric coupling in 100 nm thick Co capped by ZnO nanorods. *Nanoscale*, 10(3):1326–1336, 2018.

[62] Jing Ma, Jiamian Hu, Zheng Li, and Ce-Wen Nan. Recent Progress in Multiferroic Magnetoelectric Composites: from Bulk to Thin Films. *Advanced Materials*, 23(9):1062–1087, mar 2011.

[63] J. Irwin, S. Lindemann, W. Maeng, J. J. Wang, V. Vaithyanathan, J. M. Hu, L. Q. Chen, D. G. Schlom, C. B. Eom, and M. S. Rzchowski. Magnetoelectric Coupling by Piezoelectric Tensor Design. *Scientific Reports*, 9(1):19158, dec 2019.

[64] C L Zhang, W Q Chen, J Y Li, and J S Yang. One-dimensional equations for piezoelectromagnetic beams and magnetoelectric effects in fibers. *Smart Materials and Structures*, 18(9):095026, 2009.

Appendix A

MOKE Reference Data

This Appendix has some important reference data.

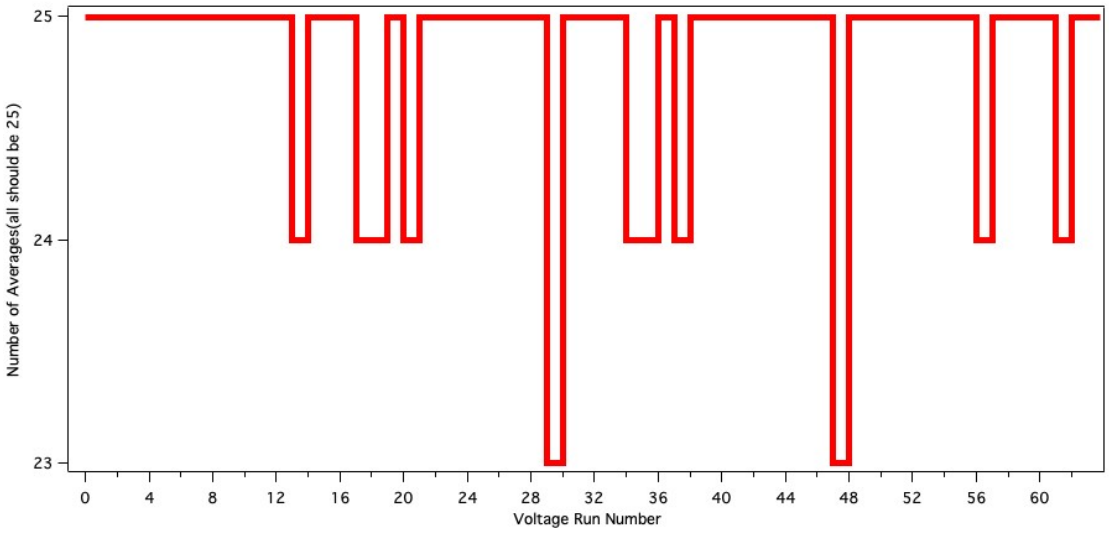

Figure A.1 Missed Trigger: Measuring Voltage and checking how many missed triggers to the oscilloscope happened. This data was used in the averaging of the MOKE data.

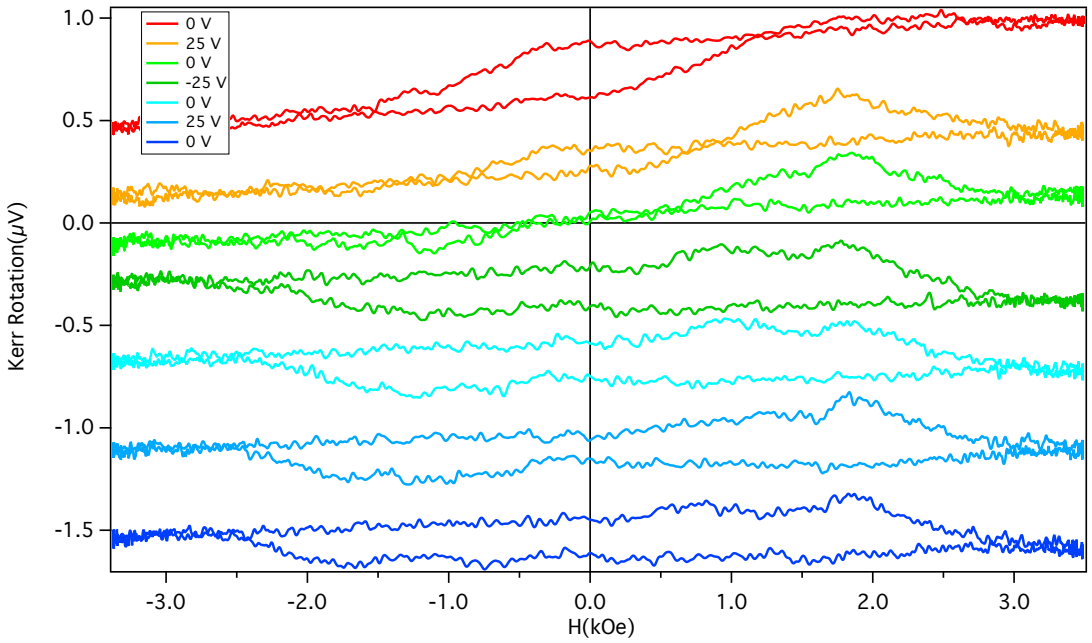

Figure A.2 MEMOKE Collapse: This shows a collapsing then expanding hysteresis loop that happened in a particular nanofiber. This exemplifies the difficulties in knowing how the stress is changing the magnetization of the CFO.

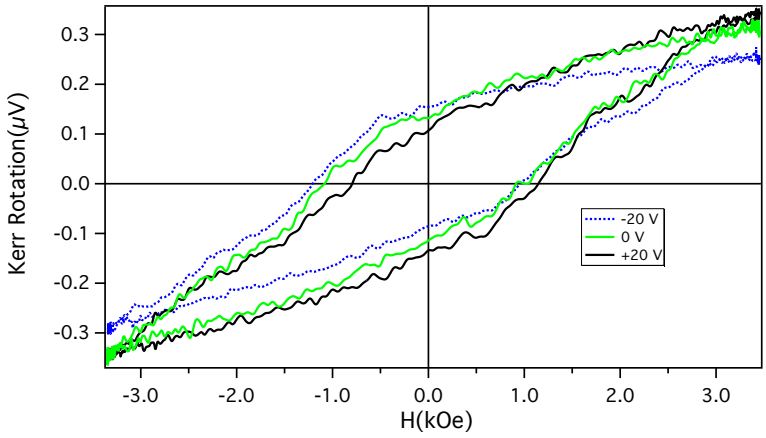

(a)

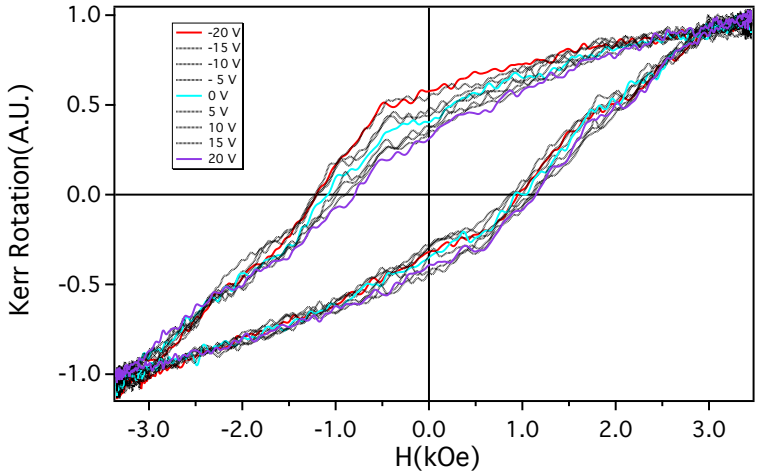

(b)

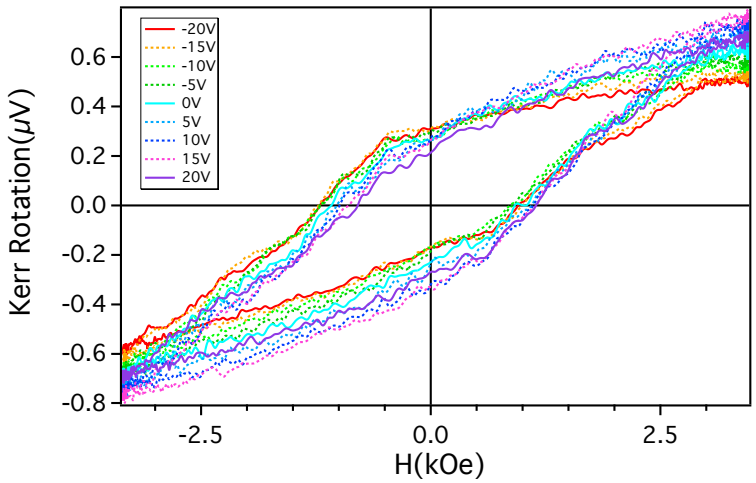

(c)

Figure A.3 Stress Hysteresis Loops: This shows the stress induced changes in a coplanar fiber oriented in the x_3 direction, a) is the ±20V and 0V, b) is the normalized curves, c) is the full Kerr rotations showing the smearing of the hysteresis loop.

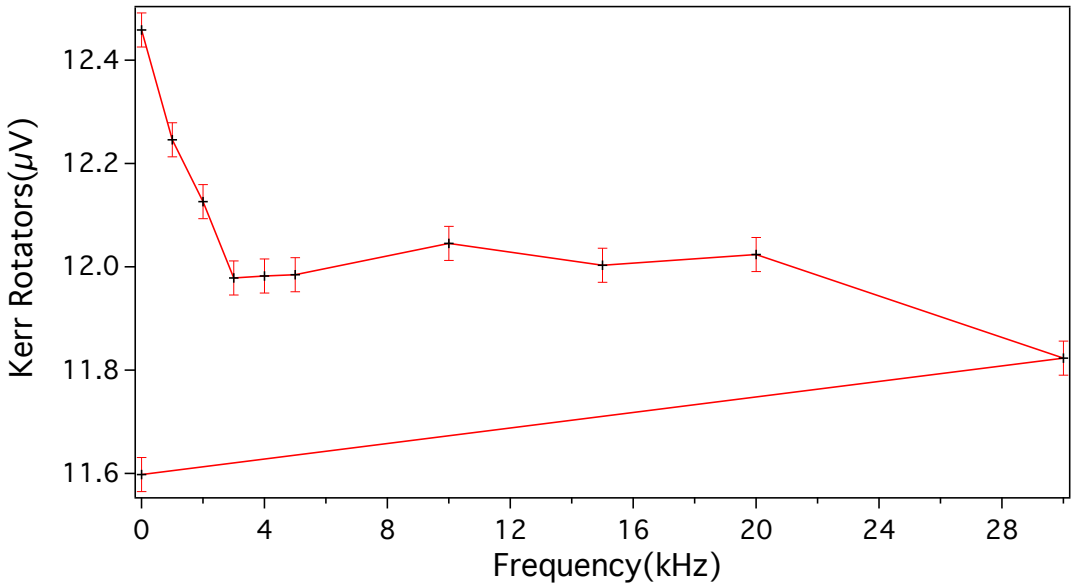

Figure A.4 Kerr Rotation Change at Different Applied Voltage Frequencies: This shows the Kerr rotation change due to an applied AC sine wave at 1Vpp and various Frequencies. Though there appears to be a change, the sample became discolored after the highest frequencies. I am not able to conclusively say what these changes are from.

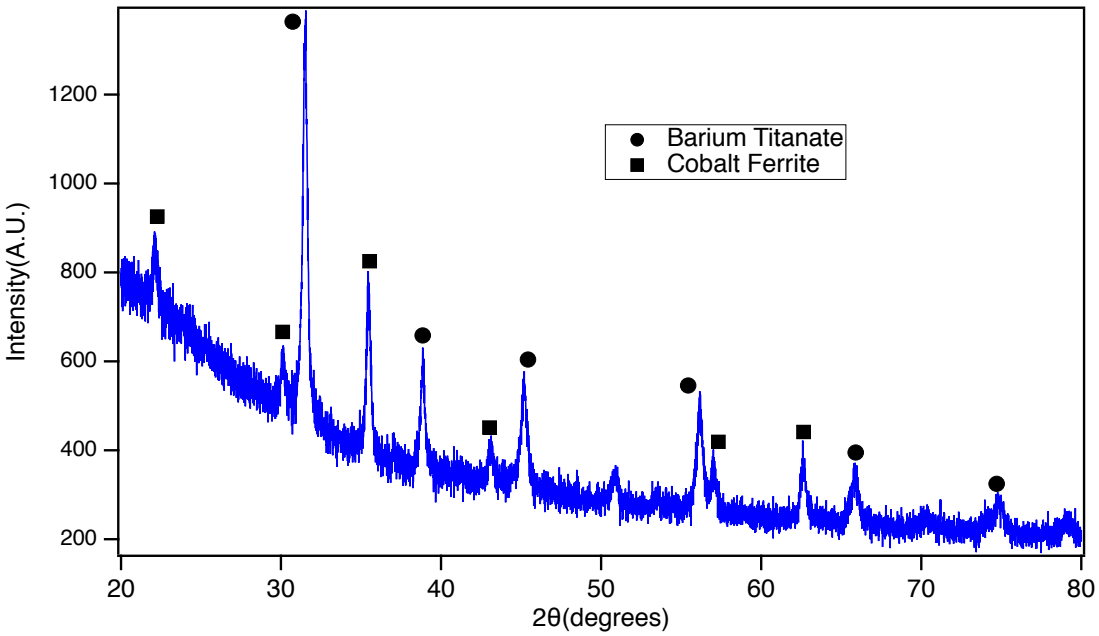

Figure A.5 XRD Data on Janus Fibers: This shows the XRD data taken on the Janus nanofibers confirming the presence of BTO and CFO.

Appendix B

Initial FORC Curves

In this appendix is the initial data on FORC curves run on the same fiber. The number of reversals was 150 but only 135 reversals are shown. The voltages applied are 0 and 25V in the coplanar geometry.

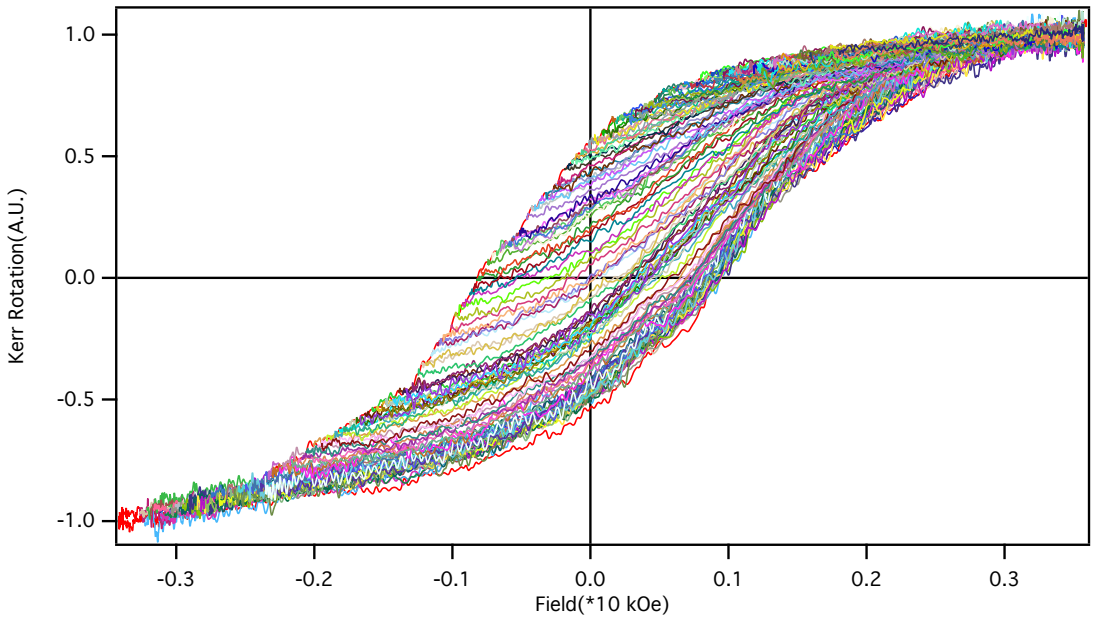

Figure B.1 First FORC Run: This FORC run was done on a nanofiber in the coplanar geometry and had 150 reversals and 0 V was applied.

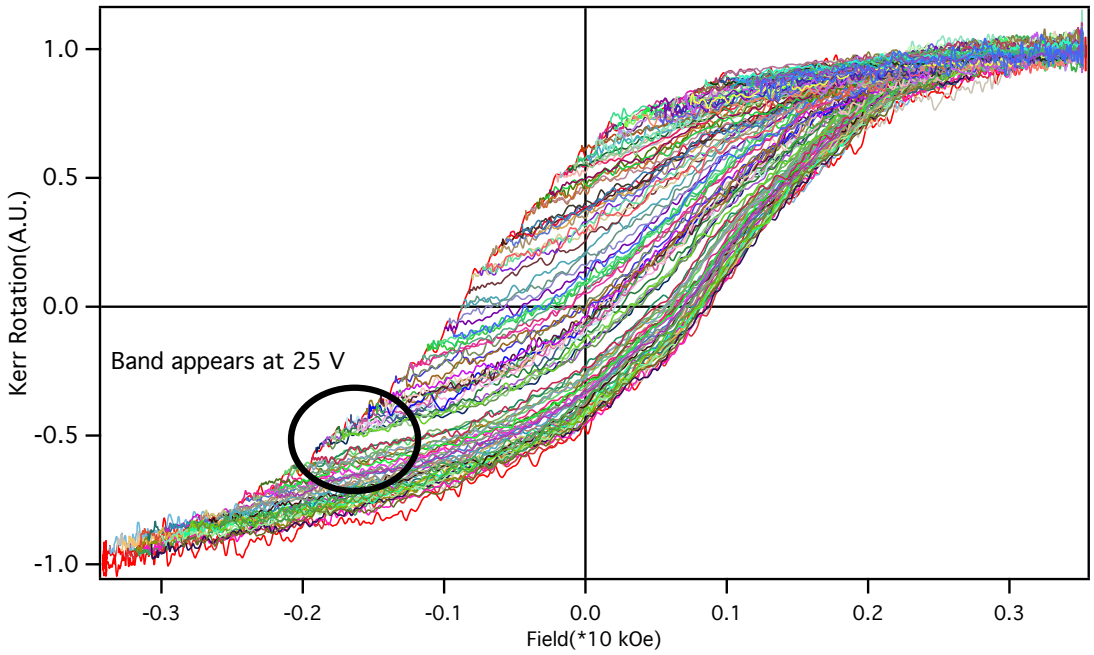

Figure B.2 Second FORC Run: This FORC run was done on a nanofiber in the coplanar geometry and had 150 reversals and 25 V was applied. This shows indications that there will be splitting in the curves.

Appendix C

Procedure for suspending Janus Nanofibers

Dispersant solution for Janus nanofibers:

1. 20ml DI water
2. Add Janus nanowires
3. Add 4.64mg citric acid
4. Heat to 80°C for 2h
5. Let cool
6. Add 54μL 0.1M NaOH to raise pH to $\approx$10
7. Add polyvinyl(alcohol) to achieve desired viscosity (around 50mg works to disperse nanowires for $\approx$45min)

PVA Solution Materials:

- 0.25g PVA
- 10mL DI water
- Water bath
- Magnetic stir bar
- Magnetic stir/hot plate
- Paper clip

- Themometer

PVA Procedure:

1. Add 0.25g PVA, 10mL DI water, and magnetic stir bar in a scintillation vial; mark the water level on the outside of the vial with a sharpie.

2. Unfold the paper clip and add it to the water bath; place water bath on hot plate

3. Suspend the vial in the water bath, making sure that water level of the bath is equal or greater than the water level of the vial.

4. Turn on the stir rate and increase as high as possible while maintaining uniform mixing in the vial

5. Increase the heat until the water bath is just below boiling(90-100°C)

6. At just below boiling the solution will take approximately 3 hours for the PVA to fully dissolve, at 90°C the solution will take at least 5 hours, sometimes more.

7. Keep an eye on the water line of the water bath and PVA solution; refill the water in both as needed.

8. Once the PVA is fully dissolved remove the vial from the heat and allow too cool. Then filter the PVA solution.

Appendix D

Magnetic Chaining and Image Analysis Code

In this section is all my code for using ImageJ and a simplified code for transforming the data before fitting is done.

General Image procedure:

1. Contrast
2. Kuwahara Filtering
3. Smooth
4. Find Edges
5. Invert
6. Otsu Threshold
7. Convert to Binary
8. Fill holes
9. Erode
10. Visual Check in original
11. Analyze Particles

D.1 ImageJ processing macro

```
macro "Chaining"{
        run("Kuwahara␣Filter", "sampling=5␣stack");
        run("Smooth", "stack");
        run("Find␣Edges", "stack");
        run("Invert", "stack");
        setAutoThreshold("Otsu");
        //run("Threshold...");
        setOption("BlackBackground", false);
        run("Convert␣to␣Mask", "method=Otsu␣background=Light␣calculate");
        run("Fill␣Holes", "stack");
        run("Erode", "stack");
        run("Analyze␣Particles...", "size=8.19-Infinity␣display␣exclude␣
            clear␣summarize␣stack");
}
```

D.2 IgorPro Code for Chaining Data

```
#pragma rtGlobals=3          // Use modern global access method and strict
    wave access.


Function st2(dibs, dwav)
        wave dibs
        wave dwav
        string name
        string name2
        string name3
        string name4
```

```
string name5
make/O stt
make/O Lst
make/O Lt
make/O rmst
make/O Llt
variable x, y, z
variable i = 0
name = "stt" + nameofwave(dwav)
name2 = "lst" + nameofwave(dwav)
name3 = "Lt" + nameofwave(dwav)
name4 = "rmst" + nameofwave(dwav)
name5 = "LogLt" + nameofwave(dwav)

z = numpnts(dibs)

for(x = 0; x<z; x+=2)
       wavestats/Q/R=[dibs[x],dibs[x]+dibs[x+1]] dwav
              if(i> 127)
                     InsertPoints i, 1, stt
                     InsertPoints i, 1, lst
                     InsertPoints i, 1, Lt
                     InsertPoints i, 1, rmst
                     insertPoints i, 1, Llt
              endif

         stt[i] = ((V_rms)^2)/V_avg
         lst[i] = log(stt[i])
         Lt[i] = V_avg
```

```
                Llt[i] = log(V_avg)
                rmst[i]= V_rms
                i +=1
        endfor

        Rename stt, $name
        Rename lst, $name2
        Rename Lt, $name3
        Rename rmst, $name4
        rename Llt, $name5
End
```

Appendix E

ME Microscope Power Supply Control Code

E.1 Voltage and Current Control Code

```
@author: bryanchavez
This program controls the voltage, current and frequency of the system
   , note you are programming in python but then controlling in VISA
   Basic"""
import pyqtgraph as pg
#import numpy as np
import time
import FreqCont as fc
import SetField as sf
import SetVolt as sv
import VoltageArrayBuilder as VAB
import sys

from PyQt5 import QtCore, QtGui, uic, QtWidgets
from PyQt5.QtCore import pyqtSlot



pg.setConfigOption('background', 'w')
pg.setConfigOption('foreground', 'k')
qtCreatorFile = "MEMicro.ui" # Enter file here.

Ui_MainWindow, QtBaseClass = uic.loadUiType(qtCreatorFile)

class MEMicro(QtWidgets.QMainWindow, Ui_MainWindow):
    def __init__(self):
        QtWidgets.QMainWindow.__init__(self)
        Ui_MainWindow.__init__(self)
        self.setupUi(self)
        self.CurrSweep.clicked.connect(self.FieldSweep2)
        self.MagSweep.clicked.connect(self.FieldSweep)
        self.SetCurr.clicked.connect(self.SetCur2)
        self.SetV.clicked.connect(self.SetVolt2)
        self.SetMag.clicked.connect(self.SetMagTo)
        self.MERun.clicked.connect(self.MERuns)
        self.setFree.clicked.connect(self.SetF)

    @pyqtSlot()
```

```
def FieldSweep2(self):
    C = self.Curr.value()
    Step2 = self.Step.value()
    Carray = VAB.VoltArray2(C, Step2)
    N = len(Carray)
    i = 0

    #print(len(Carray))
    while i < N:
        sf.SetCur(Carray[i])
        i +=1
        time.sleep(0.3)
    return

@pyqtSlot()
def SetCur2(self):
    sf.SetCur(self.Amp.value())
    return
@pyqtSlot()
def SetVolt2(self):
    sv.SetVolt(self.Volt.value())
    return

@pyqtSlot()
def SetMagTo(self):
    sf.SetField(self.ConMag.value())
    return

@pyqtSlot()
def FieldSweep(self):
    H = self.MagField.value()
    Step1 = self.Step.value()
    Harray = VAB.VoltArray2(H, Step1)
    N = len(Harray)
    i = 0
    #print(len(Harray))
    while i < N:
        sf.SetField(Harray[i])
        time.sleep(0.3)
        i +=1
    return

@pyqtSlot()
def MERuns(self):
    if self.DCBut.isChecked():
        sf.SetField(self.ConMag.value())
        sv.SetVolt(self.Volt.value())
    elif self.ACBut.isChecked():
        sf.SetField(self.ConMag.value())
        fc.SetFreq(self, self.Free.value(), self.Volt.value())
    return
@pyqtSlot()
```

```
    def SetF(self):
        fc.SetFreq(self,self.Free.value(), 1)
        return

if __name__ == "__main__":
    def run_app():
        app = QtWidgets.QApplication(sys.argv)
        window = MEMicro()
        window.show()
        app.exec_()
    run_app()
```

E.2 Magnetic Field Measurement Code

```
@author: bryanchavez
This program measures the magnetic field using a Hall probe"""
import pyqtgraph as pg
import numpy as np
import MultiM as MM
#import matplotlib.pyplot as plt
#from scipy import stats
#import pyqtgraph as pg
import sys
from PyQt5 import QtCore, QtGui, uic, QtWidgets
from PyQt5.QtCore import pyqtSlot

pg.setConfigOption('background', 'w')
pg.setConfigOption('foreground', 'k')
qtCreatorFile = "PlotField.ui" # Enter file here.

Ui_MainWindow, QtBaseClass = uic.loadUiType(qtCreatorFile)

class MeField(QtWidgets.QMainWindow, Ui_MainWindow):
    N=1
    def __init__(self):
        QtWidgets.QMainWindow.__init__(self)
        Ui_MainWindow.__init__(self)
        self.setupUi(self)
        self.TakeD.clicked.connect(self.Takedata)
        self.StopB.clicked.connect(self.Stop)
        self.MagGraph.setLabels(title='Magnetic Field vs Time',left='
           Magnetic Field(Gauss)',bottom='time(a.u.)')
        self.MagField.setText("0")
        self.zero = MM.Zero(10)
        #print(self.zero)

    @pyqtSlot()
    def Takedata(self):
        MeField.N = 1
        b = self.zero
        self.data = [MM.Averages(10, b)]
```

```
        self.curve = self.MagGraph.getPlotItem().plot(symbol='o')
        self.timer = QtCore.QTimer()
        self.timer.timeout.connect(self.updater)
        self.timer.start(0)

    def updater(self):
        b = self.zero
        self.data.append(MM.Averages(3,b))
        self.curve.setData(self.data)
        dat = np.around(self.data[MeField.N],decimals=2)
        self.MagField.setText(str(dat))
        MeField.N+=1

    @pyqtSlot()
    def Stop(self):
        self.timer.stop()
        self.data = [0]
        self.curve.setData(self.data)

if __name__ == "__main__":
    def run_app():
        #QtWidgets.QApplication.setGraphicsSystem("raster")
        app = QtWidgets.QApplication(sys.argv)
        window = MeField()
        window.show()
        app.exec_()

    run_app()
```

E.3 Miscellaneous Subroutines

```
@author: bryanchavez
SetField Subroutine"""
import visa
import numpy as np

rm = visa.ResourceManager()
res = rm.list_resources()
gpib1 = res.index('GPIB0::5::INSTR')
inst = rm.open_resource(res[gpib1])
#print(res)
inst.write("VOLT:RANG P8V")
inst.write("VOLT:LEV 8")
inst.query("MEAS:CURR:DC?")


def SetField(H_):

    Mag = H_       #Magnetic field
    Cur = Mag/15.081  #Scaling factor for current
```

```
    #print(inst.query("MEASure:VOLTage:DC?")) #Check Voltage
    #inst.write("VOLT:RANG P8V") # Select +8V output
    #inst.write("VOLT:PROT:MAX")
    #inst.write("VOLT:LEV 8") #Set Voltage Limit to 8, important to
       run in current mode
    inst.write("CURR " + str(Cur)) # Set output current to num
    inst.write("OUTP ON")
    #inst.query("MEAS:CURR:DC?")

    return

def SetCur(Cur_):
    Cur = Cur_
    #inst.write("VOLT:RANG P8V") # Select +8V output
    #inst.write("VOLT:PROT:MAX")
    #inst.write("VOLT:LEV 8") #Set Voltage Limit to 8, important to
       run in current mode
    inst.write("CURR " + str(Cur)) # Set output current to num
    inst.write("OUTP ON")
    #inst.query("MEAS:CURR:DC?")
    return

def TOF():    #Turn off all outputs
    inst.write("APPL 0, 0")
    return

def Controls():   #Check and measure
    print(res)
    print(inst.query("MEAS:VOLT:DC?"))
    print(inst.query("MEAS:CURR:DC?"))
    print(inst.query("SYST:ERR?"))
    print(inst.query("VOLT:PROT?"))
    return

def Cur(Amp_):    #Set current
    inst.write("VOLT:RANG P8V")
    inst.write("VOLT:LEV 8")
    inst.write("CURR " + str(Amp_))
    inst.write("OUTP ON")
    print(inst.query("MEAS:CURR:DC?"))
    #inst.write("APPL 0,2")
    return

@author: bryanchavez
MultiM measurement subroutines"""
import visa
import time
import numpy as np

rm = visa.ResourceManager()
res = rm.list_resources()
```

```
print(res)
#gpib3 = res.index('USB0::0x0957::0x0607::MY47008195::INSTR')
#gpib4 = res.index('USB0::0x0957::0x0407::MY44038282::INSTR')
#usb2 = res.index('USB0::0x0957::0x0607::MY47013291::INSTR')
usb3 = res.index('USB0::0x0957::0x0607::MY47008220::INSTR')
#print(usb2)

#measF = rm.open_resource(res[usb2])
meas = rm.open_resource(res[usb3])

def Averages(Av_,zero_):

    Av = Av_ #probably need to add a wait
    a = 0
    N = 0

    while N < Av_:
        a = float(meas.query("MEAS:CURR:DC?")) + a
        #print(a)
        N+=1
        time.sleep(0.03)

    #print(a)
    b = a/Av
    b = b - zero_
    mf = b*(-1)*(218.75)
    #print(b)
    #print(meas.query("MEAS:VOLT:DC?"))
    return mf

def Zero(Av_):

    Av = Av_ #probably need to add a wait
    a = 0
    N = 0

    while N < Av_:
        a = float(meas.query("MEAS:VOLT:DC?")) + a
        #print(a)
        N+=1
        time.sleep(0.03)

    #print(a)
    b = a/Av
    #print(b)
    #print(meas.query("MEAS:VOLT:DC?"))
    return b

def AveF(Av2_):


    #b = measF.query("MEAS:VOLT:DC?")
    AvF = Av2_ #probably need to add a wait
```

```
    a2 = 0
    N2 = 0

    while N2 < AvF:
        #a2 = float(measF.query("MEAS:VOLT:DC?")) + a2
        #print(a)
        N2+=1
        time.sleep(0.18)

    #print(a)
    b2 = a2/AvF
    #print(b)
    #print(meas.query("MEAS:VOLT:DC?"))
    return b2

def AveC(Ac_):

    Ac = Ac_ #probably need to add a wait
    a = 0
    N = 0

    while N < Ac_:
        a = float(meas.query("MEAS:CURR:DC?")) + a
        #print(a)
        N+=1
        time.sleep(0.03)

    #print(a)
    b = a/Ac
    #print(b)
    #print(meas.query("MEAS:VOLT:DC?"))
    return b
```

Appendix F

Igor Pro MOKE Code

MOKE Code Procedure Flow:

1. LoaderOsci(): load files
2. timesize(): resized the waves to proper size
3. badwaves(): find the bad runs that are shifted or missing due to trigger delays
4. deathstroke(): kills all the bad waves after you have checked them
5. voltav(): finds the voltages and makes a reference wave to do averaging
6. massosci(): averages the moke data and puts it into files
7. rotator(): extract Kerr rotations, ie Ms or height of MOKE loop
8. memoke(): extract coercivities and remanence

F.1 Loading Program Properly

```
#pragma rtGlobals=3          // Use modern global access method and
   strict wave access.
#include <Waves Average>
//This program specifically loads from the oscilloscope. The reason
   being is that the namin convention into igor assumes
//a naming convention coming from the osci. We assume that the name
   aloted to the file is followed by 00000.txt which is
//important for naming AND sorting files with this program.
// Make sure there are no lingering files in the root before you start
    this. It will have trouble exiting
//possibly could add a quick loop to put all files in root into a
   temporary folder, then move them back after the program runs???
function LoaderOsci()
```

```
//initialize loop variable
Variable L=0
variable FolderWatch=200
variable Sorter = 0
variable foldersorter=0
variable i=0
variable g=0
string wname,fname          //wave names and file name,
   respectively
String XorY
getfilefolderinfo/D
if (datafolderexists("A_waves")==0)
       newdatafolder/O root:A_waves
endif
if (datafolderexists("B_waves")==0)
       newdatafolder/O root:B_waves
endif
if (datafolderexists("C_waves")==0)
       newdatafolder/O root:C_waves
endif
if (datafolderexists("Timewaves_A")==0)
       newdatafolder/O root:Timewaves_A
endif
       if (datafolderexists("Timewaves_B")==0)
       newdatafolder/O root:Timewaves_B
endif
if (datafolderexists("Timewaves_C")==0)
       newdatafolder/O root:Timewaves_C
endif

newpath/O DataAnalysis S_path
//Create a list of all files that are .txt files in the folder
   . -1 parameter addresses all files.
string filelist= indexedfile(DataAnalysis,-1,"????")
filelist = SortList(filelist, ";", 16)

//Pull the prefix of the first wave, compare each prefix to
   that of the first, if it matches, name it one way, if not
   name the other.
//Begin processing the list
do
       //store the ith name in the list into wname.
       fname = stringfromlist(i,filelist)
  If  (stringmatch(fname ,".DS_Store")==1)
    i=i+1
        Fname = stringfromlist(i,filelist)
  else

            string Timename
        string name
        variable totallength=strlen(fname)
        variable namelengthvariable=0
        L=0
```

```
Do                  //pull the suffix number from the
   first non-zero digit following the name string
   readspot= Fname[totallength-9+L]
                  if (str2num(readspot)!=0)
                         string Suffix= Fname[
                            totallength-9+L,
                            totallength-5]
                  endif
           L+=1
    while(str2num(Readspot)==0)
    if(sorter==0)
                  string matchMeprefix = fname[0,1]
                  string Actualprefix = fname[0,1]
                  sorter+=1
           elseif(sorter!=0)
                  Actualprefix = fname[0,1]
           endif

           if (stringmatch(Actualprefix, "C2")==1)
           name = fname[2,totallength-10]+"_"+Suffix
              +"a"
                Timename="T_"+name

           elseif(stringmatch(Actualprefix, "C3")
              ==1)
                name = fname[2,totallength-10]+"_
                   "+Suffix+"b"  //gootta add 2
                   more indexes here for when i
                Timename="T_"+name //am moving
                   things to folders mid run.
           else
                  name = fname[2,totallength -10] +"
                     _"+Suffix +"c"
                  Timename="T_"+name

           endif
              //used to be linear Time as X axis,
                 now linear magnetic field

             string info=""

             info+="N='"+Timename+"';"
             info += "N='"+name+"';"
             info+= "N='_skip_';N='_skip_';"

                    Loadwave/a/b=info/d/J/Q/P=
                       DataAnalysis stringfromlist(i
                       ,filelist)

                   // if(i==(i+50))
                         print  "Loaded "+fname
                  //  endif
```

```
if(i == folderwatch)
if(i==1600)
print "dookie"
endif
       do
              string overflowlist=WaveList
                 ("*",";","")
              string overflowname =
                 stringfromlist(0,overflowlist)
              wave overflowwave= $overflowname
              if(stringmatch(overflowname[strlen
                 (overflowname)-1],"A")==1&&(
                 stringmatch(overflowname[0],"T
                 ")==0))
                    deletepoints/M=0 0, 5,
                       overflowwave
                    Movewave overflowwave,
                       root:A_waves:
              elseif(stringmatch(overflowname[
                 strlen(overflowname)-1],"B")
                 ==1&&(stringmatch(overflowname
                 [0],"T")==0))
                    deletepoints/M=0 0, 5,
                       overflowwave
                    Movewave overflowwave,
                       root:B_waves:
              elseif(stringmatch(overflowname[
                 strlen(overflowname)-1],"C")
                 ==1&&(stringmatch(overflowname
                 [0],"T")==0))
                    deletepoints/M=0 0, 5,
                       overflowwave
                    Movewave overflowwave,
                       root:C_waves:
              elseif(stringmatch(overflowname
                 [0],"T")==1&&stringmatch(
                 overflowname[strlen(
                 overflowname)-1],"C")==1)
                    deletepoints/M=0 0, 5,
                       overflowwave
                    Movewave overflowwave,
                       root:Timewaves_C:
              elseif(stringmatch(overflowname
                 [0],"T")==1&&stringmatch(
                 overflowname[strlen(
                 overflowname)-1],"B")==1)
                    deletepoints/M=0 0, 5,
                       overflowwave
                    Movewave overflowwave,
                       root:Timewaves_B:
```

```
                                    elseif(stringmatch(overflowname
                                       [0],"T")==1&&stringmatch(
                                       overflowname[strlen(
                                       overflowname)-1],"A")==1)
                                             deletepoints/M=0 0, 5,
                                                overflowwave
                                             Movewave overflowwave,
                                                root:Timewaves_A:

                                    endif

                                while(Countobjectsdfr(root:,1)!=0)

                           folderwatch+=200
                           endif

                  i =i+1                //move to next file
                  endif

         while(i<itemsinlist(filelist))             //end when all
            files are processed.

do
                                 overflowlist=WaveList("*",";","")
                                 overflowname =stringfromlist(0,
                                    overflowlist)
                                 wave overflowwave= $overflowname
                                 if(stringmatch(overflowname[strlen(
                                    overflowname)-1],"A")==1&&(stringmatch
                                    (overflowname[0],"T")==0))
                                             deletepoints/M=0 0, 5,
                                                overflowwave
                                             Movewave overflowwave,
                                                root:A_waves:
                                    elseif(stringmatch(overflowname[
                                       strlen(overflowname)-1],"B")
                                       ==1&&(stringmatch(overflowname
                                       [0],"T")==0))
                                             deletepoints/M=0 0, 5,
                                                overflowwave
                                             Movewave overflowwave,
                                                root:B_waves:
                                    elseif(stringmatch(overflowname[
                                       strlen(overflowname)-1],"C")
                                       ==1&&(stringmatch(overflowname
                                       [0],"T")==0))
                                             deletepoints/M=0 0, 5,
                                                overflowwave
                                             Movewave overflowwave,
                                                root:C_waves:
                                    elseif(stringmatch(overflowname
                                       [0],"T")==1&&stringmatch(
```

```
                                        overflowname[strlen(
                                        overflowname)-1],"C")==1)
                                              deletepoints/M=0 0, 5,
                                                 overflowwave
                                              Movewave overflowwave,
                                                 root:Timewaves_C:
                                     elseif(stringmatch(overflowname
                                        [0],"T")==1&&stringmatch(
                                        overflowname[strlen(
                                        overflowname)-1],"B")==1)
                                              deletepoints/M=0 0, 5,
                                                 overflowwave
                                              Movewave overflowwave,
                                                 root:Timewaves_B:
                                     elseif(stringmatch(overflowname
                                        [0],"T")==1&&stringmatch(
                                        overflowname[strlen(
                                        overflowname)-1],"A")==1)
                                              deletepoints/M=0 0, 5,
                                                 overflowwave
                                              Movewave overflowwave,
                                                 root:Timewaves_A:
                                     endif
                            while(Countobjectsdfr(root:,1)!=0)

                    Print "Presto Load-o!!"
                    //print "The next thing you want to run is NaughtyBoy()
                       "
end
```

F.2 Time Adjusting Wave Code

```
#pragma rtGlobals=3          // Use modern global access method and
   strict wave access.
//This program will resize the A_waves(MOKE), B_waves(H-Field), and
   C_waves(Voltage)
//based off the time in timewaves
// Prompt for files or get

function timesize()
       string thefolder
       string the2ndFolder
       variable startKerr1, startH1, startKerr2, startH2, lengthKerr1
          , lengthH1, lengthKerr2, lengthH2

       Execute "CreateBrowser prompt=\"Find the Folder with Magnetic
          Field Time Data\", showWaves=0,showVars=0,ShowSTRS=0"//ask
          for the data folder with waves
       SVAR S_BrowserList=S_BrowserList //no clue why this is here
                                                          All of this
           just locates the right folder full of waves.
```

```
variable pathlength1 =strlen(s_browserlist) //length, in
   numbers, of the path name..
thefolder=s_browserlist[0,pathlength1-2] //cuts the semicolon
   from the path name

Execute "CreateBrowser prompt=\"Find the Folder with MOKE Time
    Data\", showWaves=0,showVars=0,ShowSTRS=0"//ask for the
   data folder with waves
SVAR S_BrowserList=S_BrowserList //no clue why this is here
                                                    All of this
    just locates the right folder full of waves.
variable pathlength2 =strlen(s_browserlist) //length, in
   numbers, of the path name..
the2ndFolder=s_browserlist[0,pathlength2-2] //cuts the
   semicolon from the path name


variable numberofwaves = countobjectsdfr($(thefolder),1)

string dummyName = thefolder + ":" + "'" +
   GetIndexedObjNameDFr($(thefolder), 1, 0) +"'"
string dummyName2 = the2ndfolder +":" +"'"+
   GetIndexedObjNameDFR($(the2ndfolder),1,0)+"'"
//print dummyName

// cut large wave with more points down

variable vtolerance = 0.001
wave HFieldTime = $(dummyName)
wave KerrTime = $(dummyName2)

//cut endpoints
variable Hpoints = numpnts(HFieldTime)
variable Kerrpnts = numpnts(KerrTime)
if(HFieldTime[Hpoints-1] < KerrTime[Kerrpnts-1])//End of waves
       variable startT = HFieldTime[Hpoints-1]
       findValue/V=(startT)/T=(vTolerance) KerrTime
       startKerr2 = V_value +1
       lengthKerr2 = kerrpnts - V_Value -1
       print V_value, StartT, Startkerr2, lengthkerr2
else
       startT = KerrTime[Kerrpnts-1]
       findValue/V=(startT)/T=(vTolerance) HFieldTime
       startH2 = V_Value +1
       lengthH2 = Hpoints - V_value -1
       print V_Value, StartT, startH2, lengthH2
endif

//cut front points
if(HFieldTime[0] < KerrTime[0])//begining of waves
       startT = KerrTime[0]
       findvalue/V=(startT)/T=(vTolerance) HFieldTime
       startH1 = V_value -1
```

```
		lengthH1 = V_value
		print V_value, startT, startH1, lengthH1 // add delete
		   part
	else
		startT = HFieldTime[0]
		findvalue/V=(startT)/T=(vTolerance) KerrTime
		startKerr1 = V_value -1
		lengthKerr1 = V_value
		print V_Value,StartT, startKerr1, lengthKerr1 // add
		   delete part
	endif

	//now cut points

	//kill end points first then the begining points
	variable x
	if(hpoints>kerrpnts)
		setdatafolder root:B_waves
		for(x=0; x< numberofwaves-1; x+=1)
			string allthewaves = wavelist("*",";","")
			string lookingatyou = Stringfromlist(x,
			   Allthewaves)
			wave delwave = $(lookingatyou)
			deletepoints startH2, lengthH2, delwave
			deletepoints startH1, lengthH1, delwave
		endfor
	else
		setdatafolder root:A_waves
		for(x=0; x< numberofwaves-1; x+=1)
			allthewaves = wavelist("*",";","")
			lookingatyou = Stringfromlist(x,Allthewaves)
			wave delwave = $(lookingatyou)
			deletepoints startkerr2, lengthkerr2, delwave
			deletepoints startkerr1, lengthkerr1, delwave
		endfor

	endif
	setdatafolder root:
end
```

F.3 Find Bad Magnetic Field Waves:

```
#pragma rtGlobals=3          // Use modern global access method and
   strict wave access.
function badwaves() //Goal find all bad runs possible by two ways.

       string thefolder

       Execute "CreateBrowser prompt=\"Find the Folder with Magnetic
          Field Data\", showWaves=0,showVars=0,ShowSTRS=0"//ask for
          the data folder with waves
       SVAR S_BrowserList=S_BrowserList //no clue why this is here
                                                          All of this
           just locates the right folder full of waves.
       variable pathlength1 =strlen(s_browserlist) //length, in
          numbers, of the path name..
       thefolder=s_browserlist[0,pathlength1-2] //cuts the semicolon
          from the path name

       setdatafolder root:A_waves
       string AllAwaves = wavelist("*",";","")
       setdatafolder root:C_waves
       string AllCwaves = wavelist("*",";","")
       setdatafolder root:Timewaves_A
       string AllAwavesT = wavelist("*",";","")
       setdatafolder root:Timewaves_B
       string AllBwavesT = wavelist("*",";","")
       setdatafolder root:Timewaves_C
       string AllCwavesT = wavelist("*",";","")

       setdatafolder $(thefolder)

       variable numberofwaves = countobjectsdfr($(thefolder),1)
       String AllTheWaves = wavelist("*",";","")
       make/O/N=(numberofwaves) DifWave
       make/O/T/N=1 badBoysNames
       make/O/T/N=1 badBoysA_waves
       make/O/T/N=1 badBoysC_waves
       make/O/T/N=1 badBoysNames2
       make/O/T/N=1 badBoysATime
       make/O/T/N=1 badBoysBTime
       make/O/T/N=1 badBoysCTime

       variable x

       For(x=0; x<numberofwaves; x+=1)// looks at each wave and
          subtracts it from the first(ie good wave) may not be best
          way
           string firstwave = Stringfromlist(0,Allthewaves)
           string lookingatnext = Stringfromlist(x,Allthewaves)
           wave dummy = $(firstwave)
           wave dummy2 = $(lookingatnext)
```

```
        make/O/N=(numpnts(dummy)) dummy3
        dummy3 = dummy - dummy2
        wavestats/Q dummy3
        Difwave[x] = V_avg*1000

endfor
make/O/N=(numberofwaves) AvgW
for(x=0;x<numberofwaves; x+=1)
        string lookingatyou = stringfromlist(x,Allthewaves)
        wave dummy4 = $(lookingatyou)
        wavestats/Q dummy4
        AvgW[x] = abs(V_avg)

endfor

//everything below is trying to set the threshold for badboys
variable numberpt = numpnts(Difwave)
wavestats/Q AvgW //change previous Difwave
variable threshold = V_avg + 2*V_sdev
make/O/N=1 fuboys
variable i = 0

for(x=0; x<numberpt-1; x+=1)//find badboys and set index
        if(AvgW[x]> threshold || AvgW[x]< -threshold) //changed
            to AvgW from Difwave
               fuboys[i] = x
               badBoysNames[i] = Stringfromlist(x,Allthewaves)
               badBoysA_waves[i] = Stringfromlist(x,AllAwaves)
               badBoysC_waves[i] = stringfromlist(x,AllCwaves)
               badBoysATime[i] = stringfromlist(x, AllAwavesT)
               badboysBTime[i] = stringfromlist(x,AllBwavesT)
               badboysCTime[i] = stringfromlist(x,AllCwavesT)
               insertpoints i+1, 1, badBoysAtime
               insertpoints i+1, 1, badboysBtime
               insertpoints i+1, 1, badboysCtime
               insertpoints i+1, 1, badBoysA_waves
               insertpoints i+1, 1, badBoysC_waves
               insertpoints i+1, 1, badBoysNames
               insertpoints i+1, 1, fuboys
               i+=1
        endif
endfor
deletepoints i, 1, badboysAtime
deletepoints i, 1, badboysBtime
deletepoints i, 1, badboysCtime
deletePoints i,1, badBoysA_waves
deletePoints i, 1, badBoysc_waves
deletePoints i, 1, badBoysNames
deletePoints i, 1, fuboys

i=0
make/O/N=1 fuboys2
wavestats/Q AvgW
```

```
        variable threshold2 = V_avg +2*V_sdev
        for(x=0;x<numberpt-1;x+=1)//badboys find two
                if(AvgW[x]>threshold2 || AvgW[x]< -threshold2)
                        fuboys2[i] = x
                        badboysNames2[i] = stringfromlist(x,Allthewaves)
                        insertpoints i+1, 1, badboysNames2
                        insertpoints i+1, 1, fuboys2
                        i+=1
                endif
        endfor
        deletePoints i, 1, fuboys2
        deletepoints i, 1, badboysNames2

        movewave badboysAtime, root:
        movewave badboysBtime, root:
        movewave badboysCtime, root:
        movewave badboysA_waves, root:
        movewave badboysC_waves, root:
        movewave badboysNames2, root:
        movewave badBoysNames, root:
        movewave fuboys2, root:
        movewave AvgW, root:
        movewave fuboys, root:
        movewave Difwave, root:
        killwaves dummy3
        setdatafolder root:
end
```

F.4 Kill Bad Waves Code

```
#pragma rtGlobals=3          // Use modern global access method and
   strict wave access.
//this program will kill all the bad waves(badboys)

function deathstroke()
        wave fuboys
        wave/T killAwaves = badBoysA_waves
        wave/T killBwaves = badBoysNames
        wave/T killCwaves = badBoysC_waves
        wave/T killAwavesT = badBoysATime
        wave/T killBwavesT = badboysBTime
        wave/T killCwavesT = badboysCTime
        variable numBBoys = numpnts(fuboys)
        //setdatafolder root:A_waves

        variable x

        setdatafolder root:A_waves //delete A_waves
        for(x=0;x<=numBBoys-1;x+=1)
                //string Allthewaves = wavelist("*",";","")
                //string killyouA = stringfromlist(x,Allthewaves)
```

```
		string killable = killAwaves[x]
		killwaves $(killable)
	endfor

	setdatafolder root:B_waves //delete B_waves
	for(x=0;x<=numBBoys-1;x+=1)
		//string Allthewaves = wavelist("*",";","")
		//string killyouB = stringfromlist(x,Allthewaves)
		killable = killBwaves[x]
		killwaves $(killable)
	endfor

	setdatafolder root:C_waves //delete C_waves
	for(x=0;x<=numBBoys-1;x+=1)
		killable = killCwaves[x]
		killwaves $(killable)
	endfor

	setdatafolder root:Timewaves_A //delete Timewaves_A
	for(x=0;x<=numBBoys-1;x+=1)
		killable = killAwavesT[x]
		killwaves $(killable)
	endfor

	setdatafolder root:Timewaves_B //delete Timewaves_B
	for(x=0;x<=numBBoys-1;x+=1)
		killable = killBwavesT[x]
		killwaves $(killable)
	endfor

	setdatafolder root:Timewaves_C //delete Timewaves_C
	for(x=0;x<=numBBoys-1;x+=1)
		killable = killCwavesT[x]
		killwaves $(killable)
	endfor

	setdatafolder root:

end
```

F.5 Find Applied Voltages Code

```
#pragma rtGlobals=3		// Use modern global access method and
   strict wave access.
function VoltAv()

	make/O Voltage
	make/O/N=(1,2) VoltageCount1
	make/O/N=1 VoltCount1
	string thefolder
```

```
//String cdfBeore = GetDataFolder(1)
Execute "CreateBrowser prompt=\"Find the Folder with Voltage
   Data\", showWaves=0,showVars=0,ShowSTRS=0"//ask for the
   data folder with waves
//String cdfAfter = GetDataFolder(1) // Save current data
   folder afte, though seeems like this is the same as
   CDFbefore since execute doesn't set the folder unless you
   do that, just saves path
//SetDataFolder cdfBefore                                    //
   Restore current data folder.
SVAR S_BrowserList=S_BrowserList //no clue why this is here
   All of this just locates the right folder full of waves.
variable pathlength1 =strlen(s_browserlist) //length, in
   numbers, of the path name..
thefolder=s_browserlist[0,pathlength1-2] //cuts the semicolon
   from the path name

setdatafolder $(thefolder)
variable numberofwaves = countobjectsdfr($(thefolder),1)
String AllTheWaves = wavelist("*",";","")


variable x
insertpoints 127, (numberofwaves -128), Voltage

For(x=0; x<numberofwaves; x+=1)
        string lookingatyou = Stringfromlist(x,Allthewaves)
        wavestats/Q $(lookingatyou)
        Voltage[x] = V_avg*5
endfor

x=0
variable p=0
variable delta
variable length
variable firstpoint = 0
for(x=0;x<numberofwaves; x+=1)
        if(x<numberofwaves-1)
                delta = abs(Voltage[x] -Voltage[x+1])
        elseif(x==numberofwaves-1)
                wavestats/Q/R=[firstpoint,x] Voltage
                length = x -firstpoint +1
                VoltageCount1[p][0] = V_avg
                VoltageCount1[p][1] = length
                VoltCount1[p] = length
        endif

        if(delta >1)
                wavestats/Q/R=[firstpoint, x] Voltage
                length = x - firstpoint +1
                //print length
                //print p
                VoltageCount1[p][0] = V_avg
```

```
                        VoltageCount1[p][1] = length
                        VoltCount1[p] = length
                        insertPoints p+1, 1, VoltCount1
                        insertPoints p+1, 1, VoltageCount1
                        firstpoint = x+1
                        p+=1
                        //print VoltageCount
                endif
        endfor
        print numberofwaves
        setdatafolder root:
end
```

F.6 Averaging MOKE Loops Code

```
#pragma rtGlobals=3          // Use modern global access method and
   strict wave access.
//this program will average the osci scope data both the field and
   MOKE Data

function MassOsci()
        wave VoltCount1
        newdatafolder root:Kerrwaves
        newdatafolder root:MagField
        newdatafolder root:KerrwavesN
        string thefolder
        string the2ndFolder

        Execute "CreateBrowser prompt=\"Find the Folder with MOKE Data
           \", showWaves=0,showVars=0,ShowSTRS=0"//ask for the data
           folder with waves
        SVAR S_BrowserList=S_BrowserList //no clue why this is here
                                                              All of this
            just locates the right folder full of waves.
        variable pathlength1 =strlen(s_browserlist) //length, in
           numbers, of the path name..
        thefolder=s_browserlist[0,pathlength1-2] //cuts the semicolon
           from the path name

        Execute "CreateBrowser prompt=\"Find the Folder with Magentic
           Field Data\", showWaves=0,showVars=0,ShowSTRS=0"//ask for
           the data folder with waves
        SVAR S_BrowserList=S_BrowserList //no clue why this is here
                                                              All of this
            just locates the right folder full of waves.
        variable pathlength2 =strlen(s_browserlist) //length, in
           numbers, of the path name..
        the2ndfolder=s_browserlist[0,pathlength2-2] //cuts the
           semicolon from the path name

        variable numME = numpnts(VoltCount1)
```

```
variable x
variable istart = 0

for(x=0; x<numME; x+=1)

        setdatafolder $(thefolder)// set folder
        string allthewaves = wavelist("*",";","")// get
           wavenames
        string dummyname = "kerr_" + num2str(x)
        string dummynameNorm = "kerrNorm_" + num2str(x)

        string lookingatyou= stringfromlist(istart,Allthewaves)
        make/O/N=(numpnts($lookingatyou)) $(dummyname)
        wave dummy = $(dummyname)
        make/O/N=(numpnts($lookingatyou)) $(dummynameNorm)
        wave dummyNorm = $(dummynameNorm)

        variable nextmax = istart + voltcount1[x] // set be
           number of averages -1 for indexing
        variable count =0
        variable i

        for(i = istart; i< nextmax; i+=1)
                string dummy2 = stringfromlist(i,Allthewaves)
                wave dum = $(dummy2)
                dummy = dummy + dum
                count+=1
        endfor
        //print count
        dummy = (dummy/Voltcount1[x])
        variable length = numpnts(dummy)

        wavestats/Q/R=(0,100) dummy
        variable max1 = V_avg
        wavestats/Q/R=(length-100,length) dummy
        variable max2 = V_avg
        variable truemax = (max1 +max2)/2
        variable mid = Floor(length/2)
        wavestats/Q/R=(mid-200,mid+200) dummy
        variable min1 = V_avg

        dummyNorm = -1 +(((dummy - min1)*2)/(truemax -min1))

        //normalizing is done here

        movewave dummy, root:Kerrwaves:
        movewave dummyNorm, root:KerrwavesN:

        //now the
        setdatafolder $(the2ndfolder)
        string allthewaves2 = wavelist("*",";","")//get
           wavenames
        string dummyname2 = "Hfield_" + num2str(x)
```

```
                string lookingatyou2 = stringfromlist(istart,
                   Allthewaves2)
                make/O/N=(numpnts($lookingatyou2)) $(dummyname2)
                wave dummy3 = $(dummyname2)
                count =0
                for(i= istart; i<nextmax; i+=1)
                        string dummy4 = stringfromlist(i,Allthewaves2)
                        wave dum2 = $(dummy4)
                        dummy3 =dummy3 + dum2
                        count +=1
                endfor
                //print count
                dummy3 = (dummy3/Voltcount1[x])*10 //*10kOe or /10000
                   for T

                movewave dummy3, root:MagField:

                istart = nextmax
        endfor
        setdatafolder root:

end
```

F.7 Find Total Kerr Rotation Code

```
#pragma rtGlobals=3          // Use modern global access method and
   strict wave access.
//This Function will get the rotators for an arbitrary MOKE file

Function rotator()
        wave VoltCount1
        string thefolder

        Execute "CreateBrowser prompt=\"Find the Folder with MOKE Data
           \", showWaves=0,showVars=0,ShowSTRS=0"//ask for the data
           folder with waves
        SVAR S_BrowserList=S_BrowserList //no clue why this is here
                                                          All of this
            just locates the right folder full of waves.
        variable pathlength1 =strlen(s_browserlist) //length, in
           numbers, of the path name..
        thefolder=s_browserlist[0,pathlength1-2] //cuts the semicolon
           from the path name

        variable numME = numpnts(VoltCount1)

        make/O/N=(numME) rotators
        make/O/N=(numME) yoffset
        variable i

        for(i=0; i<numMe; i+=1)
```

```
                setdatafolder $(thefolder)
                string allthewaves = wavelist("*",";","")// get
                   wavenames
                string lookingatyou= stringfromlist(i,Allthewaves)

                wave dummy = $(lookingatyou)
                variable length = numpnts(dummy)

                wavestats/Q/R=(0,500) dummy // originally 100
                variable max1 = V_avg
                wavestats/Q/R=(length-500,length) dummy
                variable max2 = V_avg
                variable truemax = (max1 +max2)/2
                variable mid = Floor(length/2)
                wavestats/Q/R=(mid-300,mid+300) dummy //orginally 200
                variable min1 = V_avg
                variable rot = truemax - min1
                rotators[i] = abs(rot)
                wavestats/Q dummy
                yoffset[i] = -V_avg

        endfor
        setdatafolder root:
end
```

F.8 MEMOKE Code

```
#pragma rtGlobals=3          // Use modern global access method and
   strict wave access.
Function MEMoke()//i dont think this does anything
//This program will initially find the Coercivity by finding where the
    signal crosses zero
// and then take the average of the two point before and after

variable a,b,c,d
variable i=0
//make/o m_wavestats
//wave m_wavestats
string thefolder,fieldfolder

NewDatafolder/o root:CoercivityPiecesME

variable v_flag

       Execute "CreateBrowser prompt=\"Find the folder with MOKE data
          \", showWaves=0, showVars=0, showStrs=0" //asks you to find
           a data folder, who'se path is stored as S_browserlist
       SVAR S_BrowserList=S_BrowserList //no clue why this is here
       variable pathlength1 =strlen(s_browserlist) //length, in
          numbers, of the path name..
       Thefolder=s_browserlist[0,pathlength1-2] //cuts the semicolon
          from the path name

       Execute "CreateBrowser prompt=\"Find Folder with FIELD data\",
           showWaves=0, showVars=0, showStrs=0"
       variable pathlength2 =strlen(s_browserlist)
       fieldfolder=s_browserlist[0,pathlength2-2]

string suffix
Prompt Suffix, "what will be the suffix of coercivity wave. eg.
   coercivity_SUFFIX'\r\ for waves found in"+Thefolder
doprompt "naming", suffix

//Prompt thefolder,"root:subfolder1:subfolder2: ... :subfolderN:"
//doPrompt "full path to Kerr waves",thefolder
       //thefolder= "root:normalizedwaves:"

//Prompt fieldfolder,"root:subfolder1:subfolder2: ... :subfolderN:"
//doPrompt "full path to Fieldwaves",fieldfolder
       //fieldfolder = "root:fieldwaves:"
//setdatafolder root:CoercivityPiecesME

Variable Counter
counter= countobjectsdfr($(thefolder),1)
       String CoercivityName= fieldfolder + ":" + "Coercivity_" +
          SUFFIX
       make/o/N=(Counter) $CoercivityName
       //string wavenamey =fieldfolder + ":" + CoercivityName
```

```
        wave coer = $CoercivityName

//print numpnts(coer)
//String nameofcoercivity = "WaveNames_" + suffix
        //make/o/N=)

//setdatafolder $(fieldfolder)
//string allthefields = wavelist("*",";","")

Do//Finds Coercivity, first finds width then divides, could be made to
    find loop center
        setdatafolder $(thefolder)
        string allthewaves = wavelist("*",";","")
        string lookingatyou = stringfromlist(i, allthewaves)
        wave dummy = $(lookingatyou)
        wavestats/Q dummy
        dummy = dummy - V_avg
        variable length = numpnts(dummy)
        Findlevels/P/D=destwave dummy, 0
        variable maxi = numpnts(destwave) -1
        setdatafolder $(fieldfolder)

        string allthefields = wavelist("*",";","")
        string lookingatfield = stringfromlist(i, allthefields)
        wave thefields = $(lookingatfield)
        variable cor = thefields[Round(destwave[0])] -thefields[Round(
           destwave[maxi])]
        coer[i] = Abs(cor)
        //print destwave[0]
        //Findlevel/R=(length/2, length) dummy,0
        //print V_levelx
i+=1
while(i<counter)

String RemanceName = thefolder + ":" + "Remance_" + Suffix
make/O/N=(Counter) $RemanceName
wave rem = $RemanceName
i=0
Do
        setdatafolder $(fieldfolder)
        lookingatfield = stringfromlist(i,allthefields)
        wave thefields = $(lookingatfield)
        Findlevels/P/D=destwave thefields, 0
        //print destwave[0], destwave[1]

        setdatafolder $(thefolder)
        lookingatyou = stringfromlist(i,allthewaves)
        wave dummy = $(lookingatyou)
        rem[i] = dummy[Round(destwave[0])]
i+=1
while(i<counter)
```

```
killwaves destwave

movewave rem , root:CoercivityPiecesME:
movewave coer, root:CoercivityPiecesME:

setdatafolder root:
end
```